Rate observables for cosmology and heavy ion collision experiments

Inaugural dissertation
of the Faculty of Science
University of Bern

presented by

Greg Jackson

from South Africa

Supervisor of the doctoral thesis:

Prof. Dr. Mikko Laine

Albert Einstein Center for Fundamental Physics
Institute for Theoretical Physics, University of Bern

Rate observables for cosmology and heavy ion collision experiments

Inaugural dissertation
of the Faculty of Science
University of Bern

presented by

Greg Jackson

from South Africa

Supervisor of the doctoral thesis:

Prof. Dr. Mikko Laine

Albert Einstein Center for Fundamental Physics
Institute for Theoretical Physics, University of Bern

Accepted by the Faculty of Science.

Bern, 16 July 2020 The Dean

Prof. Dr. Zoltan Balogh

Submitted: 22 May 2020, Revised: 18 June 2020

Author: Greg Jackson[1]
Supervisor: Mikko Laine
Referee: Dietrich Bödeker

[1]Electronic address: jackson@itp.unibe.ch

Abstract

The early universe is perhaps the best conceivable multi-particle system in nature, for which the degrees of freedom are those of the Standard Model. This elementary particle plasma traced a path through its phase diagram, while evolving, that was largely determined by the underlying symmetries of the theory. Another trajectory, through the same phase diagram, is followed in a central collision between two heavy nuclei at high energies. Fortunately, theoretical methods developed and tested for heavy ion collision experiments are also proving useful in cosmology, and *vice versa*. We demonstrate this by giving context to (and summarising) the work in Refs. [1–5].

Important properties can be studied through the 'eyes' of different probes that escape a thermal medium. In this thesis we consider three: Photons, neutrinos and gravitational waves. Each of these signals is a forensic tool for one or another facet of the Standard Model at finite temperature. Among the dynamical observables, interaction rates for hot gauge theories are conceptually interesting in their own right because they are sensitive to many scales in the problem. It is therefore crucial to evaluate the predictive power of perturbative approximations, either by examining higher-order terms or by comparing them with non-perturbative information.

Keywords: perturbation theory, interaction rate, quark-gluon plasma, electroweak phase transition, gravitational radiation, hydrodynamics

Acknowledgements

I sincerely thank Mikko Laine, whose scrupulous attention to detail has repeatedly come to the author's rescue. With his deep insight and technical skill, Mikko has convinced me that few (if any) calculations are impossible. It has been a privilege to learn from him and receive his guidance over the past three years.

I am grateful to Dietrich Bödeker for agreeing to be the external referee of my thesis – his valuable feedback undoubtedly went into improving its quality. Thanks also go to Uwe-Jens Wiese for chairing my defence and his comments on the thesis. The work presented here has been enriched by the author's conversations with Simon Caron-Huot, Charles Gale, Jacopo Ghiglieri, Peter Petreczky, Rob Pisarski and in particular André Peshier. I wish to convey my genuine appreciation to friends among fellow graduate students and postdocs at the University of Bern. Let me express special thanks to Philipp Schicho and Tuomas Tenkanen, of our research group, for discussions – and distractions! Kim Jackson and James Wilsenach were kind enough to proofread parts of this thesis.

The Swiss National Science Foundation has provided the financial support for this work and enabled my participation in various conferences and schools. These include the Les Houches Summer School in 2017, the Hot Quarks workshop in 2018, the QCD Masterclass in 2019 and the 28^{th} Quark Matter conference. I also thank Brookhaven National Lab and McGill University for kindly hosting me so that I could visit them to present and discuss my work earlier this year.

To my friends and family, thank you for everything else.

Contents

1. Introduction

To fathom the universe at its earliest moments, we rely on signals that have spent the intervening history travelling to our current location in space and time. Some of these 'probes' are photons emitted by a thermal system whose radiance peaks in the microwave frequency range, now referred to as the cosmic microwave background (CMB) [6]. The observation of this source, plus its near uniformity in all directions, marked a turning point in cosmology: It ratified the hypothesis of a Big Bang origin, implying that all matter in our universe was once a hot, dense plasma [7]. Modern cosmology relies heavily on the prospect of tracing all observable phenomena to a small number of facts and laws – the primary concern of elementary particle physics. In the Standard Model (SM), matter is understood to fall into two categories: quarks and leptons [8]. Natural phenomena may be described by the interactions of these 'particles', according to four fundamental forces, namely, electromagnetism, the strong and weak forces, as well as gravity. Our current understanding implies that these forces arise due to an invariance of the non-interacting theory under certain symmetry transformations. The resulting gauge field theory leads to quanta that supplement the quarks and leptons. Mathematical self-consistency of these theories, in the context of renormalisation, supplies the guiding principle on which the SM is constructed [9]. Although the gravitational force has not yet been fully realised as a quantum field theory (QFT), the rest have – and to a degree that continues to be extremely successful in high-energy experiments. There are other issues, besides gravity's omission, that point to the need for further development, such as the observation that neutrinos have mass, as well as the CMB-based evidence for both dark matter and dark energy. Thus, the SM provides an incomplete, but coherent description of nature. Its virtues and shortcomings bear particular relevance for cosmology, in a manner that the two disciplines mutually complement one another.

In this thesis we will discuss interaction rates that pertain to many-body properties of the SM in thermal equilibrium. Specifically, we consider three quite different scenarios which nonetheless involve a similar underlying physical process: An 'external field' which is out of equilibrium with the hot environment (but can still interact with it), is either produced or absorbed by the medium. The average *net rate* is a difference between production and absorption rates and serves to thermalise the combined system. When the temperature is much higher than the rest masses of the particles considered, $k_{\mathrm{B}}T \gg mc^2$, the creation of particle-antiparticle pairs becomes prevalent. In this regime the total number of particles grows so that the mean interparticle distance shrinks with increasing T. Eventually, the particle separation becomes comparable to the thermal de Broglie wavelength $\lambda_{\mathrm{th}} \sim \hbar c/(k_{\mathrm{B}}T)$ and the system is both quantum mechanical and relativistic. However, in general, a simple extrapolation of the properties of a few particles is not sufficient to explain this high-T limit [10].

The cosmos, in its early stages, consisted of a hot SM plasma, which, apart from some possible phases of reheating, cooled down over time. If we consider $t = 0$ to correspond with the 'initial singularity', current time is

$$t_{\mathrm{now}} \quad = \quad (4.32 \pm 0.01) \times 10^{17} \text{ seconds}\,. \tag{1.1}$$

The CMB is the oldest thing we have ever seen, dating to when the universe was about 3.77×10^5 years old[2]. It defines the edge of the observable universe for electromagnetic

[2] One year is approximately $\pi \times 10^7$ seconds.

radiation. Other probes, like neutrinos and gravitational waves, interact very weakly so that their observable limit is further away (earlier) but consequently more difficult to measure in experiments. Ideally, the 'multimessenger astronomy' approach could provide snapshots of the universe at very different points in its history, see Fig. 1. Understanding the cosmological evolution requires knowledge of the many-body properties of the SM. Many sections of that evolution can be described to a good approximation by thermodynamics, since the typical 'microscopic' timescales of the local equilibration process are much smaller than those of the concurrent global dynamics. The inverse Hubble parameter $H^{-1}(t) = a(t)/\dot{a}(t)$, where a is the cosmic scale factor, sets the 'macroscopic' time. Its present-day value, of $H_0^{-1} \simeq 4.6{\times}10^{17}$ seconds, differs from (1.1) due to the *nonlinear* nature of the expansion.

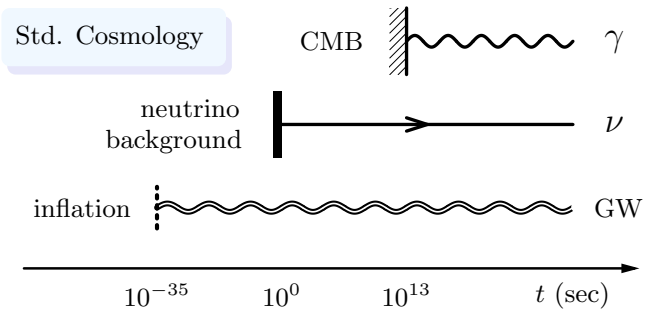

Figure 1: Three important probes of the early universe: photons (γ), neutrinos (ν) and gravitational waves (GW). They originate by different processes and thus bring information from various stages in the evolution of the universe, as far back as it became 'transparent' in that channel.

We are able to draw conclusions about times prior to the CMB by knowing that the universe is expanding and that it is made up of SM particles. In a crude sense, studying the early universe's chronology is thus akin to studying the SM as a function of temperature, i. e. its equation of state. The Friedmann equations provide a relation between the first two time derivatives of $a(t)$, the pressure, and the energy density [11]. The equation of state completes the set of coupled differential equations. The CMB marks the moment that photons decoupled and stable hydrogen was able to form through $p + e^- \to \mathrm{H} + \gamma$. After this, the formation of an electrically neutral 'gas' of atoms allowed photons to travel without further interaction. Some few thousand years prior, the bulk energy density came from ultrarelativistic particles and hence $a(t) \propto t^{1/2}$ in the radiation-dominated era. At this time, light nuclei (predominantly hydrogen and helium isotopes) could be synthesised and the observed ratio of baryons to photons of $1 : 10^9$ was set, implying a negligible hadrochemical potential. The density was high enough to be opaque to neutrinos at $t \lesssim 1$ s, when photons were the main scattering target.

Decoupling of neutrinos is called the cosmic neutrino background (CνB), which has so far remained undetected. We will focus on still earlier times, after certain 'broken symmetries' of the SM have been restored, but not so far back that serious issues (beyond even simple SM-extensions) of Grand Unification and inflation need to be taken into account. The time in (1.1) is one of six parameters in the Lambda cold dark matter (ΛCDM) model of cosmology, and calling it the age of the universe means extrapolating to times where current physical theories may not apply. (That point is the so-called Planck epoch, corresponding to $t < 10^{-43}$ seconds.) The ΛCDM model, often referred to as the 'standard model' of cosmology, needs to be taken seriously because of its ability to describe the cosmic history

over several orders of magnitude. Unfortunately, dark matter and dark energy (two of three major components in the ΛCDM) are not included in the SM (the third component, being 'ordinary matter') [12].

Our terrestrial units for time are less adequate when it comes to the early universe than its temperature (T) in units of MeV. Due to the conservation of comoving entropy density in an adiabatically expanding system, described by the Friedmann equations, T can be directly converted to time in seconds. A convenient order-of-magnitude formula is available,

$$\frac{t}{\text{sec}} \simeq \left(\frac{\text{MeV}}{k_{\text{B}}T}\right)^2 ,$$

which is approximately valid prior to recombination, i. e. $T \geq \frac{1}{4}$ eV$/k_{\text{B}}$. Many internal symmetries of the SM, which we discuss next, are 'hidden' but have been revealed (and tested) in high energy experiments. These symmetries are expected to control the phase diagram, and in particular the trajectories that are followed in extreme environments, like those which undoubtedly existed in the early cosmos.

The strong force describes how quarks and gluons interact, the latter arising from a local non-Abelian $SU_{\text{c}}(3)$ symmetry in the free theory of the former. The conserved charge associated with this symmetry is called 'colour', and the theory is known as quantum chromodynamics (QCD) [13]. In Abelian quantum field theories, such as quantum electrodynamics (QED), the gauge bosons do not carry charge[3]. However, the self-interaction that results from gluons (the mediators of the strong force) carrying a colour charge is expected to underpin the fact that quarks and gluons are *confined* to colour neutral bound states. The lightest are the pions, which exist as an isotriplet of pseudoscalars; π^0, $\pi^\pm$ and have mass $m_\pi \simeq 140$ MeV$/c^2$. That mass far exceeds the sum of individual quark masses in the u, d-pair. For other settings, this would make it energetically favourable to separate the constituents arbitrarily far apart from one another. However, in QCD, confinement means that an unbound case is not realised in nature.

The weak force was originally proposed as a solution to the problem of β-decay via the leptonic reaction $n \to p + e^- + \bar{\nu}_e$, and the (electron-type) neutrino was originally adopted to account for the missing momentum in the same process. Underlying the conversion of a neutron to a proton is the fact that weak interactions can change flavour, namely a u-quark to a d-quark. Glashow, Weinberg and Salam first realised how to unify electromagnetism with the weak force from an underlying $SU_{\text{L}}(2) \times U_{\text{Y}}(1)$ gauge symmetry [14]. The resulting electroweak (EW) sector involves three 'isospin' and one 'hypercharge' gauge fields, which are massless and interact with the quarks and leptons. In the SM, at zero temperature, that gauge symmetry is broken by the Higgs mechanism to $U_{\text{em}}(1)$ which has the effect of endowing three gauge fields with a mass: the charged $W^\pm$ and the neutral Z^0. One gauge boson remains massless, we call it the photon: γ.

Before QCD or EW theory became the widely accepted basis of the SM, various effective approaches were used to study the structure of hadrons (now known to be colour neutral bound states). Already at that time, it was recognised that the thermodynamics of strongly interacting mesons, baryons and antibaryons becomes untenable in the very early universe. One line of reasoning goes back to Hagedorn [15], who supposed that *all* resonant

[3] For QED the gauge group is $U_{\text{em}}(1)$, which is Abelian.

hadronic states be included in a statistical 'bootstrap' ensemble, omitting (to first order) their mutual interactions. The combinatorics of this ensemble implies an exponentially rising mass spectrum for those hadronic states. Figure 2 shows the actual cumulative number of known hadrons above a given mass M, collected by the Particle Data Group [16]. It roughly confirms the phenomenological form

$$\rho(M) \;=\; \frac{a}{\left(M^2+b^2\right)^{5/4}} \exp\Big[\,\frac{M\,c^2}{k_{\mathrm{B}}T_{\mathrm{H}}}\,\Big], \tag{1.2}$$

where $a \sim 0.16$ and $b = 0.5$ GeV$/c^2$ [17]. Although incomplete, this picture makes a unique and dramatic prediction; namely that thermodynamic quantities will generally be ill-defined for $T > T_{\mathrm{H}}$. Any integrals of $\rho(M)\,dM$ with a weight factor of $e^{-M/T}$ for $M \to \infty$ do not converge. Note that the flattening accumulation of resonances in Fig. 2 is most likely due to the shortage of information about hadronic states with mass $M \gtrsim 2$ GeV$/c^2$.

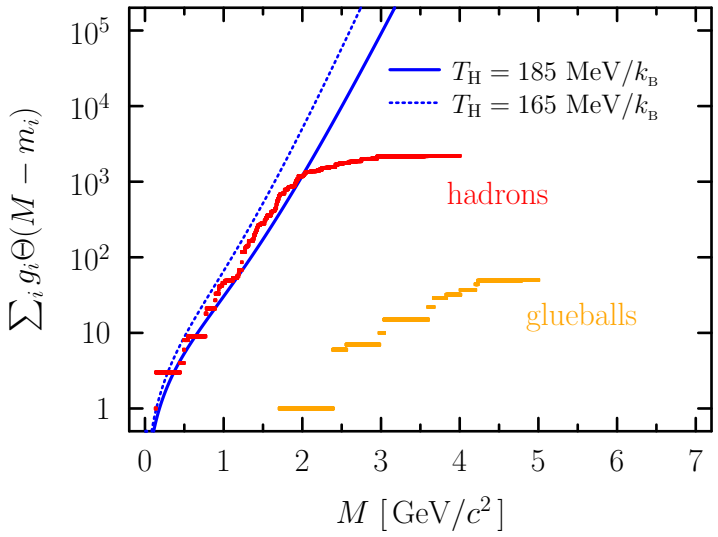

Figure 2: Cumulative number of hadronic resonances with mass greater than M, including all mesons and baryons (red) from Ref. [16]. The sum runs over all states i with a known mass m_i and degeneracy factor g_i. Glueballs (orange) may also be included, although their contribution is evidently minor, but showing that the same arguments apply to quenched QCD.

The system's temperature may rise above $T_{\mathrm{H}} \simeq 175$ MeV$/k_{\mathrm{B}}$ thanks to a remarkable feature of QCD, called asymptotic freedom [18]. This fact says that the effective colour charge diminishes at short distances, in particular at high temperatures where the interparticle separation is small. A new phase emerges where the hadronic constituents are not confined and the carriers of colour charge are mobile over macroscopic distances. Asymptotic freedom implies that as $T \to \infty$, the strong coupling diminishes logarithmically and the system gradually approaches an ideal gas called the quark-gluon plasma. This is a rigorous[4] limit of QCD, but non-perturbative lattice simulations have shown that a phase transition occurs

[4] At asymptotically large temperatures, the 'smallness' of the coupling makes perturbation theory applicable. Whether these weak-coupling predictions are robust when extrapolated to lower temperatures should be judged on a case-by-case basis.

at $T_c = 154 \pm 9$ MeV/k_B in a theory with two light and a heavier strange quark [19]. Sufficient conditions are recreated by smashing nuclei into one-another at enough center-of-mass energy (per nucleon-nucleon pair), $\sqrt{s_{NN}}$; an undertaking which is fulfilled at the Large Hadron Collider (LHC) and Relativistic Heavy Ion Collider (RHIC) [20]. The yields of photons and dileptons produced is one of many proposed 'thermometers' of the deconfined phase. Accurate predictions of thermal spectra are needed to extract such signatures on top of their large hadronic backgrounds [21].

What happens to the rest of the SM as the temperature is increased further? An EW plasma has its original symmetry restored at temperatures slightly higher than the mass of the Higgs boson, at $T_c = 159.5 \pm 1.5$ GeV/k_B, and a *smooth* transition has been shown to occur [22]. The symmetry-broken phase is characterised by a Higgs field with a non-vanishing expectation value, $\langle\phi\rangle \neq 0$. Such temperatures cannot be achieved in terrestrial experiments, but certainly existed in the early cosmos and are connected (in that context) with one of the longstanding mysteries in physics: An imbalance in matter and anti-matter in the observable universe[5]. The common interpretation is that a process of baryogenesis occurred which destroyed the perfect symmetry, generating a preferences for baryons over anti-baryons. In an argument due to Sakharov, inspired by the CMB and $\mathcal{CP}$-violation in neutral kaons, three conditions are required for baryogenesis: *i*) Baryon number violation, *ii*) $\mathcal{C}$- and $\mathcal{CP}$-symmetry violation, *iii*) thermal non-equibrium [23]. Smoothness of the transition tends to keep the system in equilibrium through its dynamical evolution, thus making processes like EW baryogenesis ineffectual [24]. However, physics beyond the SM may cure this drawback. It is possible to incorporate (heavy) right-handed neutrinos that partially account for dark matter [25]. These 'sterile' neutrinos would also explain why the left-handed neutrinos have a (small) mass and also introduce a new source of $\mathcal{CP}$-violation. Although these extensions introduce many new parameters, their values are starting to be quite constrained [26]. Whether the new models turn out to be true (or not), it stands to reason that precision EW calculations are called for.

Although the 'standard' EW transition is a mild crossover, there are plausible extensions that could still make it first-order. That would permit the system to depart from local equilibrium, making baryogenesis possible and also rendering the associated cosmological event considerably more violent [27]. Perhaps the gravitational waves emitted will be detected in the next generation of detectors, the most germane being the Laser Interferometer Space Antenna (LISA) [28, 29]. The manner of such a phase transition is similar to the boiling of water – but in reverse: As the system cools enough for the Higgs ground state $\langle\phi\rangle = 0$ to be metastable, fluctuations will seed 'bubbles' in the broken phase. These nucleated regions with non-zero $\langle\phi\rangle$ grow into the unstable (hotter) background, collide and then coalesce with one another. Friction at the planar interface of the bubbles hampers their propagation until they reach a stable velocity [30, 31]. The subsequent radiation of gravity has been studied in hydrodynamic simulations, which show that the spectrum is dominated by the combination of sound waves and turbulence [32]. In addition to the differential frequency spectrum of GWs, their total energy density would supply part of the cosmic budget in the radiation epoch [33, 34]. That would affect the values of important parameters in ΛCDM, many of which are becoming quite well constrained.

[5] Currently, neither conventional particle physics nor general relativity can explain the baryon asymmetry in the universe.

Outline

The treatment of emission and absorption rates in thermal field theory has a variety of applications [35]. We tackle three problems, which inform the organisation of this report:

§ I Electromagnetic probes

Photons and dileptons from an equilibrated QCD plasma are produced at a rate proportional to the corresponding spectral function. We investigate this function, and determine it for energies above, below and in the vicinity of the light cone [2]. The results are confronted with non-perturbative lattice data, which is sufficient to calibrate the choice of running coupling [3].

§ II Neutrino damping

In this part, we consider the rate of interactions suffered by a neutrino as it passes through a plasma in the symmetry-broken phase. The ultrarelativistic neutrino's EW interactions can be mapped to an effective three-dimensional theory that simplifies the calculation. Doing so, we push the perturbative accuracy to NLO [4].

§ III Gravitational waves

Transport of energy and momentum in the early universe would have radiated GWs. We determine the shape of the spectrum due to hydrodynamical fluctuations that arise because of friction in nucleation phase transitions [1]. The equilibrium rate is also mentioned, referring to recent work on the high-frequency radiation [5].

Although these three chapters may be read independently, the ordering above seems most natural: Topics progress from strong to weak(er) coupling. To avoid being sidetracked in these overviews, some discussions have been relegated to the Appendices. In the conclusion, we will highlight the common features in these problems and summarise the main results of each section.

It is worthwhile to comment on the framework in which we address the topics above. Our understanding of a physical problem frequently profits from knowing that two pertinent scales are clearly separated. The notion of *effective field theory* (EFT) is then a scaffold on which to base calculations at one extreme of the range [36]. In each of the three problems above, we explain how this approach is applied in the thermal setting.

Notation and conventions

We make use of the 'natural units' $\hbar = c = k_{\rm B} \to 1$, so that Planck's constant is $h = 2\pi$.

Euclidean (d-) vectors are flagged by Latin indices, like x_i. We write the boldface script,

$$\boldsymbol{x} = (x_1, x_2, \ldots, x_d)\,, \quad \text{where} \quad d = 3 \text{ (usually)}\,.$$

Summation convention will be used, and scalar products are denoted

$$\boldsymbol{xy} \;\coloneqq\; x_1y_1 + x_2y_2 + \ldots + x_dy_d \;=\; x_iy_i\,.$$

The magnitude of a vector is $x = |\boldsymbol{x}| = \sqrt{\boldsymbol{x}^2}$ and its direction $\hat{x} = \boldsymbol{x}/x$.

Components of $(d+1)$-spacetime vectors will be capitalised[6] and denoted by Greek indices, e. g. $X_\alpha = (x_0, \boldsymbol{x})$. When in local Minkowski space, the covariant metric (tensor in $d = 3$)

$$g_{\mu\nu} \;\coloneqq\; \mathrm{diag}\,(+,-,-,-)$$

and is self inverse: $g_{\mu\nu}g^\mu{}_\rho = g_{\nu\rho}$. (With curved backgrounds, we use $\eta_{\mu\nu}$ for the flat metric and $g_{\mu\nu}$ in general.) Hence the 4-products are $XY \coloneqq X_\mu Y^\mu = x_0y_0 - \boldsymbol{xy}$. After Wick rotating, (Euclidean) vectors will be written $X_{\rm E}$ where $x_0 = ix_{\rm E}^0$ and $\boldsymbol{x} = \boldsymbol{x}_{\rm E}$ so that $X_{\rm E}^2 = -X^2$. We often make use of the 4-momentum $K = (\omega, \boldsymbol{k})$ as an 'external variable' ($\omega \in \mathbb{R}$). The corresponding light cone momenta are defined as $k_\pm = \frac{1}{2}(\omega \pm k)$ and invariant mass $M = \sqrt{|K^2|}$.

Mean values for distributed quantities are represented by angular brackets, i. e. $\langle \cdots \rangle$, where the type of averaging will be specified in the main text. Often we need the thermal average, with respect to a grand canonical ensemble, entailing single particle distribution functions:

$$n_s(\omega) \;=\; \frac{1}{e^{\omega/T} - s}\,. \tag{1.3}$$

Bosons ($s = +1$) and Fermions ($s = -1$) shall be denoted $n_{\rm B}$ and $n_{\rm F}$ respectively. Extensive quantities are given Roman capitals: $E, V, N, S, \cdots$. Excepting the temperature T, intensive variables will be lower case: $\varepsilon = E/V$, $n = N/V$ and $s = S/V$ for the energy, number and entropy density respectively; and p for the pressure.

The trace over momentum[7] $K = (k_0, \boldsymbol{k})$ at finite temperature is defined by

$$\not{\int}_K = \int_{\boldsymbol{k}} T \sum_{k_0}\,; \qquad \int_{\boldsymbol{k}} = \left(\frac{e^\gamma \bar{\mu}^2}{4\pi}\right)^\epsilon \int \frac{d^dk}{(2\pi)^d}\,,$$

where γ is Euler's constant and $d = 3 - 2\epsilon$. The energy in the sum is Euclidean, $k_0 = ik_{\rm E}^0$, and covers a discrete spectrum $k_{\rm E}^0 \to \pi jT$ where j is an even (odd) integer for bosons (fermions). We also abbreviate the Dirac delta function $\delta\!\!\!^{-}(\cdots) = 2\pi\delta(\cdots)$.

Respectively, the $SU_{\rm c}(3)$-, $SU_{\rm L}(2)$- and $U_{\rm Y}(1)$-gauge couplings of the SM are:

$$\alpha_{\rm s} = \frac{g_{\rm s}^2}{4\pi}\,, \quad \alpha_{\rm w} = \frac{g^2}{4\pi} \quad \text{and} \quad \alpha_{\rm y} = \frac{g'^2}{4\pi}\,.$$

In addition, we will use $\widetilde{g} = \sqrt{g^2 + g'^2}$, the electromagnetic coupling $e = gg'/\widetilde{g}$ and sometimes $\underline{g}$ as a 'generic' coupling. For $SU(N)$ theories, we write the quadratic Casimir in the fundamental representation as $c_F = (N^2 - 1)/(2N)$, which is 4/3 for QCD.

[6] With the exception of $u_\mu = \gamma(1, \boldsymbol{u})$, the four-velocity.

[7] We shall regard k_0 in the complex plane, taking on real ($k_0 \to \omega$), and imaginary ($k_0 \to ik_{\rm E}^0$) values.

Part I

Electromagetic probes of the quark-gluon plasma

2. Phenomenological prelude

Heavy ion collisions recreate conditions that are amenable to forming a QCD plasma. Photons produced inside the plasma typically pass through the medium without further interaction, making them ideal probes [21]. That includes both real and virtual photons; the latter of which decay into lepton-antilepton pairs. Relevant particle yields, at the RHIC and LHC experiments, come from *all* stages of the nucleus-nucleus interaction, e. g. initial (hard) partons would populate the high energy part of the spectrum. Understanding specific production rates – in particular from the quark-gluon plasma (QGP) itself – is a prerequisite to explaining observations like the invariant-mass distribution displayed in Fig. 3 for e^+e^- pairs. Of course, the variety of processes that can deliver such pairs make disentangling separate mechanisms an ambitious goal.

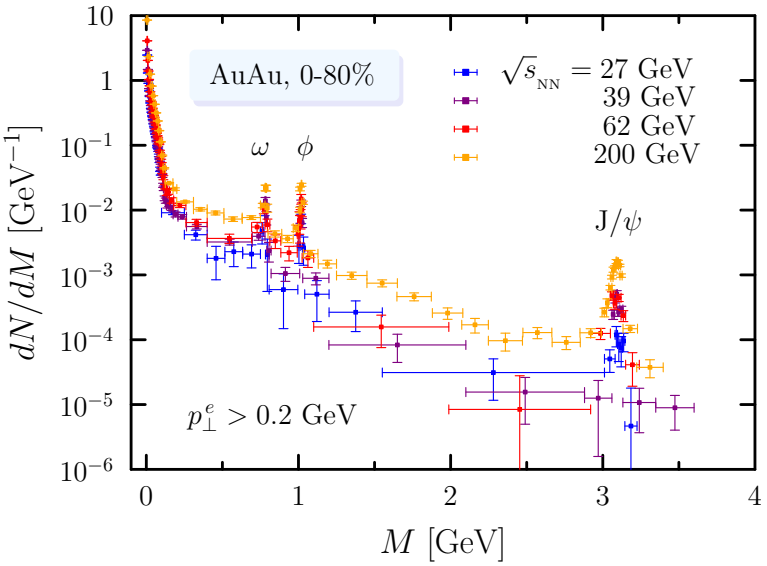

Figure 3: Several dielectron spectra measured by the STAR detector for AuAu collisions in a 0-80% centrality class at mid-rapidity $|y_{ee}| < 1$ [37, 38]. Electrons with pseudo-rapidity $|\eta^e| > 1$ and transverse momenta below $p_\perp^e < 0.2$ GeV are excluded. We indicate the peaks from narrow ω, ϕ and J/ψ resonances. Decays from $\pi^0 \to \gamma + e^- + e^+$ dominate for $M \lesssim \frac{1}{10}$ GeV.

We will consider the emission rates of *electromagnetic* probes by a fully equilibrated, QCD plasma at zero chemical potential. If $f_\gamma(\omega, \boldsymbol{k})$ denotes the phase space density of (possibly virtual) photons, then the evolution in time is [39]

$$\dot{f}_\gamma \;=\; \Gamma_{\rm e}(\omega, \boldsymbol{k})\,[1 + f_\gamma] \,-\, \Gamma_{\rm a}(\omega, \boldsymbol{k})\, f_\gamma \,, \tag{2.1}$$

where $\Gamma_{\rm e}$ is the spontaneous emission rate and $\Gamma_{\rm a}$ is the absorption rate. The two rates satisfy detailed balance: $\Gamma_{\rm a}/\Gamma_{\rm e} = e^{\omega/T}$, so that $f_\gamma = n_{\rm B}(\omega)$ is a fixed-point. Assuming that the QGP is optically thin, $f_\gamma \ll n_{\rm B}$, the right-hand side of (2.1) can be approximated by $\Gamma_{\rm e}$. This quantity may be used to calculate the production rates per unit volume, $\mathcal{R}_\gamma$ (real photons) and $\mathcal{R}_{l\bar{l}}$ (dileptons), by integrating $\dot{f}_\gamma$ over all momenta. Using the dilepton rate as an example, see Fig. 3, the invariant mass $M = \sqrt{|\omega^2 - k^2|}$ originates from the decay of an off-shell photon with $M \geq 2m_l$. For hydrodynamic simulations of heavy ion collisions,

the 'fireball' is characterised by local parameters like the temperature $T(t,\boldsymbol{x})$ and the flow velocity $u_\mu(t,\boldsymbol{x})$. The net yield is obtained by integrating over the full spacetime evolution of the system, see Fig. 4. Hyperbolic coordinates are the most natural to use, since detectors measure transverse momentum $k_\perp = p_\perp^l + p_\perp^{\bar{l}}$ and rapidity y (which may also have acceptance limits), and read

$$k(M,k_\perp,y) = \sqrt{M^2\,\mathrm{sh}^2 y + k_\perp^2\,\mathrm{ch}^2 y}\ , \qquad \omega(M,k_\perp,y) = \sqrt{M^2+k_\perp^2}\ \mathrm{ch}\, y\ .$$

The number of dileptons events is then given by the convolution:

$$\frac{dN}{dM^2\,dy} \ \propto\ \int d^4X \int_0^\infty dk_\perp \cdot k_\perp \,\frac{d\mathcal{R}_{l\bar{l}}}{d\omega d^3k}\big(M^2,k_\perp,y;\,T,u_\mu,\ldots\big)\,. \tag{2.2}$$

Isolating the thermal component is very difficult in practice due to both transport properties of the medium [40] and the many off-equilibrium sources [41]. We shall not discuss the phenomenology any further here, instead turning to the status of predictions for the rate.

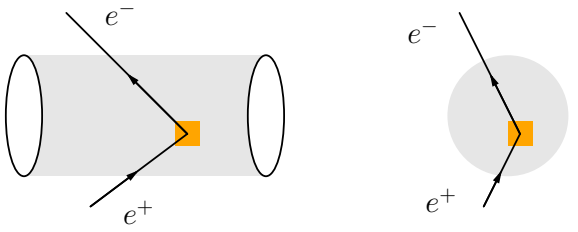

Figure 4: Longitudinal expansion of a central heavy ion collision, with a dielectron pair produced from the orange cell in the wake (shaded) of two nuclei. Sideways and transverse views are shown for the same 'event', $\gamma^\star \to e^+e^-$.

The theoretical evaluation of Γ_{e} in (2.1) has a long history, and was regarded as settled in the early 1990s when Kapusta *et al.* [42] and Baier *et al.* [43] independently arrived at the same answer for real photons. Dileptons, with $k=0$, had also been considered in the years shortly before by several authors [44–46], who concluded that radiative corrections were minor (for $\omega = M \sim T$). The leading-order (LO) rate of 'soft' photons, those with $M \ll T$, turned out to be greatly enhanced by screening effects for $k=0$ [47] and $k>0$ [48, 49]. It was later discovered that the treatment of real photons was incomplete and additional processes were incorporated by Arnold, Moore and Yaffe (AMY) [50, 51]. The same issue was addressed for soft dileptons in Ref. [52]. More recently, the accuracy of both the real photon and dilepton rates have been pushed to next-to-leading order (NLO) [53–56].

In QCD, the value of the coupling $\alpha_{\mathrm{s}} \sim \frac{1}{3}$ (for $T \gtrsim T_c$) invites suspicion on the predictive power of perturbation theory. Although the magnitude of NLO corrections goes a long way in quantifying the convergence of (truncated) *asymptotic series*, it is highly desirable to have non-perturbative information. There are different methods for the low temperature phase ($T \lesssim T_c$), to calculate rates from a hot hadronic gas [57]. Low-density expansions and chiral symmetry also provide constraints for the rate [58, 59], but there remain issues for including the baryons[8]. Emission rates for photons (both real and virtual) are given via the vector channel spectral function $\rho_{\mu\nu}$, defined below in Eq. (3.2), an object that can ultimately be reconstructed by analytic continuation of lattice data [61]. Despite significant hurdles with the ensuing systematic uncertainties [62], lattice studies have been undertaken for $k=0$ [63–65] and $k>0$ [66–68].

[8] Contemporary hydrodynamic simulations simply multiply the mesonic contribution by a factor 2 [60].

3. Minkowski to Euclidean variables

The photo-emission rate of a QGP can be derived from the (contracted) spectral function $\rho_\mu{}^\mu$, for the photon self-energy [69–71]. That quantity incorporates longitudinal and transverse polarisations of the virtual photon, with energy ω and momentum $\boldsymbol{k}$ (in the rest frame of the heat bath). We consider an equilibrium $SU(N)$-plasma with n_f massless quarks that carry electromagnetic charge. The vector current for the latter is defined by $j_\mu = e\bar{q}\gamma_\mu q$ where the coupling e is assumed much smaller than that of the non-Abelian interactions (denoted by $g_{\rm s}$). In the imaginary time formalism,

$$\Pi_{\mu\nu}(K) \;=\; -\int_0^{1/T} d\tau \int d^3\boldsymbol{x}\; e^{iKX} \left\langle\, j_\mu(X) j_\nu(0) \,\right\rangle , \tag{3.1}$$

where $\langle\cdots\rangle$ denotes the thermal average and $x_0 = i\tau$ [35]. The external energy takes on discrete Euclidean values at bosonic Matsubara frequencies $k_{\rm E}^0 = \pi j T$ (j is even). For real energies ω, the spectral function is then given by analytically continuing

$$\rho_{\mu\nu}(\omega) \;=\; {\rm Im}\big[\, \Pi_{\mu\nu}(K_{\rm E}) \,\big]_{ik_{\rm E}^0 \to (\omega + i0^+)} . \tag{3.2}$$

Because of the Ward identity, $\Pi^{\mu\nu}$ is proportional to $(K^2 g^{\mu\nu} - K^\mu K^\nu)$ at zero temperature, implying that the spectral functions for the two polarisations coincide. Let us briefly elaborate: At finite temperature $\rho_{\mu\nu}$ can be given in terms of two scalar functions, corresponding to the longitudinal and transverse polarisations,

$$\rho_{\rm L} \;=\; -\frac{K^2}{\boldsymbol{k}^2}\,\rho_{00} \;, \qquad \rho_{\rm T} \;=\; \frac{1}{d-1}\Big(\rho_\mu{}^\mu + \frac{K^2}{\boldsymbol{k}^2}\,\rho_{00} \Big) , \tag{3.3}$$

where $d = 3 - 2\epsilon$ is the number of spatial dimensions. (Since both $\rho_\mu{}^\mu$ and ρ_{00} are ultraviolet finite, one may actually set $d = 3$ above.) We introduce the useful combinations[9]

$$\rho_\Delta \;\coloneqq\; \rho_{\rm T} - \rho_{\rm L} \;, \qquad \rho_{\rm V} \;\coloneqq\; \rho_{\rm L} + (d-1)\rho_{\rm T} \;, \tag{3.4}$$

and will discuss ρ_i for $i \in \{\,{\rm L}, {\rm T}, \Delta, {\rm V}\,\}$, any two of which are sufficient to specify the full spectral function. The physical rate is proportional to $\rho_{\rm V}$ while ρ_Δ is purely thermal; at zero temperature it is identically zero.

Truncating the perturbative result for the correlator (an even function of $g_{\rm s}$) to order e^2 in the electromagnetic interactions, we denote by $\Pi_{(l)}$ the ensuing contribution from $g_{\rm s}^{2l}$ in the strong coupling expansion (cf. Ref. [72]). Naively, the series then takes the form

$$\Pi^{\mu\nu} \;=\; e^2 \Big[\, \textstyle\sum_{l=0}^{\infty} g_{\rm s}^{2l}\, \Pi_{(l)}^{\mu\nu} \,\Big] \;+\; \mathcal{O}(e^4) , \tag{3.5}$$

with a supposed ordering by powers of $g_{\rm s}^2$. For an ordinary loop expansion, the 'coefficients' of $g_{\rm s}^{2l}$ are themselves functions of ω and k but independent of $g_{\rm s}$. However their dependence on the external momentum K can (and does) spoil this power counting, e. g. when $|K^2| \lesssim g_{\rm s}^2 T^2$. This issue reveals itself explicitly in [the group factor $c_F = (N^2-1)/(2N)$]

$$\rho_{\rm V} \;\simeq\; e^2 g_{\rm s}^2\, T^2\, \frac{N c_F}{16\pi} \Big[\, 1 - 2\, n_{\rm F}(\omega) \,\Big] \log \frac{T^2}{K^2} \tag{3.6}$$

for $K^2 \ll T^2$ [44–46]. In the case of high-energy real photons (meaning $\omega = k \gg T$), it is *obligatory* to account for thermal screening to render the logarithm in Eq. (3.6) finite [42,43]. This is done by resumming 'hard thermal loops' (HTLs) [73].

[9] In Ref. [3], we used $\rho_{\rm H} = 2\rho_\Delta$ which coincides with $\rho_{\rm V}$ on the light cone for $d = 3$.

Due to its relation with the imaginary-time correlator G [74], lattice calculations could provide constraints on the photon spectral function. The former (which is 'measured' in lattice simulations) is given by an integral over all positive energies ω:

$$G_{\mu\nu}(\tau,\boldsymbol{k})\,/\,T^3 \;=\; \int_0^\infty \frac{d\omega}{2\pi T}\,\frac{\rho_{\mu\nu}(\omega,\boldsymbol{k})}{\omega\,T}\,\mathcal{F}(\omega,\tau)\,. \tag{3.7}$$

We have divided the spectral function by ωT as it will be more natural when considering the $\omega \to 0$ limit. The integration kernel is

$$\mathcal{F} \;:=\; \frac{\omega\,\mathrm{ch}\big[(\frac{1}{2}\beta-\tau)\omega\big]}{T\,\mathrm{sh}\big(\frac{1}{2}\beta\omega\big)}\,, \tag{3.8}$$

where $\beta = 1/T$ is the inverse temperature. One can view (3.7) as a collection of 'sum rules' for the spectral function [3]. Evidently G depends on ρ above, below and in the vicinity of the light cone. In contrast, the *observable* photon and dilepton rates depend on ρ for $K^2 = 0$ and $K^2 \geq 4m_l^2$ respectively, where the perturbative studies have hitherto been focused[10]. The complementary region, $K^2 < 0$, would be pertinent to the (hypothetical) deep inelastic scattering of leptons off a heat bath of quarks and gluons.

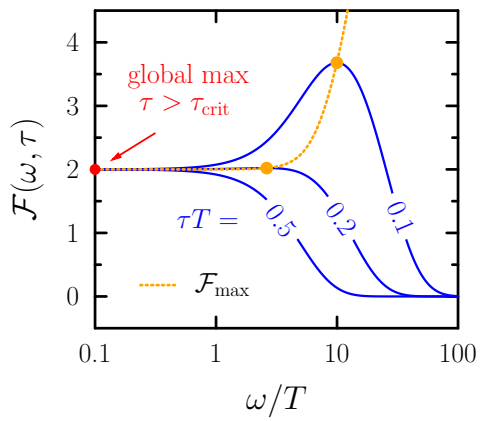

Figure 5: The natural kernel of the integral transform in (3.7), as a function of the frequency, ω, in units of the temperature. Shown here are the cases $\tau T = \{0.1, 0.2, 0.5\}$, which demonstrates the emergence of a peak at positive ω, for $\tau < \tau_{\rm crit}$ [the value of $\tau_{\rm crit}$ is given in Eq. (3.9)]. The maximum moves out as τ shrinks, implying that the imaginary time correlator becomes more sensitive to the asymptotic behaviour of $\rho_{\mu\nu}$, despite the eventual exponential decay of $\mathcal{F}$.

Formally, the inversion of (3.7) with only a finite number of sampling points is an *ill-posed* problem. The kernel of the integral transform (a Fredholm equation of the first kind), depicted in Fig. 5, has several important features. We note that $\mathcal{F}_{\rm max} = 2$ for τ exceeding the critical value

$$\tau_{\rm crit} \;=\; \frac{1}{2T}\Big(1-\frac{1}{\sqrt{3}}\Big) \;\approx\; \frac{0.211325}{T}\,. \tag{3.9}$$

For $\tau < \tau_{\rm crit}$ the extremal value of $\mathcal{F}(\omega)$ bifurcates: $\mathcal{F}(0) = 2$ becomes a local minimum, and the maximum shifts to positive frequencies. Asymptotically, as $\tau \to 0$, the global maximum shifts to $\omega \sim 1/\tau$ with $\mathcal{F}_{\rm max} \sim 1/(\tau T)$. The strength of this maximum gives the integrand in (3.7) substantial weight there, but the eventual exponential decay $\mathcal{F} \to e^{-\omega/T}$ still overrides this beyond the peak.

Many existing approaches use a maximum likelihood estimator to reconstruct $\rho(\omega,\boldsymbol{k})$ as a continuous function [61]. But a subtlety arises in the large ω limit of $\rho_\mu{}^\mu$, which gives a divergence in $G_{\mu\nu}$ for $\tau \simeq 0$ that spoils the analytic continuation [75, 76]. To remedy

[10] Including the special case $m_l \to 0$.

this issue, it has been suggested to rather use (3.7) with a particular linear combination of transverse and longitudinal spectral functions bereft of ultraviolet 'contamination' [67]. The spectral function ρ_Δ defined in (3.4) is a good candidate, because it is both entirely thermal and finite for large frequencies. Moreover, the first term in an operator product expansion (OPE) is $\sim k^2T^4/K^4$, making ρ_Δ highly suppressed in the ultraviolet [77].

Consequences of the operator product expansion

Around the same time that AMY identified a class of higher-order diagrams that ought to be included for the LO (real) photon rate, a dispute arose about the nature of *infrared* divergences in loop integrals for virtual photons. A residual cut-off sensitivity was found in Refs. [78, 79] that had not been observed prior. This is usually forbidden, at zero-temperature, by the Kinoshita-Lee-Nauenberg (KLN) theorem [80, 81]. The result was called into question by the authors of earlier works, wherein the cut-off parameter did not remain [82]. A slightly different calculation seemed to suggest that the KLN theorem was respected at finite-T [83], but the contention remained [84].

The verdict came from Caron-Huot, who approached $\rho_{\mu\nu}$ using OPE techniques and (on very general grounds) ruled out the presence of lingering infrared divergences [77]. In the OPE formalism, spectral functions are constructed from the admissible operators at time-like separations much smaller than the typical wavelength of the plasma $\sim T^{-1}$. The 'vector-vector correlator' is precisely the same spectral function that is needed for the photon rate. The expansions[11] for large $K^2 = \omega^2 - k^2$ are

$$\begin{aligned} \mathrm{Im}\big[\, g_{\mu\nu}\Pi^{\mu\nu}_{(1)}\,\big] &= 4Nc_F\Big\{\,\frac{3K^2}{4(4\pi)^3} - \int_{\boldsymbol{p}}\frac{p}{\pi}\frac{(n_{\mathrm{B}}-4\,n_{\mathrm{F}})}{3\,K^4}\Big(\omega^2+\frac{k^2}{3}\Big)\,\Big\} + \ldots\,, \\ \mathrm{Im}\big[\,\Pi^{00}_{(1)}\,\big] &= -4Nc_F\Big\{\,\frac{k^2}{4(4\pi)^3} - \int_{\boldsymbol{p}}\frac{p}{\pi}\frac{(n_{\mathrm{B}}-4\,n_{\mathrm{F}})k^2}{9\,K^4}\,\Big\} + \ldots\,. \end{aligned} \tag{3.10}$$

Distribution functions are evaluated at $p = |\boldsymbol{p}|$. The leading term in each channel is the vacuum result and is $3c_F/(4\pi)^2$ times $\Pi_{(0)}$ for $T \to 0$ [see ahead to Eq. (4.2)]. Thermal corrections would start at $\mathcal{O}(T^2)$, but this term is absent – a prediction of the OPE method. Using known integrals of the distribution functions, namely $\int_{\boldsymbol{p}} p\, n_{\mathrm{B}} = \pi^2T^4/30$ and $\int_{\boldsymbol{p}} p\, n_{\mathrm{F}} = 7\pi^2T^4/240$, one finds that for (3.4)

$$\rho_\Delta \;=\; g^2c_FN\,\frac{2\pi\,k^2T^4}{27\,K^4} \;+\; \mathcal{O}\Big(\frac{T^6}{K^4}\Big)\,. \tag{3.11}$$

The OPE limit thus implies that ρ_Δ approaches zero from above and respects the general requirement that the whole spectral function should vanish for $k = 0$.

A less obvious consequence of Eq. (3.11) follows by analytic continuation. Consider Fourier transforming the imaginary time correlator for ρ_Δ from (3.7), and regard it for 'large' Euclidean energy $k_0 = ik^0_{\mathrm{E}}$. Since

$$\int_0^{1/T} d\tau\, e^{k_0\tau}\,\mathcal{F}(\omega,\tau) \;=\; \frac{2\omega^2}{T(\omega^2-k_0^2)} \;=\; -2\frac{\omega^2}{T\,k_0^2} \;+\; \mathcal{O}\Big(\frac{\omega^4}{T\,k_0^4}\Big)\,, \tag{3.12}$$

and G_Δ cannot contain a term proportional to k_0^{-2}, we arrive at the sum rule

$$\int_0^\infty d\omega\,\omega\,\rho_\Delta(\omega,\boldsymbol{k}) \;=\; 0\,. \tag{3.13}$$

[11] See Ref. [2] for a direct way of obtaining the expansions for $M^2 \gg T^2$. The assumption $\omega \gg T, k$, considered by Ref. [77], is a somewhat stricter limit and is included as a special case of (3.10).

Together with the approach to zero, this constraint means that ρ_{Δ} must be positive at some point and there is at least one frequency $\omega^* > 0$ such that $\rho_{\Delta}(\omega^*, \boldsymbol{k}) = 0$. Sum rules for other spectral functions, seem to be of limited practical use [85, 86].

It would be profitable to use Eq. (3.7) as a means to verify perturbative approaches to $\rho_{\mu\nu}$. But, in aspiring to use the integral transform, we require the spectral function for all ω (given $\boldsymbol{k}$). The calculation must be split into two main parts: Photons having *i*) moderate invariant mass $M^2 \sim T^2$, and *ii*) low invariant mass $M^2 \ll T^2$. These two regimes must be treated differently. In *i*) we may directly compute the 2-loop corrections, whereas *ii*) involves summing a whole class of relevant topologies to recover the correct parametric dependence on g_{s}. The latter hence includes some of the former, under the assumption of small M^2 [87]. To avoid double counting in the combined result, we need to identify the overlap and subtract it.

4. Perturbation theory: $M^2 \sim T^2$

The first term in (3.5), for which $l = 0$, represents the leading order (LO) result. Resolving the two polarisations in terms of $\Pi_{\mu}^{\ \mu}$ and Π_{00}, we have

$$\begin{aligned} g_{\mu\nu}\Pi^{\mu\nu}_{(0)} &= 4(d-1)N \oint\!\!\!\!\!\!\sum_{P} (PL)\widetilde{\Delta}_P\widetilde{\Delta}_L\,, \\ \Pi^{00}_{(0)} &= -4N \oint\!\!\!\!\!\!\sum_{P} (p_0\ell_0 + \boldsymbol{p}\boldsymbol{\ell})\widetilde{\Delta}_P\widetilde{\Delta}_L\;; \quad L = K - P\,. \end{aligned} \tag{4.1}$$

Here $\Delta_P \equiv 1/P^2$ and the tilde just indicates that the sum-integral is over fermionic modes,[12] *viz.* $p_0 = i(2n+1)\pi T$ for integers n. A particular case where analytic expressions can be found, obtainable by assuming $\omega, k \ll T$, is the HTL limit ($c = \omega/k$ is the velocity)

$$g_{\mu\nu}\Pi^{\mu\nu}_{(0)}\,\big|_{\mathrm{HTL}} = N\frac{T^2}{3}\,, \qquad \Pi^{00}_{(0)}\,\big|_{\mathrm{HTL}} = N\frac{T^2}{6}\Big(2 - c\log\frac{c+1}{c-1}\Big)\,.$$

However, of course, this is not applicable for $K^2 \sim T^2$. Both the real and imaginary parts of (4.1) are known without the HTL assumption [88]. We are interested in the imaginary parts because they give the spectral function:

$$\begin{aligned} \mathrm{Im}\big[\, g_{\mu\nu}\Pi^{\mu\nu}_{(0)}\,\big] &= K^2\frac{N}{4\pi}\ \Big\{\quad \Theta(k_-) + 2\frac{T}{k}\log\frac{1+e^{-\beta k_+}}{1+e^{-\beta|k_-|}}\ \Big\}\,, \\ \mathrm{Im}\big[\, \Pi^{00}_{(0)}\,\big] &= -k^2\frac{N}{4\pi}\ \Big\{\ \frac{1}{3}\Theta(k_-) + 4\frac{T^2}{k^2}\Big(\mathrm{Li}_2\big(-e^{-\beta k_+}\big) + \mathrm{sgn}(k_-)\mathrm{Li}_2\big(-e^{-\beta|k_-|}\big)\Big) \\ &\qquad + 8\frac{T^3}{k^3}\Big(\mathrm{Li}_3(-e^{-\beta k_+}) - \mathrm{Li}_3(-e^{-\beta|k_-|})\Big)\ \Big\}\,. \end{aligned} \tag{4.2}$$

Here Li_2 and Li_3 are the second and third order polylogarithms respectively. We abbreviated the light cone momenta $k_{\pm} = \frac{1}{2}(\omega \pm k)$ and Θ is the Heaviside step function. Note that the formulae in (4.2) hold above and below the light cone. The vanishing of $\mathrm{Im}\big[\, g_{\mu\nu}\Pi^{\mu\nu}_{(0)}\,\big]$ for $K^2 = 0$ reflects the fact that $q\bar{q} \to \gamma$ has no available phase space. One may show analytically (although it is rather tedious) that ρ_{Δ} obtained from the above LO expression does satisfy the sum rule Eq. (3.13), which ought to hold order by order.

[12] Performing frequency sums over two variables is outlined in the appendices of Ref. [73]. We will not repeat that discussion here, but simply make use of the final expressions [2].

In the limit $k \to 0$, it is possible to use (3.7) to obtain an analytic expression[13] for the imaginary-time correlation function. Importantly, the large frequency behaviour of (4.2) is quadratic. Hence, replacing $\mathcal{F} \to e^{-\omega\tau}$ in (3.7), would give $\int_0^\infty d\omega\, \omega^2 e^{-\omega\tau} = \frac{2}{\tau^3}$. This singularity for small τ is entirely due to the vacuum contributions to $\Pi_{\mu\nu}$. This was the issue referred to earlier, and does not occur for ρ_Δ because it is exclusively thermal.

The QCD corrections start with $\Pi^{\mu\nu}_{(1)}$, termed the next-to-leading order (NLO) result and derivable from the diagrams in Fig. 6. (A diagram containing a piece like  , automatically vanishes due to colour conservation.) The loop momenta are abbreviated by

$$L \;=\; K - P\,; \quad V \;=\; K - Q\,; \quad R \;=\; K - P - Q\,. \tag{4.3}$$

It is possible to to write the NLO expression for the self-energy like in Eqs. (4.1), which is gauge invariant and somewhat compact. $\Pi_\mu^{\ \mu}$ can be cast into the form

$$\begin{aligned} g_{\mu\nu}\Pi^{\mu\nu}_{(1)} \;=\; &- \; 4\,d\,N c_F \oint\!\!\!\!\!\!\int_{P,Q} \Big[\; 2d\big(\,L^2(PQ) - 2(LP)(LQ)\,\big)\;\widetilde{\Delta}_L \\ &+ \; \Big\{\,(d-6)(LV)(QP) - (d-2)\big(\,(LP)(VQ) + (LQ)(VP)\,\big)\Big\}\;\widetilde{\Delta}_V\;\Big] \\ &\times \; \widetilde{\Delta}_P\;\widetilde{\Delta}_Q\;\Delta_R\;\widetilde{\Delta}_L\;, \end{aligned} \tag{4.4}$$

and the counterpart, also with the shorthand in (4.3), for Π^{00} reads

$$\begin{aligned} \Pi^{00}_{(1)} \;=\; &- \; 4N c_F \oint\!\!\!\!\!\!\int_{P,Q} \Big[\; 2\,d\big(\,L^2(p_0q_0 + \boldsymbol{pq}) - 2(p_0\ell_0 + \boldsymbol{p\ell})\,LQ\,\big)\;\widetilde{\Delta}_L \\ &+ \; \Big\{\,(d-4)\big(\,(LQ)(PV) - (LV)(PQ)\,\big) + 2(d-2)\big(\,p_0q_0\,LV + \ell_0v_0\,PQ\,\big) \\ &+ \; 4\big(\,\ell_0q_0\,PV + p_0v_0\,LQ\,\big) + d\big(\,(QV)(LP) - 2\ell_0p_0\,QV - 2q_0v_0\,LP\,\big)\Big\}\;\widetilde{\Delta}_V\;\Big] \\ &\times \; \widetilde{\Delta}_P\;\widetilde{\Delta}_Q\;\Delta_R\;\widetilde{\Delta}_L\;. \end{aligned} \tag{4.5}$$

However, instead of using these representations directly, we will show how they may be broken up into a (larger) set of 'master integrals' that are individually simpler. Moreover, only the imaginary parts of these masters are of interest to us – not the entire self-energy given above. We defer to Refs. [2, 53] for their properties and (numerical) evaluation.

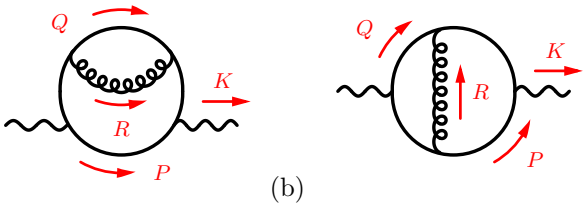

Figure 6: The $O(\alpha_{\rm em}\alpha_{\rm s})$ corrections to $\Pi_{\mu\nu}$ are depicted in (a) and (b). Flow of momentum is shown by red arrows, see the labelling in Eq. (4.3) which satisfies $Q + P + R = K$.

[13] At LO and $k = 0$, the imaginary-time correlator reads

$$G_{\rm V}(\tau,0) \;=\; e^2 6T^3\Big[\,(\pi-\vartheta)\frac{1+\cos^2\vartheta}{\sin^3\vartheta} + 2\frac{\cos\vartheta}{\sin^2\vartheta}\,\Big]\,; \qquad \vartheta = 2\pi\tau\,.$$

For non-zero momentum, and even for $G_\Delta(\tau,0)$, there is no closed form. However, the integrals are quite simple to evaluate numerically and we shall use them to judge how significant the NLO corrections are.

Before discussing the master integrals, let us pause to consider the physical content of Eqs. (4.4) and (4.5). The 2-loop topologies each generate several cuts, yielding partial amplitudes for processes like $q\bar{q} \to g\gamma^*$ and $q\bar{q}g \to \gamma^*$ (so called 'real' corrections[14]), but also α_s corrections to the leading order $q\bar{q} \to \gamma^*$ (so called 'virtual' corrections) [89]. To understand this better, consider a cut of Fig. 6 (a) or (b) having momenta P, Q and R all on-shell. The amplitude may develope a singularity from the internal propagator if

$$(K-P)^2 \;=\; K^2 - 2p\big(\,\omega - k\cos\theta_{kp}\,\big) \;\approx\; 0\,, \tag{4.6}$$

where θ_{kp} is the angle between $\boldsymbol{k}$ and $\boldsymbol{p}$. The conditions for some θ_{kp} to satisfy Eq. (4.6) are inferred according to the sign of K^2: If $K^2 \geq 0$ then p must be in the interval $I = [k_-, k_+]$ ($k_\pm$ are the light cone momenta). While if $K^2 < 0$, (4.6) can be satisfied if and only if p is in the complementary region $I^c = \mathbb{R}\backslash I$.

As a consequence of Eq. (4.6),

$$(R+Q)^2 \;=\; 2rq(1-\cos\theta_{rq}) \;\approx\; 0$$

so that the momenta $\boldsymbol{q}$ and $\boldsymbol{r}$ are collinear. Such configurations only make sense when $\boldsymbol{q}$ and $\boldsymbol{r}$ are identified to the same 'observable'. This means that the cut considered should be combined with the amplitude where Q and R are virtual but their sum is on-shell. In that case $(K-P)^2 = (Q+R)^2 = 0$, so that the phase space coincides with where (4.6) can be fulfilled. This was all demonstrated explicitly in Ref. [2].

Let us now derive the (scalar) master integrals for the two diagrams in Fig. 6. The contribution from the first topology (a) is

$$\Pi^{(\mathrm{a})}_{\mu\nu} = g_s^2 e^2 N c_F \int\!\!\!\!\!\!\diagup_{P,Q} n^{(\mathrm{a})}_{\mu\nu}\; \widetilde{\Delta}_P\, \widetilde{\Delta}_L^2\, \Delta_R\, \widetilde{\Delta}_Q\;. \tag{4.7}$$

The fermion traces go into the 'numerator' $n^{(\mathrm{a})}$, which is defined by

$$n^{(\mathrm{a})}_{\mu\nu} \;=\; -\,\mathrm{tr}[\gamma_\mu \not{P} \gamma_\nu \not{L} \gamma_\alpha \not{Q} \gamma_\beta \not{L}]\Big(\, g^{\alpha\beta} - (1-\xi)\frac{R^\alpha R^\beta}{R^2}\,\Big)\,.$$

This (gauge dependent) diagram is clearly associated with an insertion of the 1-loop quark self-energy. The other topology in Fig. 6, associated with the correction to the photon-quark vertex, is

$$\Pi^{(\mathrm{b})}_{\mu\nu} = g_s^2 e^2 N c_F \int\!\!\!\!\!\!\diagup_{P,Q} n^{(\mathrm{b})}_{\mu\nu}\; \widetilde{\Delta}_P\, \widetilde{\Delta}_Q\, \Delta_R \widetilde{\Delta}_L\, \widetilde{\Delta}_V\;. \tag{4.8}$$

The numerator reads

$$n^{(\mathrm{b})}_{\mu\nu} \;=\; \mathrm{tr}[\,\gamma_\mu \not{P} \gamma_\alpha \not{V} \gamma_\nu \not{Q} \gamma_\beta \not{L}\,]\Big(\, g^{\alpha\beta} - (1-\xi)\frac{R^\alpha R^\beta}{R^2}\,\Big)\,.$$

Decomposition into master integrals: $\Pi_\mu^{\ \mu}$ and Π_{00}

We use $\gamma_\rho \not{Q} \gamma^\rho = (1-d)\not{Q}$ and then express $n_\mu^{\ \mu}$ in terms of four-products between the momenta. In $d = 3-2\epsilon$ dimensions, we find (for $\xi \to 1$ since the final result can be shown to be ξ-independent, although we do not it prove here)

$$\begin{aligned} g^{\mu\nu} n^{(\mathrm{a})}_{\mu\nu} \;&=\; 4(d-1)^2\big(\, L^2(PQ) - 2(LP)(LQ)\,\big) \\ &=\; 2(d-1)^2\big(\, 2L^2(KQ) - (K^2-P^2)(L^2+Q^2-R^2)\,\big)\,, \end{aligned} \tag{4.9}$$

[14] If $\omega < k$, three-body decays such as $g \to q\bar{q}\gamma^*$ are present and counted among the real corrections.

The second line was obtained by expressing $PQ = KQ - LQ$ and then using

$$LP = \tfrac{1}{2}(K^2 - P^2 - L^2)\,, \qquad LQ = \tfrac{1}{2}(L^2 + Q^2 - R^2)\,.$$

Putting this together with the other factors in (4.7), and writing out the scalar propagators explicitly ($\widetilde{\Delta}_Q = 1/Q^2$, etc.) we have

$$\begin{aligned}\Pi^{(\mathrm{a})\,\mu}_{\ \mu} \;=\; 2\,g_{\mathrm{s}}^2 e^2 (d-1)^2 \Big\{ \int\!\!\!\!\!\!\diagup_{L,R} \Big[\frac{1}{L^4\,R^2} \;-\; \frac{K^2}{L^4\,R^2\,P^2} \Big] \\ +\; \int\!\!\!\!\!\!\diagup_{L,Q} \Big[\frac{1}{L^2\,Q^2\,R^2} \;-\; \frac{1}{L^4\,Q^2} \;+\; \frac{K^2}{L^4\,Q^2\,P^2} \Big] \;+\; \int\!\!\!\!\!\!\diagup_{P,Q} \Big[\frac{K(2Q-K)}{P^2\,Q^2\,L^2\,R^2} \Big] \Big\}\,.\end{aligned} \tag{4.10}$$

The original labelling of Fig. 6 has been kept, although it is possible to rename integration variables provided the statistical nature is respected. (R is bosonic, the rest are fermionic.)

Next up is the numerator in (b). To simplify this trace, we shall use

$$\gamma_\alpha \not{L} \gamma_\mu \not{P} \gamma^\alpha = (d-5)\not{P}\gamma_\mu\not{L} - 2(d-3)\big(L_\mu \not{P} + \not{L} P_\mu - (LP)\gamma_\mu \big)\,.$$

Then

$$\begin{aligned} g^{\mu\nu} n^{(\mathrm{b})}_{\mu\nu} \;&=\; (d-5)\mathrm{tr}[\gamma_\mu \not{Q}\not{P}\gamma^\mu \not{L}\not{V}\,] \\ &-\; 2(d-3)\Big(\mathrm{tr}[\not{L}\not{Q}\not{P}\not{V}\,] + \mathrm{tr}[\not{P}\not{Q}\not{L}\not{V}\,] - LP\,\mathrm{tr}[\gamma_\mu \not{Q}\gamma^\mu \not{V}\,] \Big)\,. \end{aligned} \tag{4.11}$$

These traces can be decomposed into combinations of products between the quark momenta P, Q, L and V (as usual). Because each momentum appears once in the product, it should be possible to express (4.11) as a linear combination of the three ways to form two four products between them.

The first trace in (4.11) can be simplified with ordinary techniques to give

$$\mathrm{tr}[\gamma_\mu \not{Q}\not{P}\gamma^\mu \not{L}\not{V}\,] = 4(d+1)(LV)(QP) + 4(d-3)\big((LP)(VQ) - (LQ)(VP) \big)\,.$$

In $d = 3$ dimensions, this is not necessarily the only contribution; the second line of (4.11) will be non-zero if a divergence can offset the small prefactor. Let us err on the side of caution and calculate the other traces. The last trace in (4.11) above is the simplest – it is

$$\mathrm{tr}[\gamma_\mu \not{Q}\gamma^\mu \not{V}\,] = -4(d-1)(VQ)\,.$$

The remaining traces in (4.11) are the same, by cyclicity. They are both equal to

$$\mathrm{tr}[\not{L}\not{Q}\not{P}\not{V}\,] \;=\; \mathrm{tr}[\not{P}\not{Q}\not{L}\not{V}\,] \;=\; 4\big((LV)(QP) + (LQ))(VP) - (LP)(VQ) \big)\,.$$

Putting these together, we find

$$g^{\mu\nu} n^{(\mathrm{b})}_{\mu\nu} \;=\; 4(d-1)\Big\{ (d-7)(LV)(QP) - (d-3)\big[(LP)(VQ) + (LQ)(VP) \big] \Big\}\,. \tag{4.12}$$

Each term can be recast into a form that depends only on the norms of the propagating momenta and $K^2 = \omega^2 - k^2$. Indeed 'completing the square' in each pair leads to the following multiplication table:

$$\begin{array}{lll|lll} LV &=& \tfrac{1}{2}(R^2 + K^2 - Q^2 - P^2) & PQ &=& \tfrac{1}{2}(R^2 + K^2 - L^2 - V^2) \\ PL &=& \tfrac{1}{2}(K^2 - P^2 - L^2) & QV &=& \tfrac{1}{2}(K^2 - Q^2 - V^2) \\ QL &=& \tfrac{1}{2}(L^2 + Q^2 - R^2) & PV &=& \tfrac{1}{2}(V^2 + P^2 - R^2) \end{array} \tag{4.13}$$

And hence that (4.12), after some massaging, is equal to

$$\begin{aligned} g^{\mu\nu} n^{(\mathrm{b})}_{\mu\nu} \;=\; & (d-1)\Big\{ 4(K^2+R^2)(P^2+Q^2+L^2+V^2) \;+\; (d-7)(P^2+Q^2)(L^2+V^2) \\ & -\,(d-3)\Big((P^2+L^2)(Q^2+V^2) + (P^2+V^2)(Q^2+L^2) \Big) \\ & +\,2(d-7)\,K^2R^2 \;-\; 4(K^4+R^4) \Big\}\,. \end{aligned} \tag{4.14}$$

To simplify these expressions when combining (4.14) with the propagators in (4.8), observe that the integration variables are symmetric under the simultaneous exchange of any two pairs from $\{P,Q,L,V\}$, e. g. $P \leftrightarrow Q$ and $L \leftrightarrow V$. For this reason, one *may* replace

$$(P^2+Q^2+L^2+V^2) \;\to\; 4V^2 \quad \text{and} \quad (L^2+V^2) \;\to\; 2V^2\,,$$

in the first line of (4.14). Similarly, we may replace the second line of (4.14) by $-2(d-3)V^2(P^2+Q^2+2L^2)$. We also find it convenient to replace $R^2 = (L-Q)^2 \;\to\; (2V^2) - \frac{1}{2}K^2$, but *only* once, and in the term $R^4 = R^2 \cdot R^2$.

Collecting everything back into (4.8), and changing some integration variables,

$$\begin{aligned} \Pi^{(\mathrm{b})\,\mu}_{\mu} \;=\; & 4\,g_{\mathrm{s}}^2 e^2 (d-1) \Big\{ \mathchoice{\int\!\!\!\!\!\!\int}{\int\!\!\!\!\!\!\int}{\int\!\!\int}{\int\!\!\int}_{P,Q} \Big[\frac{2}{P^2Q^2L^2} \;-\; \frac{d-3}{P^2Q^2R^2} \Big] \;-\; \mathchoice{\int\!\!\!\!\!\!\int}{\int\!\!\!\!\!\!\int}{\int\!\!\int}{\int\!\!\int}_{P,R} \frac{2}{P^2R^2L^2} \\ & -\; \mathchoice{\int\!\!\!\!\!\!\int}{\int\!\!\!\!\!\!\int}{\int\!\!\int}{\int\!\!\int}_{L,Q} \frac{2}{Q^2L^2R^2} \;+\; \mathchoice{\int\!\!\!\!\!\!\int}{\int\!\!\!\!\!\!\int}{\int\!\!\int}{\int\!\!\int}_{P,Q} \Big[\frac{4K^2}{P^2Q^2L^2R^2} \;+\; \frac{\frac{1}{2}(d-6)K^2}{P^2Q^2L^2V^2} \;-\; \frac{K^4}{P^2Q^2L^2V^2R^2} \Big] \Big\}\,. \end{aligned} \tag{4.15}$$

Again, the statistics of the propagating momenta are implied by their definitions above and are in accordance with Fig. 6. Because the self-energy in (a) can occur on either quark line, the full result is $2\,\Pi^{(\mathrm{a})}_{\mu\nu} + \Pi^{(\mathrm{b})}_{\mu\nu}$ which is evidently a linear combination of integrals.

Having now calculated the trace of the self-energy $\Pi_{\mathrm{V}} = \Pi_{\mu}^{\mu}$ at NLO, it will be sufficient to calculate any combination of polarisations that is independent from it. We will evaluate the time-time entry: Π_{00} (which is proportional to Π_{L}), again for the topologies in Fig. 6. Being guided by Eqs. (4.10) and (4.15), let us define a more generic class of 2-loop spectral functions.

We introduce the notation

$$\mathcal{I}^{(m,n)}_{abcde}(K) \;\equiv\; \mathchoice{\int\!\!\!\!\!\!\int}{\int\!\!\!\!\!\!\int}{\int\!\!\int}{\int\!\!\int}_{P,Q} p_0^m q_0^n\, \widetilde{\Delta}^a_P \widetilde{\Delta}^b_Q \Delta^c_R \widetilde{\Delta}^d_L \widetilde{\Delta}^e_V\,, \tag{4.16}$$

where the abbreviations from Eqs. (4.3) are used; L, V and R depend on P, Q and K. The imaginary parts of integrals of this type were studied in Ref. [2] and help to organise our evaluation of Eqs. (4.4) and (4.5). Introducing $m,n>0$ is necessary to deal with Π_{00} and is sufficient because we can always use identities like $\boldsymbol{pq} = p_0q_0 - PQ$ to favour powers of the energies. [Also note that KQ in (4.10) can be traded for a negative power of $\widetilde{\Delta}_V$.]

It quickly becomes convenient to reduce the photon self-energy to the integral basis, prescribed by (4.16), with the help of a symbolic manipulation system. There are many on the market, but here we use one called FORM [90]. Generating the master integrals using automatic code is less error prone, but we have also checked these results by hand. Listing 1 provides a module for proccessing the topologies in Fig. 6. The local variables may be further manipulated by procedures defined in Appendix A. Symmetries and other relations between the integrals $\mathcal{I}$ can be used to put a canonical ordering on the basis, so that we arrive at a representation which is 'minimal'. We also set $d = 3-2\epsilon$ and take the limit $\epsilon \to 0$.

```
symbol D, xi;
dimension D;
vectors k, p, q, r, l, v;
cfunction prop;
indices mu,nu,al,be;

local DiagA = (d_(al,be)+xi*r(al)*r(be)*prop(r))*
              g_(1,mu,-p,nu,l,al,q,be,l)*
              prop(p)*prop(q)*prop(r)*prop(l)^2;

local DiagB = (d_(al,be)+xi*r(al)*r(be)*prop(r))*
              g_(2,mu,-p,al,-v,nu,q,be,l)*
              prop(p)*prop(q)*prop(r)*prop(l)*prop(v);

local PI = 2*DiagA + DiagB;
.sort

drop DiagA, DiagB;
local PMN = d_(mu,nu)*PI;
local P00 = d_(0,mu)*d_(0,nu)*PI;
tracen,1;
tracen,2;
id prop(p?) = 1/p.p;
.sort
```

Listing 1: First two modules of code in the FORM language to carry out the Dirac algebra in calculating the 2-loop diagrams for $\Pi_\mu^{\ \mu}$ and Π_{00}. The variables `DiagA` and `DiagB` correspond to the explicit topologies in Eqs.(4.7) and (4.8) respectively and `xi` is used in place of $(1-\xi)$.

For the spectral function, defined via Eq. (3.2), we need the imaginary part of the master integrals: $\rho = \mathrm{Im}[\,\mathcal{I}\,]$. In this notation the relevant parts of the self-energy read (with $\epsilon \to 0$)

$$\begin{aligned}
\mathrm{Im}\big[\, g_{\mu\nu}\Pi^{\mu\nu}_{(1)}\,\big] \;&=\; && (4.17)\\
8(1-\epsilon)Nc_F\;&\Big\{\;\; 2(1-\epsilon)K^2\big(\rho^{(0,0)}_{11020}-\rho^{(0,0)}_{10120}\big)+2\rho^{(0,0)}_{11010}+2\epsilon\,\rho^{(0,0)}_{11100}\\
&\quad -\;\tfrac{1}{2}(3+2\epsilon)K^2\rho^{(0,0)}_{11011}-2(1-\epsilon)\rho^{(0,0)}_{1111(-1)}+4K^2\rho^{(0,0)}_{11110}-K^4\rho^{(0,0)}_{11111}\;\Big\}\,,\\
\mathrm{Im}\big[\,\Pi^{00}_{(1)}\,\big] \;&=\; && (4.18)\\
4Nc_F\;&\Big\{\;\; 2(1-\epsilon)\rho^{(0,0)}_{10110}+2\epsilon\rho^{(0,0)}_{11100}+(1+\epsilon)k^2\,\rho^{(0,0)}_{11011}-2(1-\epsilon)\rho^{(0,0)}_{1111(-1)}\\
&\quad +\;4\big[\,(1-2\epsilon)\omega^2-k^2\,\big]\rho^{(0,0)}_{11110}+8\epsilon\,\omega\,\rho^{(1,0)}_{11110}-8(1-\epsilon)\omega\,\rho^{(0,1)}_{11110}\\
&\quad +\;\big[\,(1-2\epsilon)\omega^2+k^2\,\big]K^2\rho^{(0,0)}_{11111}+4\epsilon\,K^2\,\rho^{(1,1)}_{11111}-4(1-\epsilon)K^2\,\rho^{(2,0)}_{11111}\;\Big\}\,.
\end{aligned}$$

Here we already took the liberty to drop any of the 'master' functions that are zero because they have no ω-dependence prior to taking the imaginary part, specifically

$$\rho^{(0,0)}_{01020}=\rho^{(0,0)}_{00120}=\rho^{(0,0)}_{01110}=0\;.$$

Other terms in (4.17) and (4.18) also fall away, in particular those proportional to ϵ without a compensating divergence in the master integral. It is important to keep some of these terms so that the vacuum result is recovered, but (for that reason) $\rho^{(0,0)}_{11100}$ and $\rho^{(1,1)}_{11111}$ end up not contributing at all. And we have used exact relations like[15]

$$K^2\rho^{(0,0)}_{11020} - 4\omega\rho^{(1,0)}_{11020} + 4\rho^{(2,0)}_{11020} \;=\; 0\,, \tag{4.19}$$

The masters $\rho^{(0,0)}_{11010}$ and $\rho^{(0,0)}_{1111(-1)}$ bear discontinuities across the light cone, see Ref. [2].

Figure 7 shows the energy dependence of the NLO spectral functions ρ_{T} and ρ_{L}, for several momenta. The transverse component ρ_{T} includes the prevailing log-divergence in (3.6), which is evidently fainter for small-k and disappears entirely for $k=0$. The factor of K^2 is enough to ensure that ρ_{L} is zero on the light cone. Both polarisations approaches zero for $\omega\to 0$, as expected on general grounds: $\Pi^*_{\mu\nu}(\omega,k)=\Pi_{\mu\nu}(\omega^\star,k)$ [91]. In Fig. 7 we also note that the $k=0$ limit the curve is compatible with $\Delta\rho=0$. Away from the light cone, the natural magnitude of $\rho^{\mu\nu}_{(1)}$ [in (3.5)] is considerably less than $\rho^{\mu\nu}_{(0)}$ which, at the very least, does not harm the perturbative expansion. The large ω behaviour is not shown here, but we have checked that Eq. (3.11) and the other OPE predictions[16] hold, see Ref. [2].

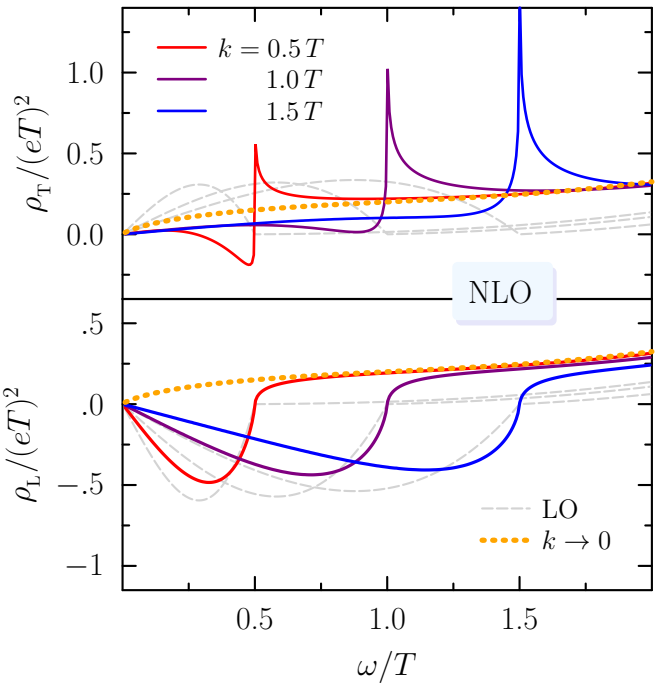

Figure 7: The two NLO spectral functions according to (4.4) and (4.5) are shown for $k/T=\{0.5,1,1.5\}$. We used $g_{\mathrm{s}}=3$ in the NLO result for visual purposes to enhance the QCD component. The dashed (gray) curves display the 'free' (or LO) limit [given in Eq. (4.2)]. Since $\rho_{\mathrm{T}}=\rho_{\mathrm{L}}$ for $k=0$, the dotted (orange) curves in the upper and lower panels are identical.

[15] This one follows from $K^2=4k_+k_-$ and the explicit integration of this factorisable topology in Refs. [2,53].
[16] The OPE expansions converge very slowly, and are only accurate for $\omega\gtrsim 30\,T$.

5. Perturbation theory: $M^2 \ll T^2$

In the previous section, we have seen that the spectral function develops a log-divergence, cf. Eq. (3.6), for $M^2 = |K^2| \to 0$ in the strict perturbative expansion. This singularity is unphysical since the (real) photon rate is a well-defined observable. Moreover, some universal arguments imply that the spectral function should be both finite *and* continuous across the light cone [92]. The central issue, and the first hurdle, can be easily understood from the tree-level QCD cross sections for photon production, shown in Fig. 8. In kinetic theory, and for $K^2 = 0$, these are the only contributions.

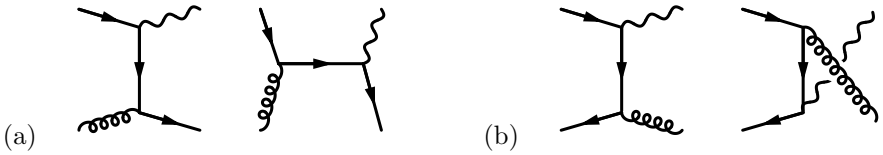

Figure 8: Leading-order QCD photon production from $2 \to 2$ interactions: (a) Compton scattering $qg \to q\gamma$, (b) quark-antiquark annihilation $q\bar{q} \to g\gamma$. The square matrix elements (plus other interference terms) follow by taking the imaginary parts of the self energy diagrams in Fig. 6.

In the original treatment of Ref. [42], the authors approximate the distributions of the incoming particles by Boltzmann functions, and conclude

$$\frac{d\mathcal{R}_i}{d^3\boldsymbol{k}} \simeq \frac{e^{-\omega/T}}{(2\pi)^6}\,\frac{T}{32\omega}\int\frac{ds}{s}\,\log\left(1 \pm e^{-s/(4\omega T)}\right)^{\pm 1}\int dt\,\big|\mathcal{M}_i\big|^2\,. \tag{5.1}$$

for the process $i = \{\text{Compton, annihilation}\}$ and $\omega \gg T$. Here tree-level matrix elements are squared and summed over all internal degrees of freedom of the incoming partons,

$$\big|\mathcal{M}_{\text{annihil}}\big|^2 = \frac{\mathcal{N}}{2}\left(\frac{u}{t}+\frac{t}{u}\right), \quad \text{and} \quad \big|\mathcal{M}_{\text{Compton}}\big|^2 = -\mathcal{N}\left(\frac{s}{u}+\frac{u}{s}\right), \tag{5.2}$$

with a common normalisation factor $\mathcal{N} = e^2 g_{\rm s}^2\, 2^6\, \sum_i Q_i^2$, where the sum of charge fractions[17] squared runs over the light flavors [16]. The t-integral over two-body phase space in (5.1) diverges due to the behavior of the amplitudes (5.2) for $t \to -s$ and $t \to 0$. This arises due to the long-range Coulomb interaction and necessitates a decomposition of phase space. The singular parts can be cut off by imposing the constraint

$$-s - t^\star \le t \le t^\star\,, \tag{5.3}$$

where $t^\star < 0$. Those interactions excluded by (5.3) need to be evaluated using the 'hard thermal loop' (HTL) approximation for the *dressed* quark propagator. Once this is done, any dependence on $t^\star$ drops out of the combined result but the parametric dependence on the strong coupling is modified $d\mathcal{R}_\gamma/d^3\boldsymbol{k} \propto \alpha_{\rm em}\alpha_{\rm s}T^2\left[\log\left(\omega/(\alpha_{\rm s}T)\right) + \bar{c}\,\right] e^{-\omega/T}$ as opposed to the strict ordering in Eq. (3.5). As already mentioned, this is not the full story. Aurenche and collaborators [94] noticed that other situations with successive multiple scatterings of the quark can suppress the radiation, i. e. would modify $\bar{c}$, the 'constant under the log'.

Multiple scatterings become comparable with those in Fig. 8, when the outgoing photon and quark (Compton) or two incoming quarks (annihilation) are collinear. Although the $2 \to 2$ processes are still dominant at weak-coupling, a rigorous LO result must include the

[17] In j_μ, (3.1), we omitted the quark charge fractions, $Q_i = (1 \pm N)/(2N)$ for the SM with N colours [93].

Landau-Pomeranchuk-Migdal (LPM) effect [95, 96]. In a QCD medium, it is possible that many soft gluons slightly deflect the quark within the photon's formation time [97]. This causes a suppression of radiation due to the interference between several different emission points. The LPM effect for real photons was handled in Refs. [50, 51]. Their work was generalised to 'soft' dileptons, i. e. $|K^2| \lesssim g_{\rm s}^2 T^2$, in Refs. [52, 98]. By now there are also several alternative approaches to obtain those results, which require summing an infinite number of 'ladder' diagrams, see Fig. 9. The same contributions can be found by setting up the Boltzmann equation for an appropriate linear-response to an external electromagnetic field [99]. Alternatively, the photon rate can also be obtained from the generating function of the HTL effective theory itself [100].

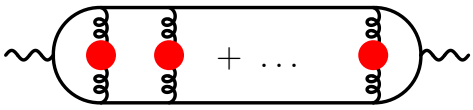

Figure 9: Ladder diagrams of arbitrary length; each rung is an HTL gluon. The valence quarks take on their asymptotic thermal mass.

In Fig. 9, the rungs are uncrossed and there are no 3- or 4-point gluon vertices between the valence quarks. We do not repeat the analysis that proves these are the only diagrams, but we will explain how to calculate their contribution. Such ladder-approximations are solved by a Bethe-Salpeter integral, which can be reformulated as a differential equation. Here we give details about how to solve this problem for the LPM effect [101].

The spectral functions can be calculated from

$$\rho_{\rm T,L} \;=\; e^2\, K^2 \frac{4N}{\pi^2\,\omega}\big(e^{\omega/T}-1\big)\int dp\, d\ell\; n_{\rm F}(p) n_{\rm F}(\ell)\delta(\omega-p-\ell)\;\chi_{\rm T,L}(p,\ell)\,, \tag{5.4}$$

where the (dimensionless) functions $\chi_{\rm T}$ and $\chi_{\rm L}$ will be explained shortly. Each is symmetric in p and ℓ, permitting (5.4) to be written as an integral from $p = \frac{1}{2}\omega$ to positive infinity. This integral needs to be done numerically. For that, it is handy to define the leading order (asymptotic) thermal mass of a hard quark as well as a shifted kinematical mass:

$$m_\infty^2 \;\coloneqq\; g_{\rm s}^2 T^2\,\frac{c_F}{4}\,, \quad M_{\rm eff}^2 \;\coloneqq\; m_\infty^2 - \frac{p\ell}{\omega^2}K^2\,. \tag{5.5}$$

We assume a photon with energy $\omega \sim T$ and invariant mass $|K^2| \lesssim m_\infty^2$.

Before specifying $\chi_{\rm T,L}$ above, we focus on the general setup. The integral equation that accounts for ladder resummation can be framed as an ordinary differential equation, by Fourier transforming the momentum $\boldsymbol{p}_\perp$ (orthogonal to $\boldsymbol{k}$) into an transverse 'impact parameter' coordinate. In conjugate space, we need to solve a Schrödinger-type equation of the form

$$\big[\,(\kappa-\nabla_{\boldsymbol{x}}^2)+i\lambda\mathcal{V}(x)\,\big]\phi(\boldsymbol{x},\boldsymbol{x}') \;=\; \delta^{(2)}(\boldsymbol{x}-\boldsymbol{x}')\,, \tag{5.6}$$

were κ and λ are real constants and (using K_0 to denote the modified Bessel function of the first kind) the imaginary potential is

$$\mathcal{V}(x) = \frac{1}{2\pi}\Big(\,\log\frac{x}{2}+\gamma+K_0(x)\,\Big)\,.$$

Here the two dimensional conjugate coordinate has been rescaled by the Debye mass so that $\boldsymbol{x}$ is dimensionless.

To carry out the integration in Eq. (5.4), $\chi_{\rm T}$ and $\chi_{\rm L}$ should be disclosed; they are functions of $g_{\rm s}$, ω, k, p and ℓ. (Energy conservation promptly sets $\ell = \omega - p$.) We can obtain them from ϕ, with a solution space described by the two real quantities:

$$\kappa = \frac{M_{\rm eff}^2}{m_D^2}\,, \qquad \lambda = 8\frac{p\ell}{\omega T}\frac{m_\infty^2}{m_D^2}\,,$$

which specify the governing equation (5.6). Then $\chi_{\rm L}$ and $\chi_{\rm T}$ are (respectively) proportional to the imaginary parts of $\phi(\boldsymbol{x},\boldsymbol{x})$ and $\nabla^2_{\boldsymbol{x}}\phi(\boldsymbol{x},\boldsymbol{x})$ near the origin.

Therefore, we proceed to discuss the admissible solutions ϕ. Since D is a function of the magnitude $x = |\boldsymbol{x}|$, the solution may be written $\phi(\boldsymbol{x}) = \sum_\ell \phi_\ell(x) e^{i\ell\theta}$, where θ parametrises the azimuthal direction with respect to the $\boldsymbol{k}$-axis. (The azimuth is the same for $\boldsymbol{x}$ and $\boldsymbol{x}'$, as dictated by the δ-function.) Then the Fourier coefficients satisfy a radial equation, which we prefer to express in terms of $U_\ell(x,x') \equiv \sqrt{xx'}\,\phi_\ell$. Then (5.6) gives instead, for each $\ell \in \mathbb{Z}$,

$$\left[-\partial_x^2 + \frac{\ell^2 - \frac{1}{4}}{x^2} + \kappa + i\lambda\mathcal{V}(x)\right] U_\ell(x,x') \;=\; \frac{\delta(x-x')}{2\pi}\,. \tag{5.7}$$

It is possible to write the solution, following [102], as

$$U_\ell(x,x') = A_\ell\, u_\ell^{>}\big(\,\max(x,x')\,\big)\, u_\ell^{<}\big(\,\min(x,x')\,\big)\,,$$

where $u_\ell^{>}(x)$ and $u_\ell^{<}(x)$ solve the homogenous version of (5.7), but are regular as $x \to \infty$ and as $x \to 0$ respectively. The overall factor A_ℓ is specified by the discontinuity in the derivative of U_ℓ at $x = x'$, namely

$$\frac{1}{2\pi} = \partial_x U_\ell\big|_{x=x'-0} - \partial_x U_\ell\big|_{x=x'+0} = A_\ell\,\mathcal{W}(u_\ell^{<}, u_\ell^{>}\,; x')\,, \tag{5.8}$$

where $\mathcal{W}$ is the Wronksian of two solutions: $\mathcal{W}(f,g\,;x) = \dot{f}g - f\dot{g}$. The quantity A_ℓ is indeed a constant because $\mathcal{W}$ in (5.8) is independent of x'. Let us determine its value from our solutions at $x' = 0$.

By substituting $u_\ell \sim x^p$ into the homogenous form of (5.7), and solving the resultant indicial equation for small x, we find that there is (for any ℓ) a regular solution

$$u_\ell^{\rm reg.}(x) \;\sim\; x^{\frac{1}{2}+|\ell|}\,, \qquad (x \to 0)\,. \tag{5.9}$$

These solutions are such that $\phi(x)$ and all of its derivatives are finite at $x = 0$. The other root provides asymptotic behaviour that leads to $\phi(x)$ having an essential singularity at $x = 0$. (When $\ell = 0$, the root $p = \frac{1}{2}$ is repeated.) Asymptotically, we define these solutions by[18]

$$u_0^{\rm sing.}(x) \;\sim\; x^{\frac{1}{2}}\log(x) \quad \text{and} \quad u_{|\ell|\geq 1}^{\rm sing.}(x) \sim x^{\frac{1}{2}-|\ell|}\,, \qquad (x \to 0)\,. \tag{5.10}$$

From them it is possible to construct $u_\ell^{>}$ and $u_\ell^{<}$, up to an overall normalisation. Indeed $u_\ell^{<}$ must be proportional to $u_\ell^{\rm reg.}$, but the function $u_\ell^{>}$ can also contain $u_\ell^{\rm sing.}$ in a combination that ensures $u_\ell^{>}(x \to \infty) = 0$. For example, we could take

$$u_\ell^{<}(x) \;=\; u_\ell^{\rm reg.}(x)\,, \tag{5.11}$$

$$u_\ell^{>}(x) \;=\; u_\ell^{\rm sing.}(x) - B_\ell\, u_\ell^{\rm reg.}(x)\,; \qquad B_\ell \equiv \lim_{x\to\infty}\frac{u_\ell^{\rm sing.}(x)}{u_\ell^{\rm reg.}(x)}\,.$$

[18] Although $u_0^{\rm sing.}$ is technically not singular, it has an infinite slope at $x = 0$.

In that case $u_\ell^>(x \to 0)$ will be imaginary only if B_ℓ is, because the regular and singular solutions will in general be imaginary for $x > 0$. Notice that this choice gives

$$\mathcal{W}(u_\ell^<, u_\ell^>; 0) \;=\; \Big[\, u_\ell^{\text{sing.}} \frac{du_\ell^{\text{reg.}}}{dx} - u_\ell^{\text{reg.}} \frac{du_\ell^{\text{sing.}}}{dx} \,\Big]_{x\to 0}\,, \tag{5.12}$$

which can be calculated from the expressions above. The resulting $A_0 = -1/(2\pi)$ and $A_{-\ell} = A_\ell = 1/(4\pi\,\ell)$ for $\ell \geq 1$, fully specify the solution to (5.6).

Setting $x = x'$ and $\theta = 0$ in the expression for $\phi(\boldsymbol{x}, \boldsymbol{x'})$ reveals the small-x behaviour:

$$\phi(x,x) \sim \frac{1}{2\pi}\Big[\,\gamma + B_0 - \sum_{\ell\geq 1} \frac{B_\ell x^{2\ell}}{\ell}\,\Big].$$

Thus we need B_ℓ for the imaginary part. By differentiating the limiting quantity in B_ℓ, with respect to x, one finds

$$\frac{d}{dx}\left(\frac{u_\ell^{\text{sing.}}(x)}{u_\ell^{\text{reg.}}(x)}\right) \;=\; \frac{-1}{2\pi A_\ell\,[u_\ell^{\text{reg.}}(x)]^2}\,. \tag{5.13}$$

And therefore B_ℓ can be written as an integral up to $x = \infty$ which involves only the regular function as it appears above. If we start the integration from $x = 0$, the real part of B_ℓ would not be defined. However it is sufficient for the imaginary part. For the general function ϕ, we find

$$\lim_{x\to 0}\ \text{Im}\ \partial_x^{2m}\phi(x,x) \;=\; \frac{(2m)!}{\pi}\ \text{Im}\int_0^\infty \frac{dx'}{[u_m^{\text{reg.}}(x')]^2}\,.$$

This in turn leads to the expressions[19]

$$\chi_{\text{L}} = \frac{p\ell}{2\omega^2}\int_0^\infty dx\ \text{Im}\ \frac{1}{[u_0^{\text{reg.}}(x)]^2}\ ; \quad \chi_{\text{T}} = \frac{p^2+\ell^2}{2p\ell\,K^2}\int_0^\infty dx\ \text{Im}\ \frac{m_D^2}{[u_1^{\text{reg.}}(x)]^2}\,. \tag{5.14}$$

This is useful for a numerical treatment because the integral over x in (5.14) and the determination of $u_{1,2}^{\text{reg.}}(x)$ can be performed simultaneously. Consider writing the integral with a variable upper limit. The derivative of that integral is given by the integrand – which is a simple function (real and imaginary parts) of the solution to another differential equation. Since the small-x behaviour in (5.9) sets the boundary condition, the two integrals together with $\text{Re}[u_\ell^{\text{reg.}}]$, $\text{Im}[u_\ell^{\text{reg.}}]$, $\text{Re}[\partial_x u_\ell^{\text{reg.}}]$ and $\text{Im}[\partial_x u_\ell^{\text{reg.}}]$ for $\ell = \{0,1\}$ constitute a system of ten real, first-order differential equations. Once the value of the integral in (5.14) is constant, the numerical quadrature can be terminated. That still needs to be inserted in Eq. (5.4) for a final integration over the loop momentum.

Test case: $\mathcal{V}$ = const.

If we replace the function $\mathcal{V}(x)$ by a constant, say $\mathcal{V} \to 1$, Eq. (5.6) the regular solution is

$$u_\ell^{\text{reg.}}(x) = (c^\ell\,\ell!)\sqrt{x}\,J_\ell\big(2x/c\big)\ ; \quad c \equiv \frac{2}{\sqrt{-\kappa - i\lambda}}\,,$$

[19] The function g and $\boldsymbol{f}$ in Eq. (21) of Ref. [52] and their governing differential equation need to be converted into the notation used here. We have encoded them both into the solution ϕ.

where J_ℓ is the Bessel function of the first kind. In this case we could find the associated B_ℓ in (5.11) from its derivative in Eq. (5.13), thanks to a tabulated integral [103]:

$$\int dx \frac{1}{u_\ell^{\text{reg.}}(x)^2} \;=\; \frac{\pi}{2c^{2\ell}(\ell!)^2}\frac{Y_\ell(2x/c)}{J_\ell(2x/c)}\,. \tag{5.15}$$

The function above is actually equal to the ratio $u_\ell^{\text{sing.}}/u_\ell^{\text{reg.}}$ (for general x), and B_ℓ is obtained from the limit $x \to \infty$. For that, the limiting ratio, we find a small x-behaviour,

$$\begin{aligned}
\ell = 0 \quad &: \quad \gamma + \log(x/c) + \dots \\
\ell = 1 \quad &: \quad \frac{1}{x^2} - \frac{2}{c^2}\big[\,\gamma + \log(x/c) - \tfrac{3}{4}\,\big] + \dots \\
\ell \geq 2 \quad &: \quad \frac{1}{x^{2\ell}} + \frac{2\ell\, x^2}{c^2(\ell^2-1)x^{2\ell}} + \dots
\end{aligned}$$

We note that in the case $\ell = 0$, one obtains from (5.15) evaluated between $x = 0$ and ∞,

$$B_0 \;=\; \frac{\pi}{2}\Theta(-\kappa) - \frac{1}{2}\arctan\big(\lambda/\kappa\big)$$

If the imaginary potential is dropped entirely,

$$B_0\big|_{\lambda=0} = \frac{\pi}{2}\,\Theta(-\kappa)\;, \qquad B_1\big|_{\lambda=0} = \frac{\pi}{8}\,\kappa\,\Theta(-\kappa)\,. \tag{5.16}$$

Hence, if λ may be neglected, the spectral function only receives support where M_{eff}^2 in Eq. (5.5) is negative. This will be useful later.

6. Interpolation between hard and soft regimes

The full LPM calculation includes the NLO result under simplifying assumptions (namely $K^2 \ll T^2$ and $\omega \sim T$), along with a whole host of other corrections that become increasingly important as one nears the light cone. To approximate $\rho_{\mu\nu}$ in (3.1) for all K^2, let us take up the approach advocated in [101]. The parts to order g_{s}^2 are subtracted from the full LPM results and the remainder is coupled with the full NLO truncation.

In view of Eq. (3.5), this amounts to

$$\rho \;\approx\; e^2\Big[\;\rho_{(0)} + g_{\text{s}}^2\rho_{(1)} + \textstyle\sum_{l>1} g_{\text{s}}^{2l}\rho_{(l)}\big|_{\text{LPM}}\;\Big]. \tag{6.1}$$

To isolate the LPM contributions that go *beyond* the scope of the NLO result, the shared terms can be subtracted from the former. That avoids double counting in an interpolation between the two regimes. We may identify the mutual parts from a 'naive' expansion of (5.4) in powers of g_{s}^2 and assume that $K^2 \sim T^2$.

Note that κ and λ involve the effective mass M_{eff}^2 from (5.5). That combination implies the LPM results depend on g_{s} and k only in the combination[20] K^2/g_{s}^2 [52]. Because the

[20] To be explicit, the $\chi_{\text{T,L}}$ from (5.14) are fully described by κ and λ (and the combination K^2/m_D^2 as it appears in the transverse case). Therefore, the functional structure takes the form

$$\chi\Big(g_{\text{s}}, \frac{\omega}{T}, \frac{k}{T}\Big) \;=\; f\Big(\frac{\omega}{T}, \frac{K^2}{g_{\text{s}}^2T^2}\Big),$$

in terms of non-dimensional variables. This non-trivial scaling behaviour can be checked numerically, but it also indicates that K^2 is connected to the Debye scale m_D^2 in this regime.

coupling constant only appears as an argument via $K^2/g_{\rm s}^2$, one may re-expand in $g_{\rm s}$ by considering large K^2. For χ up to terms $\mathcal{O}(g_{\rm s}^2)$, it is enough to treat $\kappa \gg \lambda$ and thus recover the simpler case studied earlier. Referring back to Eq. (5.16), we have $\chi_{\rm T,L}$ computed in closed form,

$$\chi_{\rm L} = \pi\,\Theta(-M_{\rm eff}^2)\,\frac{p\ell}{4\,\omega^2}\;, \quad \chi_{\rm T} = -\,\pi\,\Theta(-M_{\rm eff}^2)\,M_{\rm eff}^2\,\frac{p^2+\ell^2}{16p\ell\,K^2}\,. \tag{6.2}$$

The actual spectral functions require that we discuss the integral needed in (5.4). It has measure with diminished support and takes the form

$$\int dp\,d\ell\;\delta(\omega-p-\ell)\Theta\big(-M_{\rm eff}^2\big)\,F(p,\ell)\;, \tag{6.3}$$

where F is a function of the momenta. Energy conservation fixes one of the momenta, say $\ell = \omega - p$, and the negativity of $M_{\rm eff}^2$ reduces the support of the integrand. (The p-range is a finite interval above the light cone, and its complement below.) The integration regions are enclosed by the particular values

$$p_{\rm min}^{\rm max} \;=\; \frac{\omega}{2}\bigg(1 \pm \sqrt{1-\frac{m_\infty^2}{4K^2}}\;\bigg),$$

where $m_\infty^2 = g^2 c_F T^2$ is the thermal mass of a hard quark. For present concerns, LO and NLO parts can be obtained by setting $m_\infty^2 \to 0$ in these limits and focusing on the integrand. The remaining integral depends on the sign of K^2:

$$\int\!{}'\,dp \;=\; \Theta(K^2)\int_0^\omega dp - \Theta(-K^2)\Big[\;\int_{-\infty}^0 dp + \int_\omega^\infty dp\;\Big], \tag{6.4}$$

With (6.2), we can now formulate the desired re-expansion. Taking on the notation from (3.5), $\rho_{(l)}$ gives the coefficient of $e^2 g_{\rm s}^{2l}$ from the LPM result. Equation (5.4) yields

$$\begin{aligned} g_{\mu\nu}\rho_{(0)}^{\mu\nu}\,\big|_{\rm LPM} \;&=\; K^2\frac{N}{4\pi}\;\Big\{\quad \Theta(K^2) \;+\; 2\frac{T}{\omega}\log\big[\,\tfrac12(1+e^{-\beta\omega})\,\big]\;\Big\}\,, \\ \rho_{(0)}^{00}\,\big|_{\rm LPM} \;&=\; -\,k^2\frac{N}{4\pi}\;\Big\{\;\frac13\Theta(K^2) + 4\frac{T^2}{\omega^2}\Big(\,{\rm Li}_2\big(-e^{-\beta\omega}\big) - {\rm sgn}(K^2)\frac{\pi^2}{12}\,\Big) \\ &\qquad\qquad + 8\frac{T^3}{\omega^3}\Big({\rm Li}_3\big(-e^{-\beta\omega}\big) + \frac{3\zeta(3)}{4}\,\Big)\;\Big\}\,. \end{aligned} \tag{6.5}$$

These expressions coincide with those from Eqs. (4.2) assuming $k_+ \approx \omega$ and $k_- \approx 0$, as they should. QCD corrections only occur in the transverse channel of Eqs. (6.2) due to the effective mass. We thus find

$$\begin{aligned} \rho_{(1)}^{00}\,\big|_{\rm LPM} \;&=\; 0\,, \\ g_{\mu\nu}\rho_{(1)}^{\mu\nu}\,\big|_{\rm LPM} \;&=\; T^2\frac{Nc_F}{8\pi}\bigg\{\,\big[\,\tfrac12 - n_{\rm F}(\omega)\,\big]\Big(\,\log\frac{|K^2|}{m_\infty^2}+1\Big) + \int\!{}'\,dp\,\mathcal{A}(p)\;\bigg\}\,, \end{aligned} \tag{6.6}$$

where

$$\mathcal{A}(p) \;=\; \frac{1}{p}\big[\,\tfrac12 + n_{\rm F}(\omega) - n_{\rm F}(p) - n_{\rm F}(\omega-p)\,\big] - \frac{1}{\omega}\big[\,1 - n_{\rm F}(p) - n_{\rm F}(\omega-p)\,\big]\,.$$

Indeed, the transverse polarisation concedes the well-known logarithmic divergence as well as a finite part that is discontinuous across the light cone.

The singularity at $\omega \to k$ that plagues a strict perturbative series is eliminated by LPM resummation. Not only is the result finite there, but it is also continuous. That imposes a check on our NLO calculation: The discontinuity in (6.6) should *exactly* match another found in the 'full' result (4.4). We can demonstrate this explicitly by appealing to the list of master integrals given: Only two are actually discontinuous, $\rho^{(0,0)}_{11010}$ and $\rho^{(0,0)}_{1111(-1)}$, and taking them into account gives [2]

$$g_{\mu\nu}\rho^{\mu\nu}_{(1)}\big|_{\text{disc}} \;=\; T^2\frac{Nc_F}{8\pi}\bigg(\int_{-\infty}^{+\infty}\frac{dp}{\omega-p}\Big[\,n_{\text{F}}(0)+n_{\text{F}}(\omega)-n_{\text{F}}(p)-n_{\text{F}}(\omega-p)\,\Big]-1\bigg).$$

As for the LPM, only the peculiar integration over $\mathcal{A}(p)$ gives a discontinuity. From the definition (6.4), one has

$$\text{disc}\int{}'dp \;=\; \int_{-\infty}^{+\infty}dp\,, \tag{6.7}$$

to be considered with the second term in (6.6). All that remains to check $g_{\mu\nu}\rho^{\mu\nu}_{(1)}\big|_{\text{disc}}$, is whether the second term in the definition for $\mathcal{A}(p)$ gives

$$\int\frac{dp}{\omega}[1-n_{\text{F}}(p)-n_{\text{F}}(\omega-p)]=1\,,$$

which is trivially verified. (An alternative matching of discontinuities is given in Ref. [3].)

Comparison with quenched and 2-flavour lattice data

We are now ready to discuss the results. Following Ref. [3], we implement Eq. (6.1) as

$$\rho_{\mu\nu}\big|^{\text{resummed}}_{\text{NLO}} \;=\; \rho_{\mu\nu}\big|^{\text{fixed-order}}_{\text{NLO}}+\Big(\,\rho_{\mu\nu}\big|^{\text{full}}_{\text{LPM}}-\rho_{\mu\nu}\big|^{\text{expanded}}_{\text{LPM}}\,\Big)\times\varphi\,. \tag{6.8}$$

The fixed order result is obtained from the numerical evaluation[21] of the master integrals in Eqs. (4.4) and (4.5) [2]. The full LPM is also determined numerically, with the approach described below (5.14), from Eq. (5.4). From that, we subtract the 'double counted' parts attributed to LO (6.5) and NLO (6.6) re-expansions. For $\varphi\to 1$, we recover the interpolation described at the beginning of this section.

Bearing in mind that the integral transform in (3.7) samples the spectral function over many frequencies, running of the strong coupling cannot be ignored. For QCD, the renormalisation-group equations to ℓ-loop accuracy are [16]

$$\frac{\partial\alpha_{\text{s}}}{\partial\log\mu} \;=\; -2\pi\sum_{k=0}^{\ell}\beta_k\Big(\frac{\alpha_{\text{s}}}{\pi}\Big)^{k+2}\,.$$

We will use $\ell=5$ (having checked that $\ell=\{3,4\}$, gives barely any difference) [105]. The NLO spectral function is a fixed-α_{s} calculation and the LPM version involves resumming loops, whose vacuum parts produce the running. Strictly speaking, the scale at which to evaluate the running coupling should be an outcome of the physical process. Of course, for renormalization-group invariant approximations, the choice of 'the' argument of the running coupling $\alpha_{\text{s}}(\mu)$ is arbitrary: rescaling $\mu\to\tilde{\mu}$ is compensated by emerging $\alpha_{\text{s}}(\tilde{\mu})\log(\tilde{\mu}/\mu)$ correction terms. These terms should either be included, or be minimised by an *optimal* choice of scale for the relevant processes. We will choose μ_{opt} by drawing on more complete

[21] The code for this task is available online [104].

knowledge in the following cases: For large $K^2 \gg T^2$, the vacuum self-energy is dominant and $\mu_{\rm opt}^2 = |K^2|$ from the N^{4}LO result [106]. On the other hand, in the LPM limit, i. e. for $K^2 \sim g_{\rm s}^2 T^2$, the framework can be understood from a dimensionally reduced theory[22] called *electrostatic* QCD (EQCD) [92]. The coupling parameters of this theory have been studied and would suggest $\mu_{\rm opt} \sim \pi T$ [107, 108]. As a compromise between the virtuality and the thermal scale, we choose

$$\mu_{\rm opt} \;=\; \sqrt{Q_T^2 + M^2} \;\;; \quad Q_T = \iota \cdot \pi T \,, \tag{6.9}$$

where $M^2 = |K^2|$ is the invariant mass squared. (The parameter ι is adjusted; Q_T would be the lowest fermionic Matsubara frequency if $\iota = 1$.) The argument of the coupling is

$$\frac{\mu}{\Lambda_{\overline{\rm MS}}} \;=\; \Big(\frac{\mu}{T}\Big)\Big(\frac{T}{T_c}\Big)\, t_c \;,$$

in terms of the perturbative parameter $t_c = T_c/\Lambda_{\overline{\rm MS}}$. Our model in (6.8) depends on $\mu_{\rm opt}$ in units of the temperature and T/T_c is fixed in lattice simulations. Note that $\mu_{\rm opt} \geq Q_T$ implies an upper bound on $\alpha_{\rm s}$ that is attain on the light cone. We will take $\iota_{[n_f=0]} = 1$ and $\iota_{[n_f=2]} = 2$ in what follows. Varying $\mu = [1,2] \times \mu_{\rm opt}$ puts us in line with findings based on fastest apparent convergence in EQCD.

Lattice data with $k > 0$ are available in the quenched approximation ($n_f = 0$) [66]. For $T = 1.1 T_c$ the momenta studied there are $k_j = j \cdot 2\pi T/3$ where $j = \{1, 2, 3\}$. According to Ref. [109], $t_c = 1.24$ with uncertainties of about 10 %. In Fig. 10 we display the spectral functions $\rho_{\rm V}$ and ρ_Δ, calculated according to (6.8) with $\varphi \to 1$ and for the lattice momenta. To assess the potential influence of higher order terms, the genuine NLO LPM result of Ref. [56] as been incorporated (details in [3]).

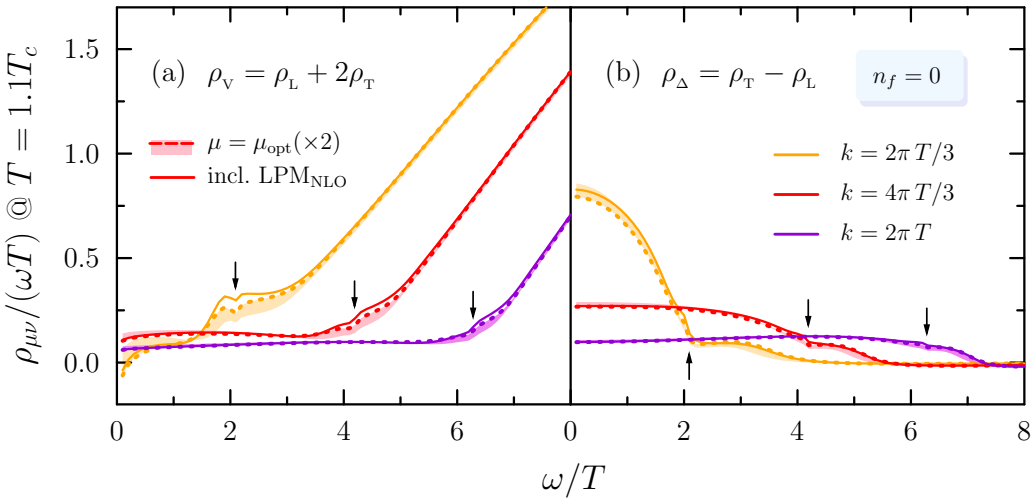

Figure 10: The resummed NLO spectral function from Eq. (6.8) in quenched QCD, as a function of frequency. We present (a) the contracted function, needed for physical rates, and (b) the difference in transverse and longitudinal polarisations. The inset arrows point out the light cone value.

[22] We shall make used of this fact later, in § II, to calculate a neutrino correlator on the light cone.

Recently, calculations of $n_f = 2$ Wilson-fermions have obtained G_Δ at temperatures $T \simeq 1.2T_c$. They have simulated several momenta, but we will focus on two of them[23], namely $k = \{\pi, \sqrt{7/2}\,\pi\}T$ [68]. To fix parameters, we use $T_c \simeq 167$ MeV [110] and the value of $\Lambda_{\overline{\rm MS}}$ from Ref. [111], giving $t_c = 0.56$, but with substantial uncertainties $\sim 25\%$. We display the ensuing spectral functions for our model in Fig. 11, as described in the quenched case. The temperature $T = 1.2T_c$ is quite low, yet there is no *prima facie* evidence to suggest that perturbation theory is failing: the 'error bands' are quite mild. For all ω, the strong coupling $\alpha_{\rm s} \lesssim 0.3$ in both the quenched and physical cases.

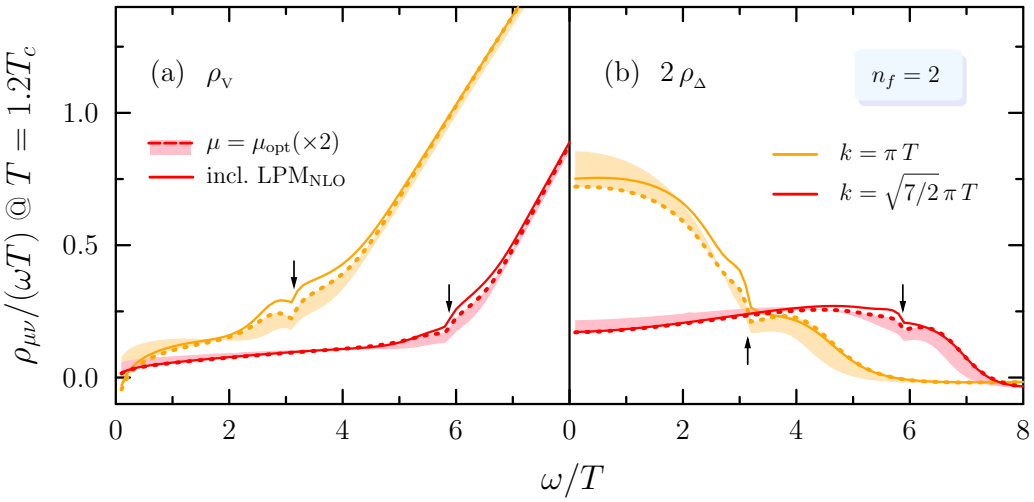

Figure 11: Like Fig. 10, but for 2-flavour QCD. The overall magnitude is the same as in the quenched approximation, flavour dependence only occurs via m_D (in the LPM-framework) and our choice of coupling. ρ_Δ has been multiplied by 2 for plotting purposes, but also to illustrate better that it coincides with $\rho_\mu^{\ \mu}$ at the light cone.

At last we come to a comparison with the imaginary-time correlator, as evaluated on the lattice. Equation (3.7) enables us to transform the spectral functions shown in Figs. 10 and 11 into $G_{\mu\nu}$ as a function of $\tau \in [0, \beta]$ where $\beta = 1/T$. (Since $G_{\mu\nu}$ is actually symmetric on this interval, we may consider it for $0 < \tau < \frac{1}{2}\beta$.) There are separate issues for attaining the trace $G_\mu^{\ \mu}$ and the difference G_Δ. In the former, thermal effects are negligible at large frequencies and so for $\omega > 30T$ we adopt the N^{4}LO result instead[24] [106]. Sensitivity to the matching point is sub-percent level for our consideration. For the latter correlator, we should preserve the sum rule in (3.13). But there is no assurance that the LPM part of (6.8) will respect it. Moreover, by introducing running coupling, the fixed-order part will violate the sum rule up to higher orders in $\alpha_{\rm s}$. A 'quick fix', that solves both problems, is to define $\varphi = \Theta(\omega^\star - \omega)$ and switch off the LPM resummation for $\omega > \omega^\star$, choosing $\omega^\star$ so that the sum rule is protected. Numerically, we obtain $\omega^\star \simeq 1.7\,k + 12.8\,T$.

[23] For convenience, we state the numerical values of k/T studied here:

$2\pi/3$	π	$4\pi/3$	$\sqrt{7/2}\,\pi$	2π
(2.09440)	(3.14159)	(4.18879)	(5.87738)	(6.28319)

[24] Using only NLO accuracy would spoil the result for $\tau T \lesssim 0.2$.

To compare our resummed spectral function with the $n_f = 0$ lattice data, ρ_{V} has been determined on a equally spaced array $\omega = \{0.1, 0.2, 0.3, \ldots, 10^3\} \times T$. The integral in (3.7) has been checked using various quadrature routines, which are all consistent. For plotting purposes, to account for the small-τ singularity, we divide G_{V} by the 'free' result, i. e. $\alpha_{\mathrm{s}} = 0$, for non-zero momentum. (An analytic formula only exists for $k = 0$, see Footnote 13.) To then distinguish the honest NLO behaviour, we subtract unity from that quantity and show the outcome in Fig. 12. The level of agreement with the lattice data is quite remarkable, given the low temperature, with moderate uncertainty bands for the largest momentum ($k = 2\pi T$). For small τ, the Euclidean correlator is mostly determined by the high-order vacuum result [62]. (Asymptotic freedom sets in very slowly, as a $\sim 2\%$ deviation from G_{free} is visible for $\tau \simeq 0$.) While the lattice results tend to fall below our estimates, τ-dependence is generally similar. Having factored-out the leading QED contribution, the non-perturbative reduction may reveal an aspect of confinement: Strong interactions restrict the thermodynamic fluctuations, limiting the currents that produce photons.

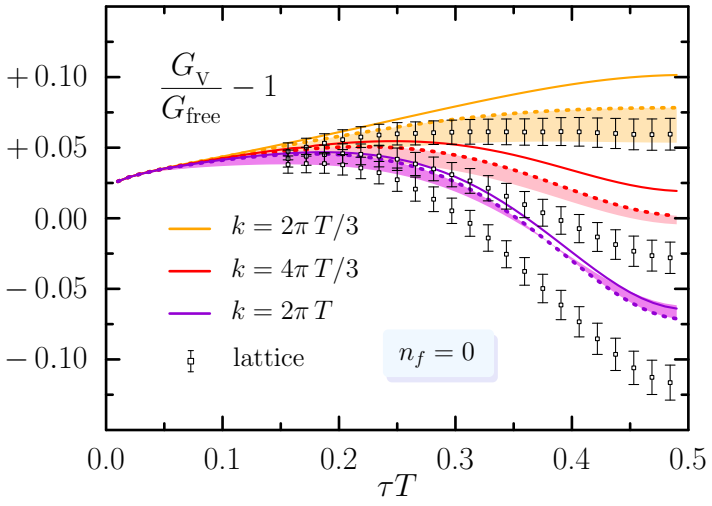

Figure 12: The imaginary-time correlator for the contracted spectral function $G_{\mathrm{V}} = G_{\mu}{}^{\mu}$, for $T = 1.1T_c$, with quenched lattice data from Ref. [66]. Here we have rescaled the result so that any deviation from zero is a QCD effect. The curves (and shaded bands) match those in Fig. 10, with the ω-integration as explained in the text.

Large ω is highly suppressed in ρ_{Δ} and there is no vacuum part, hence for its Euclidean correlator (3.7) we can get away with a smaller array $\omega = \{0.1, 0.2, 0.3, \ldots, 30\} \times T$ at the momenta from Refs. [67, 68]. In order to compare with the lattice measurements, we need to normalise by χ_{q}, the quark number susceptibility. The free value is $\chi_{\mathrm{free}} = T^2$. For $n_f = 2$, lattice and perturbation theory give $\chi_{\mathrm{q}}/T^2 = 0.9 \pm 0.1$ at $T \simeq 1.2T_c$ [112]. Due to G_{Δ} being solely thermal, it can simply be scaled by the temperature cubed. Figure 13 shows the result, alongside the corresponding free function. The estimated uncertainty of our perturbative model is relatively large, due to the fact that this spectral function is far more sensitive to infrared scales. Despite that, the NLO resummation tends to bring the function into alignment with the lattice results. The reconstructed spectral functions obtained in Ref. [68] also compare rather favourable with ours (cf. Fig. 10).

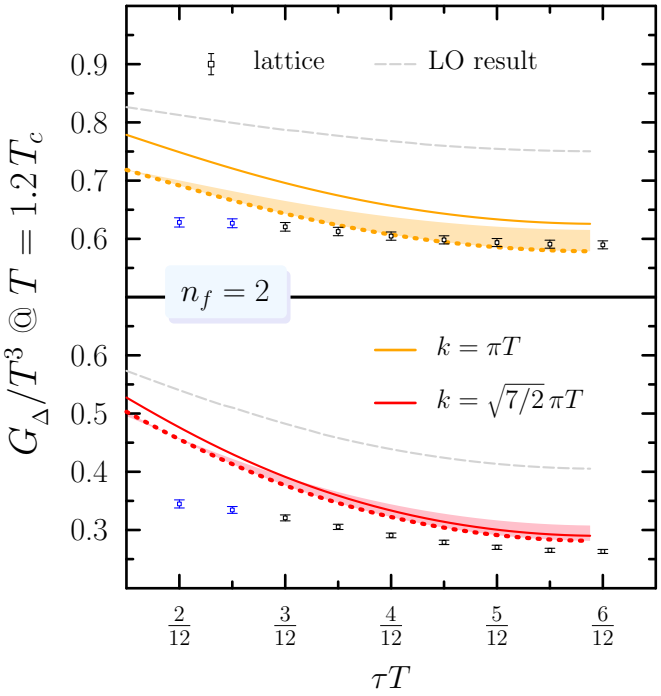

Figure 13: The correlator G_Δ as a function of τ for 2-flavour QCD, for $k = \pi T$ (upper) and $k = \sqrt{7/2}\,\pi T$ (lower). (The blue points for $\tau T < \frac{1}{4}$ are a preliminary continuum extrapolation, not included in the final version of Ref. [68].) To obtain the same correlator, lattice values have been multiplied by $\chi_{\rm q}/T^2$ and include its uncertainty.

As a side remark, we point out that spectral functions for $\omega, k \ll T$ are where we find substantial uncertainties in our prediction. Indeed, the photon's wavelength is then large compared with the 'microscopic' interparticle distance and the preceeding analysis is not strictly justified [113]. The hydrodynamic equations of motion take over in the long wavelength regime [114]. (We will discuss this topic further in Sec. 13.) In this limit, the spectral functions are known to be

$$\frac{\rho_{\rm T}}{\omega} \,=\, -\sigma \qquad \text{and} \qquad \frac{\rho_{\rm L}}{\omega} \,=\, -\sigma \frac{K^2}{\omega^2 + D^2 k^4} \tag{6.10}$$

where σ and D are the transport coefficients attributed to (charge) conductivity and diffusion respectively. They are linked by $\sigma = \chi_{\rm q} D$ according to the fluctuation-dissipation theorem. For fixed k, the combination $\rho_{\rm V} = \rho_{\rm L} + 2\rho_{\rm T}$ for $\omega \to 0$ goes negative at $k < 1/(\sqrt{2}\,D)$. [This can be seen in Fig. 10 (a).] From that we estimate that $DT \lesssim 0.3$ (for $T = 1.1$), which is consistent with lattice findings at the same temperature [115]. However, the precise functional form in (6.10) is not recovered in existing approximations [116].

We end by reiterating the twofold benefit of our results: *i*) The weak-coupling assumption may be tested, *ii*) we can scrutinise spectral reconstruction methods with 'mock' data. Juxtaposing Figs. 12 and 13, we confirm that G_Δ has improved resolution in its ability to discriminate between 'input' spectral functions. We find in both cases, the perturbative results slightly overestimate the lattice data.

Part II

Neutrino damping in the symmetry-broken phase

7. Basics: known and unknown

Both production and absorption rates of particle excitations follow from their collisional width, denoted Γ. The latter complies with (and may be derived from) the structure of the particle's dispersion relation in a thermal medium. Modifying Eq. (2.1) for fermions, the absorption rate is given by multiplying Γ with the suppression factor $\big(1-n_{\rm F}(\omega)\big)$. In this section we focus on how the medium attenuates, or 'damps', propagating modes[25]. Damping construes a reduction in the amplitude of an oscillation, e. g. by dissipating energy to its surroundings. A *drag force* is responsible for the work done and can occur, in a thermal system, by the microscopic interactions between particles. This contrasts with the (more important) 'decoherence' rate for neutrinos, which does not compel a transfer of energy. We consider the damping of an ultrarelativistic neutrino below the EW crossover.

In the SM, neutrinos are massless – but this cannot be true because experiments have proven that the three known flavours can oscillate among one another [117, 118]. Their mass-eigenstates ν_i, where $i=\{1,2,3\}$, are expressible as a superposition of those defined by the weak charge:

$$\nu_i = U_{1i}\,\nu_e + U_{2i}\,\nu_\mu + U_{3i}\,\nu_\tau\,.$$

The (unitary) lepton mixing matrix contains four parameters that cannot be trivially eliminated, as is the case in the quark-sector. It can be expressed by[26]

$$U \;=\; \begin{pmatrix} 1 & 0 & 0 \\ 0 & c_{23} & s_{23} \\ 0 & -s_{23} & c_{23} \end{pmatrix} \begin{pmatrix} c_{13} & 0 & s_{13}e^{-i\delta} \\ 0 & 1 & 0 \\ -s_{13}e^{i\delta} & 0 & c_{13} \end{pmatrix} \begin{pmatrix} c_{12} & s_{12} & 0 \\ -s_{12} & c_{12} & 0 \\ 0 & 0 & 1 \end{pmatrix}, \tag{7.1}$$

where $s_{ij}=\sin\theta_{ij}$ and $c_{ij}=\cos\theta_{ij}$ [119]. The exact values of the parameters in U depend on two inequivalent orderings of the masses m_i, each compatible with the inferred mass splittings: $\Delta_{12}\ll\Delta_{13}\simeq\Delta_{23}$ where $\Delta_{ij}:=|m_i^2-m_j^2|$. In either ordering, one finds $\theta_{12}\simeq 34^\circ$, $\theta_{23}\simeq 50^\circ$ and $\theta_{13}\simeq 8.6^\circ$ with uncertainties at the level of a few percent [120]. The value of δ is consistent with $\frac{1}{2}\pi$, showing a preference for maximal $\mathcal{CP}$-violation, although uncertainties $\mathcal{O}(30^\circ)$ are still considerable [121]. The absolute square-mass difference has been observed for solar neutrinos: $\Delta_{\rm sol}=6.9\times10^{-5}$ eV^2 [122] and atmospheric neutrinos: $\Delta_{\rm atm}=2.5\times10^{-3}$ eV^2 [123]. Together with $\Delta_{13}\simeq\Delta_{23}$, this imples that two of the three neutrino types have masses on the order of 8×10^{-3} eV or more. Stringent requirements from the β-decay of tritium [124] and cosmology [125] put sub-eV upper limits on the masses.

Despite the progress, open questions remain as to how massive ν-fields are engineered into the SM. All other fermions have a Dirac structure, entailing left- and right-handed components. This may be so for neutrinos, but since $\nu_{\rm R}$ is a singlet under every gauge group, it can also have a *Majorana mass* term without violating local symmetries. Right-handed or 'sterile' neutrinos are hypothetical, but well motivated on theoretical grounds: they explain neutrino masses [126–128], provide a dark matter candidate [129] and allow for baryon asymmetry [130]. Another consequence might be neutrinoless double β-decay, a process not yet observed [119]. If they exist, sterile neutrinos would be extremely elusive because they are uncharged with respect to every interaction in the standard model. Detection is, however, possible if they mix with the left-handed counterparts [131]. That is one of several motivations for the future Search for Hidden Particles (SHiP) facility at CERN [132].

[25] This observable is inverse of production, like that considered Part I for QCD.

[26] The completely unknown Majorana phase-differences are omitted.

The masses of the right-handed neutrinos can be brought down to the GeV level in an extension of the SM, which adds three almost mass-degenerate sterile neutrinos, called the νMSM (neutrino Minimal Standard Model) [133]. Here, both Dirac and Majorana terms are included and the seesaw mechanism gives the sterile neutrinos ($\nu_{\rm R}$) a much larger mass than the active ones ($\nu_{\rm L}$) [128]. For the νMSM, the sterile sector is fully specified by its (Majorana) masses and Yukawa couplings [134]. The latter must be very small, because we do not observe photons from $\nu_{\rm R} \to \nu_{\rm L} + \gamma$. That allows them to depart earlier from thermal equilibrium in the universe making them *relics* for possible lepton/baryon number violation. Evidently, precision studies of neutrinos will bring clarity to number of puzzling phenomena [26].

Let us recall, by a simple argument, how active neutrinos decoupled from the hot early universe [11]. Because the temperature T drops as the the universe evolves, the equilibrium distribution function $n_{\rm F}$ changes with time. Once the neutrinos free stream, the phyical momenta themselves become redshifted but their distribution is locked-in. Denote the phase space density of neutrinos $f_\nu(t,\boldsymbol{k})$ and suppose it deviates slightly from the 'running' equilibrium. The distribution function then obeys (assuming rotational symmetry) [35]

$$\Big(\frac{\partial}{\partial t} - Hk\frac{\partial}{\partial k}\Big) f_\nu \;=\; -\Gamma(k)\big[\, f_\nu - n_{\rm F}(\omega)\,\big] + \ldots . \tag{7.2}$$

From the Friedmann equations, $H = \sqrt{8\pi\,\varepsilon/(3m_{\rm Pl}^2)}$ where $\varepsilon(T)$ is the system's energy density. Γ is the microscopic interaction rate that represents how quickly the neutrinos are able to return to equilibrium. Presumably the universe included photons, electrons and neutrinos at this stage. Hence we may approximate[27] $\Gamma \simeq \langle n_\nu\,\sigma\rangle$ with the cross section $\sigma(T) \simeq 2.1\,G_F^2 T^2$ and n_ν is the number of neutrinos per volume. Number and energy density are well approximated by the the Stefan-Boltzmann limit,

$$n_\nu(T) \;\approx\; \frac{3\zeta(3)}{4\pi^2} T^3\, g_\nu\;, \quad \varepsilon(T) \;\approx\; \frac{\pi^2}{30}\,T^4\big(g_\gamma + \tfrac{7}{8}(g_e + 3g_\nu)\big)\,,$$

where the degeneracies for each particle are $g_\gamma = 2$, $g_e = 4$ and $g_\nu = 2$. For $\Gamma \gtrsim H$ interactions are efficient enough to keep f_ν close to the equilibrium distribution. This continues until a time $t_{\rm dec}$ at which $H = \Gamma$ and the temperature $T_{\rm dec} \approx 2.0$ MeV. The right-hand side of (7.2) vanishes for $\Gamma \ll H$ and the solution for $t > t_{\rm dec}$ is given by $f_\nu(t,\boldsymbol{k}) = f_\nu\big(t_{\rm dec}\,,\, k\,a(t)/a(t_{\rm dec})\big)$, where a is the scale factor. This CνB may never be directly measured, but there is indirect evidence for its existence [135]. In fact, the CMB itself also allows the number of neutrino species to be estimated quite accurately (we shall discuss this further in Sec. 14).

8. Neutrinos and lightlike correlators

We are interested in the *active* (left-handed) neutrino's interaction rate in a thermal medium below the electroweak crossover [136]. The neutrino can be regarded as an external 'probe' that suffers interactions with the weak sector of the SM, due to minimal coupling of the lepton doublet (cf. textbooks like [8])

$$\mathcal{L}_{\rm lept} \;=\; \bar\ell_{\rm L} i\gamma^\mu\Big(\partial_\mu - \frac{ig}{2}\vec W_\mu\cdot\vec\sigma - \frac{ig'}{2}B_\mu\Big)\ell_{\rm L}\,, \quad \ell_{\rm L} = \begin{pmatrix}\nu_e\\ e_{\rm L}\end{pmatrix}, \tag{8.1}$$

[27] We have assumed that neutrinos travel at the speed of light. Also note that the total cross section in the Fermi theory is $\sigma = G_F^2\, s/(3\pi)$ where s is the squared centre of mass energy. We used the average value $\langle s\rangle = \int_{12}(P_1+P_2)^2 f_1 f_2/(\int_{12} f_1 f_2) \simeq 19.86\,T^2$ in this estimate.

where $\vec{W}_\mu, B_\mu$ are the $SU_{\rm L}(2)$ and $U_{\rm Y}(1)$ gauge fields respectively. Here we use a vector notation for the weak isospin group, and write e. g. $\vec{\sigma} = (\sigma_1, \sigma_2, \sigma_3)$ for the associated Pauli matrices. We assigned a hypercharge $Y = +\frac{1}{2}$ to the left-handed doublet.

The rate of approach to equilibrium Γ of a 'test particle' can be obtained from the imaginary part of the particle's self-energy Σ, evaluated at an energy $k_0 = \omega + i0^+$ [137]. For a massless fermion, and in the medium's rest frame,

$$\Gamma(\omega) \;=\; -\frac{1}{2\omega}\,\mathrm{tr}\big[\not{K}\,\mathrm{Im}\,\Sigma(K)\big]\,. \tag{8.2}$$

(In an arbitrary frame, ω in the denominator can be replaced by Ku where u_μ is the flow velocity.) As a relation between statistical mechanics and field theory, Eq. (8.2) provides the starting point of a perturbative evaluation.

The full neutrino propagator is of the form

$$\langle \nu(K)\bar{\nu}(Q)\rangle \;=\; \frac{i}{\not{K} + \Sigma(K)}\;\delta^{(d+1)}(K-Q)\,, \tag{8.3}$$

where the self-energy reads $\Sigma(K) = -a\not{K} - b\gamma_0$ [138]. Evidently a does not contribute to Γ if $K^2 = 0$, however at higher-order the pole in the propagator moves off the light cone, calling for (8.2) to be modified. We will return to this subtlety later[28].

The fields interacting with the neutrino in (8.1) are taken to be in thermal equilibrium at a high temperature, but below the EW crossover. Spontaneous breaking of the weak gauge symmetry into $U_{\rm em}(1)$ explains how the (electrically) charged $W^\pm$ and neutral Z^0 bosons acquire masses, while the photon remains massless. Since this topic pervades almost all textbooks, we do not repeat that discussion here. But to be specific about notation, let us introduce the Lagrangian

$$\begin{aligned}\mathcal{L}_{\rm EW} \;=\;& -\tfrac{1}{4}\vec{W}_{\mu\nu}\cdot\vec{W}^{\mu\nu} \;-\; \tfrac{1}{4}B_{\mu\nu}B^{\mu\nu} \\ &+\; (D_\mu\Phi)^\dagger(D^\mu\Phi) \;-\; \mu^2\Phi^\dagger\Phi \;+\; \lambda\big(\Phi^\dagger\Phi\big)^2\,.\end{aligned} \tag{8.4}$$

The Higgs field is Φ, a complex doublet, that has non-zero (vacuum) expectation value $\big\langle\Phi^\dagger\Phi\big\rangle = \frac{1}{2}v^2$ where $v = \sqrt{\mu^2/\lambda}$. The physical Higgs mass is given by $m_H = \sqrt{2\mu^2}$ which has a measured value of 125.18(16) GeV [16].

We take the covariant derivative to act on the Higgs doublet as

$$D_\mu\Phi \;=\; \Big(\partial_\mu - \frac{ig}{2}\,\vec{W}_\mu\cdot\vec{\sigma} + \frac{ig'}{2}\,B_\mu\Big)\Phi\,. \tag{8.5}$$

The physical gauge fields in the broken phase are

$$W^\pm_\mu = \frac{W^1_\mu \mp iW^2_\mu}{\sqrt{2}}\,,\quad Z_\mu \;=\; \cos\theta\,W^3_\mu + \sin\theta\,B_\mu \quad\text{and}\quad A_\mu \;=\; -\sin\theta\,W^3_\mu + \cos\theta\,B_\mu\,,$$

where θ is Weinberg's mixing angle: $\cos\theta = g/\widetilde{g}$. Here we introduced the coupling $\widetilde{g} = \sqrt{g^2+g'^2}$. The masses of the gauge fields are $m_W = \frac{1}{2}gv$, $m_Z = \frac{1}{2}\widetilde{g}v$ and $m_A = 0$.

[28] In general, the two coefficients are given by

$$a(K) \;=\; \frac{1}{4k^2}\big(\mathrm{tr}[\not{K}\Sigma] - k_0\,\mathrm{tr}[\gamma_0\Sigma]\big)\,,\quad b(K) \;=\; \frac{1}{4k^2}\big(K^2\mathrm{tr}[\gamma_0\Sigma] - k_0\,\mathrm{tr}[\not{K}\Sigma]\big)\,.$$

We are interested in the imaginary part of b, which reduces to Eq. (8.2) for $\omega = k$.

Perturbation theory for EW-scale physics is less fragile than it is for QCD. The Debye screening mass $m_D \sim gT$ and $m_W(v) = \frac{1}{2}gv$ are suppressed with respect to the temperature T, where $v^2 = 1/(\sqrt{2}\,G_F)$ is the gauge-fixed Higgs expectation value in vacuum. More generally, $v(T)$ is a decreasing function of the temperature which reaches zero at $T = T_c$. Therefore, even in the symmetry-broken phase, we can distinguish 'low' ($\pi T < gv$) and 'high' ($gv \lesssim \pi T < \pi T_c$) temperature regimes. In the latter case, although m_D may not be parametrically smaller than m_W, thermal screening plays a crucial role. [Recall the discussion around Eq. (6.9); we shall return to this point later.]

Let us begin by considering 'low' temperatures, $\pi T < g\,v(T)$ and therefore ignore screening effects for thermal particles. (The range of validity for this approximation will emerge *a posteriori*.) The neutrino self-energy receives three contributions to leading order, depicted in Fig. 14. Only the first two have an imaginary part. They are topologically the same, but differ in the vertices and masses of the propgating W- and Z-bosons [139].

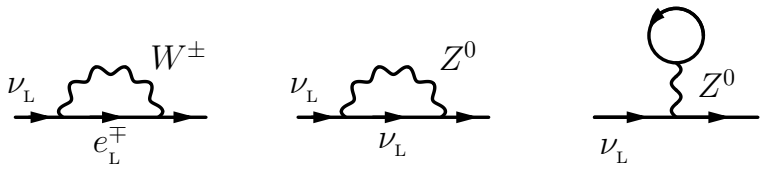

Figure 14: The active neutrino self-energy receives three contributions at LO in the symmetry-broken phase. Note that the tadpole contribution, which has any fermion in the loop, gives no discontinuity.

By taking the imaginary part of these 1-loop graphs, we obtain rates for the neutrino to scatter with gauge bosons. In Ref. [136] this was dubbed the 'Born $1 \leftrightarrow 2$' rate. Given that the on-shell ($\omega = k$) self-energy is gauge invariant, we may set $\xi = 1$ to obtain

$$\Gamma(\omega) \;=\; \frac{1}{\omega}\Big[\, 2\,g^2\mathcal{B}(m_W,\omega) + \big(g^2+g'^2\big)\mathcal{B}(m_Z,\omega)\,\Big], \tag{8.6}$$

in terms of the same function $\mathcal{B}$ of the propagating boson for each diagram in Fig. 14, which can be found by carrying out the trace in Eq. (8.2). Without any approximation, it reads

$$\mathcal{B}(m_V,\omega) \;=\; \frac{m_V^2 T}{32\pi\omega}\log\left(\frac{1+\exp\big[-m_V^2/(4\omega T)\big]}{1-\exp\big[-(\omega^2+m_V^2)/(4\omega T)\big]}\right). \tag{8.7}$$

To briefly explain where this expression comes from, let us give some details on the associated 1-loop diagram for general K ($\omega \geq k$). The sum-integrals are similar to those encountered in Eq. (4.1), but with a propagating massive gauge boson in the loop. According to the Feynman rules, and because terms with an odd number of γ_5-matrices do not contribute, the result reads

$$\mathcal{B}(m_V,K) \;=\; \frac{(d-1)}{8}\,\mathrm{Im}\Big[\,\mathop{\not\sum\!\!\!\!\int}_{P}(KL)\Delta_P\widetilde{\Delta}_L\Big]\,; \quad L = K-P\,.$$

Here the fermionic loop momentum L is massless, but $P^2 = m_V^2$ after taking the imaginary part. Conservation of energy and momentum implies that $KL = \frac{1}{2}(K^2 - m_V^2)$. After doing the frequency sum, and satisfying the integration with respect to angles in $d^3\boldsymbol{p}$, the radial

integration can be put into the form,[29] (we also take $d \to 3$)

$$\mathcal{B}(m_V, K) \;=\; \frac{m_V^2 - K^2}{32\pi\, k} \int_{p_{\rm min}}^{p_{\rm max}} dp \,\big(1 + n_{\rm B}(p) - n_{\rm F}(k_0 - p)\big)\,, \tag{8.8}$$

with limits that are dictated by kinematics: [as before, $k_\pm = \frac{1}{2}(\omega \pm k)$]

$$p_{\rm min} \;=\; k_+ + \frac{m_V^2}{4k_+} \quad \text{and} \quad p_{\rm max} \;=\; k_- + \frac{m_V^2}{4k_-}\,.$$

We assumed $K^2 < m_V^2$ in writing the limits above; they are reversed if $K^2 > m_V^2$ and coincide for $K^2 = m_V^2$. (This is a credible assumption since $\omega, k \sim T$ while $m_V \sim gv$.) The expression for $\mathcal{B}$ is recovered by taking the limit $\omega \to k$, once the integration in (8.8) is carried out.

Equation (8.6) is parametrically $\sim \underline{g}^4\, v^2/T$ where $\underline{g}$ represents one order in either weak isospin or hypercharge couplings. One might expect that if $T \gtrsim gv$, the masses of the gauge bosons can be replaced by $m_D \sim gT$. That would (incorrectly) give $\Gamma \sim \underline{g}^4 T$. The flaw in this reasoning is revealed by returning to the kinematic integration in (8.8). For $K^2 \to 0$ the lower and upper limits are approximated by $\omega + m_V^2/(2\omega)$ and $+\infty$ respectively. If, on the other hand, m_V is taken to be of the order gT from the beginning, one should be able to take the limit $m_V^2 \to 0$ in (8.8) before identifying the external momentum K to the light cone. This would yield integration limits of $p_{\rm min} = k_-$ and $p_{\rm max} = k_+$. The main issue is brought to bear after taking $\omega \to k$ so that near $p \simeq p_{\rm min}$ the integrand is dominated by the distribution function $n_{\rm B}\big(m_V^2/(4k_-)\big) \simeq 1/g^2$. This demonstrates that the naive power counting is invalid because of soft gauge particles 'lifted' the rate. As we shall see, the correct magnitude for the width is $\Gamma \sim \underline{g}^4 T^3/m_D^2 \sim \underline{g}^2 T$. The influence of soft exchanges implies that their propagators need to be resummed even at LO.

For 'high' temperatures $\pi T > g\, v(T)$, the NLO damping rate is of the order $g^4 T$ and hence Eq. (8.2) needs to be corrected. To clear up this subtlety, we decompose the exact propagator (8.3) into helicity eigenstates,

$$\big(\not{K} + \Sigma(K)\big)^{-1} \;=\; \frac{\gamma_0 - \boldsymbol{\gamma}\,\hat{k}}{2}\Delta_+(K) + \frac{\gamma_0 + \boldsymbol{\gamma}\,\hat{k}}{2}\Delta_-(K)\,,$$

where $\hat{k} = \boldsymbol{k}/k$. The two projections

$$\Delta_\pm^{-1} \;=\; (1+a)(k_0 \mp k) + b\,, \tag{8.9}$$

have zeros at $k_0 = \omega_\pm(k)$ that describe the propagation of particle excitations (+) and a plasmino mode (−) [140]. The latter has a negative ratio of chirality to helicity and arises due to the influence of the medium. In what follows, we focus on ω_+ which corresponds to the energy of an on-shell active neutrino.

For hard momenta $k \sim T$, the particle dispersion relation is given by $\omega_+(k) = k + \delta k$ where δk is a small correction. Specifically, we take the (in general complex) correction $\delta k \sim g^2 T$ to be of the same order as $b(\omega, k)$ and suppose that $a \sim g^4 T$. We introduce $S(\delta k) \coloneqq b(k + \delta k, k)$. To this order, the propagator in the vicinity of the pole reads

$$\Delta_+(k_0, k)\Big|_{k_0 = k + \delta k} \;\approx\; \frac{\mathcal{Z}}{\Big[\,\delta k + \dfrac{S(0)}{1 + S'(0)}\,\Big]}\,. \tag{8.10}$$

[29] For details, see Appendix B of Ref. [2].

Corrections of order $\delta k\, S''(0) \sim g^6$ were dropped. The residue $\mathcal{Z} = \big(1 + S'(0)\big)^{-1}$ concerns wave function renormalisation, i. e. the fields in the action are rescaled by $\sqrt{\mathcal{Z}}$. In general, Γ from (8.2) is given by the imaginary part of the solution to the particle dispersion relation. Therefore the physical damping rate reads

$$\Gamma(k) \;=\; 2\,\mathrm{Im}\Big[\,\frac{S(0)}{1+S'(0)}\,\Big] + \mathcal{O}(g^6 T)\,. \tag{8.11}$$

So, to achieve the desired accuracy, we need b and its first energy derivative on the light cone (i. e. $\delta k = 0$). (The first derivative is only needed up to LO.)

With the particle solution to Eq. (8.9) in mind, it seems desirable to reformulate $\mathcal{L}_{\rm lept}$ for a neutrino moving in the z-direction, i. e. $\boldsymbol{k} = (0,0,k)$. The negative helicities go on-shell for $k_0 \to \omega_+$. In the Weyl basis, these states are the lower components of spinors ν_e and $e_{\rm L}$ and we denote them via

$$\nu_e \;=\; \begin{pmatrix} \cdot \\ \psi \end{pmatrix}, \qquad e_{\rm L} \;=\; \begin{pmatrix} \cdot \\ \chi \end{pmatrix}.$$

Taking ψ and χ as dynamical fields, insofar as they can fluctuate about their on-shell point, relevant part of the Lagrangian (8.1) is

$$\begin{aligned} \mathcal{L}_{\rm lept} \;&\simeq\; \psi^\dagger\Big[i(\partial_z - \partial_t) + \tfrac{1}{2}\widetilde{g}(Z_0 + Z_3)\Big]\psi \\ &+\; \chi^\dagger\Big[i(\partial_z - \partial_t) + \tfrac{1}{2}\widetilde{g}(Z'_0 + Z'_3)\Big]\chi \;+\; \frac{g}{\sqrt{2}}\Big[\,\psi^\dagger\big(W_0^+ + W_3^+\big)\chi + \text{c.c.}\,\Big]. \end{aligned} \tag{8.12}$$

The ψ and χ fields couple only to temporal and 'parallel' third components of the gauge fields. For convenience, have complemented the standard definitions in (8.5) with

$$Z'_\mu \;:=\; -\cos\theta\, W^3_\mu + \sin\theta\, B_\mu\,.$$

Evidently Z'_μ is just the linear combination of Z_μ and A_μ that couples to χ. The free correlators for ψ and χ can be read off from (8.9), and we could calculate the thermal width for these 'nearly on-shell' neutrinos. Before proceeding, we review a marvelous trick that dramatically simplifies this calculation – and amounts to evaluating the long-time tails of a lightlike Wilson line.

Zero mode dominance

Let us consider some transformation properties of the frequency summation under Lorentz boosts [92]. Suppose $f(\tau, \boldsymbol{x})$ is a covariant function of (imaginary) time and space, such as an appropriate two-point function, which is periodic in τ. That implies the function f at zero time may be expressed as

$$f(\tau = 0, \boldsymbol{x}) \;=\; \sum\!\!\!\!\!\!\int_K \exp\big[\,i\,\boldsymbol{x}\boldsymbol{k}\,\big]\,\widetilde{f}(k_0, \boldsymbol{k})\,, \tag{8.13}$$

where $k_0 = ik^0_{\rm E}$. If the Euclidean energies are bosonic, which we will assume for argument's sake, then $f(\tau, \boldsymbol{x}) = f(\tau + T^{-1}, \boldsymbol{x})$. For fermions, f would be antiperiodic.

One can imagine doing the same thing for a frame moving in the z-direction [only space-like points can be reached from (8.13)]. The condition that the new function $f'(\tau', \boldsymbol{x}') = f(\tau, \boldsymbol{x})$ be periodic in *its* imaginary time is modified, see Fig. 15. If the primed frame is moving at velocity v with respect to the original one, periodicity implies

$$f'(\tau', \boldsymbol{x}_\perp, z') \;=\; f'\Big(\,\tau' + \frac{\gamma}{T},\; \boldsymbol{x}_\perp,\; z' - \gamma v \frac{i}{T}\,\Big), \tag{8.14}$$

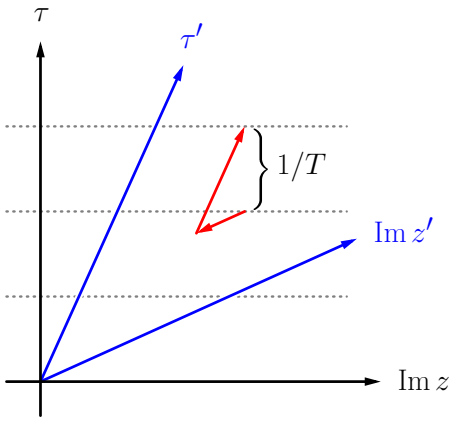

Figure 15: Minkowski diagram, with imaginary time on the vertical axis. The dotted horizontal lines are equally spaced and represent periodicity of the function f in $\tau = it$. Under boosts along the z-axis (blue, primed), the density matrix changes $\exp[-\beta H] \to \exp[-\beta\gamma(H' + vp'_z)]$ and periodicity in the imaginary time direction gets 'twisted' (red, connecting $1/T$) with respect to the old coordinates. Notably, the coordinate parallel to the boost receives an imaginary part, see Eq. (8.16).

where $\gamma = 1/\sqrt{1-v^2}$ is the boost factor and $\boldsymbol{x}_\perp = (x, y)$. The new 'Matsubara frequencies', $k'_0 = k_0/\gamma - vk'_z$, respect the modified periodicity. Not only does the original k_0 shrink by a factor of γ, but k'_0 also acquires a real part from the *physical* momentum k'_z in the boosted reference frame.

Let us extend (8.13) to the primed coordinates and evaluate it at zero time. The Euclidean representation of f' reads (in terms of the original k_0-sum)

$$f'(\tau' = 0, \boldsymbol{x}') \;=\; \frac{T}{\gamma}\sum_{k_0}\int_{\boldsymbol{k}'} \exp\big[\, i\,\boldsymbol{x}'\boldsymbol{k}'\,\big]\; \widetilde{f}'\Big(\frac{k_0}{\gamma} - vk'_z, \boldsymbol{k}'\Big)\,. \tag{8.15}$$

By now returning to the unprimed frame, we obtain an expression for f evaluated at $\tau \neq 0$ where $v = t/z$ (recall that $\tau = it$). That leads to the expression

$$f(\tau, \boldsymbol{x}) \;=\; \oint\!\!\!\!\!\!\sum_{K} \exp\big[\, -k_0\tau + i\boldsymbol{k}_\perp\boldsymbol{x}_\perp + i\big(k_z + k_0 v\big)z\,\big]\; \widetilde{f}\big(\,k_0, \boldsymbol{k}_\perp, k_z + k_0 v\,\big)\,, \tag{8.16}$$

which differs from (8.13) by the argument of f in momentum space: k_z is fettered to an imaginary part from the Euclidean energy $i\pi jTv$ (j is even). Likewise, momenta running in loops get transformed in the same way. Although $v < 1$ in Eq. (8.15) is implied by physical boosts[30], we are interested in correlators for $z/t \leq 1$ (i. e. $v \geq 1$). Formally the limit $v \nearrow 1$ can be used to set $t = z$ above, since the boost is actually undone in the end. The key step is to quantise the system along a 'hyperplane' parallel to $vz = t$, which is certainly possible on the light-front. Thus (8.16) can be utilised for lightlike observables, as we shown in the next section for the neutrino width considered in this thesis. Jet quenching in QCD was the first application of this idea, put forward in Ref. [92] (where more details can be found). We also point out that the LPM resummation detailed in Sec. 5 may also be understood in this framework, which paved the way for NLO accuracy in Ref. [56].

9. Three-dimensional electroweak theory

A dimensionally reduced version of the fundamental four-dimensional Lagrangian (8.4), can be constructed as an effective field theory [141]. There are two main steps in the process of dimensional reductions at finite T. In the first, one *integrates out* all fields with wavemodes

[30] Relating points in the domain of f for causally connected regions of spacetime.

of the order πT, i. e. 'hard' [142]. This amounts to including only the zero Matsubara frequencies in sums like (8.16), which makes this approach (potentially) beneficial for light-like observables. Since fermions satisfy antiperiodic boundary conditions in the imaginary time formalism, their Matsubara frequencies are all hard. The resulting EFT is entirely bosonic with momenta of the order gT or less, i. e. 'soft' [143]. The second step involves integrating over fields with soft spatial momenta to leave an effective Lagrangian for the 'ultrasoft' momenta. This scheme consistently divides the treatment of momentum scales into three parts. The programme has been implemented for the SM and has been successful in a variety of contexts: The EW phase transition [144], The QCD equation of state [145], susceptibilities for baryogenesis [146]. And, as we have seen in the previous section, it may also be used to treat observables on the light cone [92]. We will apply this formalism to evaluate (8.11), for $\pi T > g\,v(T)$ in the broken phase.

The temporal components of the gauge fields, $\vec{W}_0$ and B_0, are 'demoted' to scalar fields with a thermal mass. Since the new total space corresponds to $(d = 3)$-Euclidean dimensions, we can write down the effective action

$$\begin{aligned}\mathcal{S}_{\text{eff}} \;=\; \frac{1}{T}\int_{\boldsymbol{x}} \Big\{ \;& \tfrac{1}{4}\vec{W}_{ij}\cdot\vec{W}_{ij} \;+\; \tfrac{1}{4}B_{ij}B_{ij} \;+\; (D_i\Phi)^\dagger(D_i\Phi) \;-\; \mu_D^2\Phi^\dagger\Phi \;+\; \lambda\big(\Phi^\dagger\Phi\big)^2 \\ &+\; \tfrac{1}{2}(D_i\vec{W}_0)\cdot(D_i\vec{W}_0) \;+\; \tfrac{1}{2}m_D^2\vec{W}_0^{\,2} \;+\; \tfrac{1}{4}\lambda_{\scriptscriptstyle W}\vec{W}_0^{\,4} \\ &+\; \tfrac{1}{2}(\partial_i B_0)(\partial_i B_0) \;+\; \tfrac{1}{2}m_D'^2 B_0^2 \;+\; \tfrac{1}{4}\lambda_{\scriptscriptstyle B}B_0^4 \\ &+\; \tfrac{1}{4}g^2\,\vec{W}_0^{\,2}\Phi^\dagger\Phi \;+\; \tfrac{1}{4}g'^2\,B_0^2\Phi^\dagger\Phi \;-\; \tfrac{1}{2}gg'\,B_0\Phi^\dagger\big(\vec{W}_0\cdot\vec{\sigma}\big)\Phi \;\Big\}. \end{aligned} \tag{9.1}$$

Repeated indices are summed over, taking values $i, j \in \{1, \ldots, d\}$ where $d = 3 - 2\epsilon$. All the fields are bosonic and have units of [GeV] and the couplings g, g' and λ are dimensionless[31]. The first line resembles $\mathcal{L}_{\text{EW}}$ without the temporal gauge fields, whose contribution is given in the second and third line. (We shall not need to consider the quartic couplings $\lambda_{\scriptscriptstyle W} \sim g^4$ and $\lambda_{\scriptscriptstyle B}$ to compute the neutrino self-energy at NLO.) The last line gives the mutual interactions between the new scalar fields and Φ.

The covariant derivatives now act with spatial indices, e. g.

$$D_i\vec{W}_0 \;=\; \partial_i\vec{W}_0 + g\big(\vec{W}_i\times\vec{W}_0\big),$$

and similarly for the Higgs doublet, which has $Y = -\frac{1}{2}$ according to (8.5). Fermions do not appear as dynamical fields, but are taken in account in the parameters of the dimensionally reduced theory. Specifically, we include quarks in the full theory. The top interacts with the Higgs via $\mathcal{L}_{\text{Yukawa}} = y_{\text{t}}\big(\,\bar{q}_{\text{L}}\,\widetilde{\Phi}\,t_{\text{R}} + \text{c.c.}\,\big)$ where $\widetilde{\Phi} = i\sigma_2\Phi^*$. All the other Yukawa couplings may be neglected[32].

The scalar masses in (9.1) incorporate the effect of $j \neq 0$ modes [cf. Eq. (8.16)]. For example, the shape of the Higgs potential is modified by the medium through μ_D and this is what drives the symmetry restoration [147]. To be specific, we parametrise the Higgs sector by real fields ϕ_0 (the Higgs), ϕ_1, ϕ_2 and ϕ_3 (the remaining Goldstone bosons)

$$\Phi \;=\; \frac{1}{\sqrt{2}}\begin{pmatrix} \phi_2 + i\phi_1 \\ v + \phi_0 + i\phi_3 \end{pmatrix} \;\in\; \mathbb{C}^2, \tag{9.2}$$

[31] It is more standard to use couplings with dimension [GeV] and bosonic fields with dimension $[\text{GeV}]^{\frac{1}{2}}$. However, we have introduced an overall prefactor of $1/T$ in (9.1) to avoid this as it makes the tree-level comparison with $\mathcal{L}_{\text{EW}}$ more direct. This scaling originates from $\int d\tau \to 1/T$ multiplying the action.

[32] All other fermions have highly suppressed couplings to the Higgs, while $y_{\text{t}} \simeq 1$ and cannot be neglected at the scale of electroweak interactions (with respect to the other couplings).

where $v = \sqrt{\mu_D^2/\lambda}$. Ordinarily, at $T = 0$, the physical Higgs mass is given by $m_H = \sqrt{2\mu^2}$ where μ appears in (8.4). At finite temperature,

$$\mu_D^2 \;=\; \mu^2 - \frac{T^2}{16}\Big[\, g'^2 + 3g^2 + 8\lambda + 4y_{\mathrm{t}}^2 \,\Big], \tag{9.3}$$

and the thermal contribution will override the vacuum expectation value if T is sufficiently large. When this happens, the quantity $v(T) \to 0$ in Eq. (9.2) and symmetry is 'restored' for $T > T_c$. The masses of the temporal gauge fields are

$$m_D^2 \;=\; \frac{11}{6}g^2T^2 \quad \text{and} \quad m_D'^2 \;=\; \frac{11}{6}g'^2T^2\,. \tag{9.4}$$

As mentioned, no fermions appear in Eq. (9.1); they were 'integrated out' because their Matsubara frequencies are odd and therefore never zero. Fermionic effects *are*, however, included by the EFT procedure of matching to the original theory. The thermal masses, Eqs. (9.3) and (9.4), include the contribution from fermions and bosons running in loops. Therefore, the Feynman rules automatically resum a certain subclass of higher order diagrams. The rules are listed in Appendix B in a general R_ξ gauge. As dynamical fields for the Higgs sector (9.2), we follow tradition and introduce $\phi^\pm := (\phi_2 \pm i\phi_1)/\sqrt{2}$, so that

$$\Phi^\dagger\Phi = \frac{1}{2}\Big\{\,(v+\phi_0)^2 + \phi_3^2 + 2\phi^+\phi^-\,\Big\}.$$

The gauge dependence appears in the masses of the longitudinal gauge bosons and the Goldstone modes $\phi^\pm, \phi_3$.

One ramification of endowing the temporal gauge fields with a thermal mass, is to spoil the usual pattern of symmetry breaking. Specifically, the shifted masses modify the usual mixing angles, i. e. those below Eq. (8.5). This deserves some elaboration.

Mixing angle for scalars

At zero temperature, and in the full four-dimensional theory, rotating the gauge fields makes them diagonal in the masses generated by the Higgs mechanism [8]. After inserting (9.2) into the scalar kinetic term, one obtains

$$\mathcal{L}_{\mathrm{EW}} \;\supset\; m_W^2 W_\mu^+ W^{-\mu} + \frac{1}{2}\big[\, m_Z^2 Z_\mu Z^\mu + 0\cdot A_\mu A^\mu \,\big], \tag{9.5}$$

where the mass eigenstates are $m_W = \frac{1}{2}gv$ and $m_Z = \frac{1}{2}\widetilde{g}v$ with $\widetilde{g} = \sqrt{g^2+g'^2}$. The photon remains massless: $m_A = 0$.

However, in the process of dimensional reduction, W_0^3 and B_0 acquired thermal masses of their own, thus interfering with the second term in Eq. (9.5). A further step is necessary to diagonalise these temporal scalars. Note that, with the new terms,

$$\frac{1}{2}m_Z^2\big(\,\cos\theta\, W_0^3 + \sin\theta\, B_0\,\big)^2 + \frac{1}{2}m_D^2(W_0^3)^2 + \frac{1}{2}m_D'^2 B_0^2 \;=\; \frac{1}{2}\big[\,\alpha(W_0^3)^2 + 2\beta W_0^3 B_0 + \gamma B_0^2\,\big],$$

where the coefficients read

$$\alpha = m_Z^2\cos^2\theta + m_D^2\,, \quad \beta = m_Z^2\cos\theta\,\sin\theta\,, \quad \gamma = m_Z^2\sin^2\theta + m_D'^2\,.$$

We can rotate by an angle $\widetilde{\theta}$ to bring the matrix into a diagonal form, *viz.*

$$\begin{pmatrix} \alpha & \beta \\ \beta & \gamma \end{pmatrix} \;=\; \begin{pmatrix} \widetilde{c} & -\widetilde{s} \\ \widetilde{s} & \widetilde{c} \end{pmatrix} \begin{pmatrix} m_+^2 & 0 \\ 0 & m_-^2 \end{pmatrix} \begin{pmatrix} \widetilde{c} & \widetilde{s} \\ -\widetilde{s} & \widetilde{c} \end{pmatrix} ; \quad \widetilde{c} = \cos\widetilde{\theta}\,,\; \widetilde{s} = \sin\widetilde{\theta}\,.$$

The mass eigenvalues are given by

$$m_\pm^2 \;=\; \frac{1}{2}\big(m_Z^2 + m_D^2 + m_D'^2 \pm \sqrt{\mathcal{D}}\,\big)\,, \tag{9.6}$$

where the discriminant reads

$$\mathcal{D} \;=\; m_Z^4 + 2\big(m_D^2 - m_D'^2\big)\, m_Z^2 \cos 2\theta + (m_D^2 - m_D'^2)^2\,.$$

Because two non-trivial mass eigenvalues arise, we can already see that there will no longer be a massless gauge field. For $m_D = m_D' = 0$, the original Z^0 and photon masses are recovered from m_+ and m_- respectively. But (in general) the temporal scalar fields are instead diagonalised by

$$\widetilde{Z}_0 \;=\; \widetilde{c}\, W_0^3 + \widetilde{s}\, B_0 \qquad \text{and} \qquad \widetilde{A}_0 \;=\; -\widetilde{s}\, W_0^3 + \widetilde{c}\, B_0\,.$$

On the other hand, the temporal components of the original charged W-bosons still diagonalised their mass matrix: $W_0^\pm = (W_0^1 \pm i W_0^2)/\sqrt{2}$, but they *do* acquire an additive thermal correction. To summarise, the scalar masses are

$$m_{\widetilde{W}}^2 = m_W^2 + m_D^2\,; \quad m_{\widetilde{Z}}^2 = m_+^2\,; \quad m_{\widetilde{A}}^2 = m_-^2\,. \tag{9.7}$$

The new rotation angle $\widetilde{\theta}$ satisfies the two conditions[33]:

$$\sin 2\widetilde{\theta} \;=\; \frac{m_Z^2 \sin 2\theta}{\mathcal{D}}\,, \quad \cos 2\widetilde{\theta} \;=\; \frac{m_D^2 - m_D'^2 + m_Z^2 \cos 2\theta}{\mathcal{D}}\,.$$

It follows that for large T, this modified mixing angle is approximately

$$\widetilde{\theta} \;\simeq\; \frac{m_Z^2 \sin 2\theta}{2\big(m_D^2 - m_D'^2\big)}\,. \tag{9.8}$$

Taking m_Z to be independent of the temperature, this is proportional to $1/T^2$. But because $v(T)$ is a decreasing function of T, according to Eq. (9.3), $\widetilde{\theta}$ reaches zero at the same moment that m_Z does.

For completeness, let us state the free propagators:

$$\langle W_i^+(\boldsymbol{k}) W_j^-(\boldsymbol{q})\rangle \;=\; \Big[\,\frac{\delta_{ij}}{k^2 + m_W^2} + \frac{k_i k_j}{m_W^2}\bigg(\frac{1}{k^2 + m_W^2} - \frac{1}{k^2 + \xi m_W^2}\bigg)\Big]\, \bar{\delta}^{(d)}(\boldsymbol{k} + \boldsymbol{q})\,, \tag{9.9}$$

which can be obtained directly from the corresponding covariant propagator with obvious changes to $g_{\mu\nu} - K_\mu K_\nu / K^2$ and $K^2 - m_i^2$. Therefore we do not give the expressions for Z_i

[33] From Eq. (9.7), one can show that the new mixing angle satisfies two useful identities,

$$m_{\widetilde{Z}}^2 - m_{\widetilde{W}}^2 \;=\; m_W^2 \tan\theta \tan\widetilde{\theta} \qquad \text{and} \qquad m_{\widetilde{W}}^2 - m_{\widetilde{A}}^2 \;=\; m_W^2 \tan\theta \cot\widetilde{\theta}\,.$$

These often allow the differences between two temporal propagators to be written as a single term, in using one of these identities for the numerator.

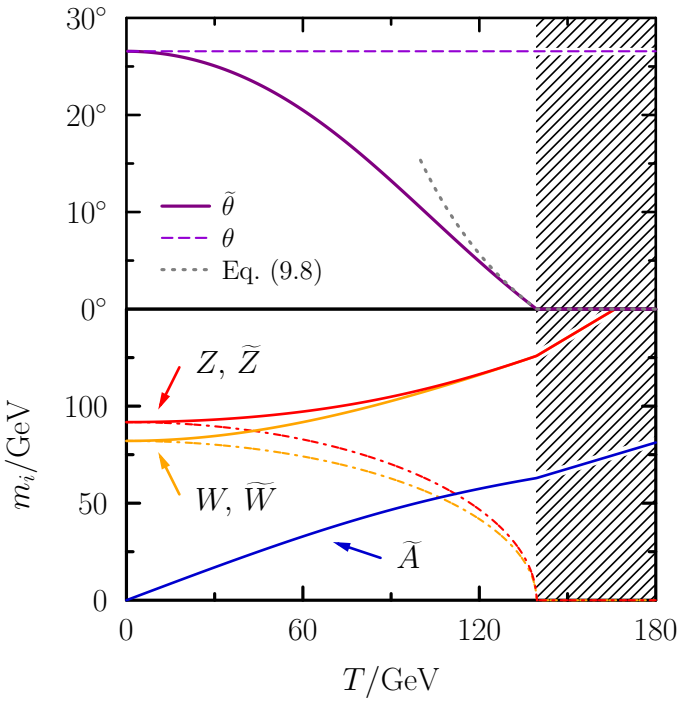

Figure 16: Top: Mixing angles as a function of temperature. Bottom: Physical masses for the spatial gauge fields (Z, W; dash-dotted) and temporal ones ($\widetilde{Z}, \widetilde{W}, \widetilde{A}$; solid). The hatched region is where $v = 0$, corresponding to the symmetric phase, as predicted by Eq. (9.3). See text for details.

and A_i. The scalar fields that interact with the neutrino (8.12) have propagators

$$\begin{aligned}
\langle W_0^+(\boldsymbol{k}) W_0^-(\boldsymbol{q})\rangle &= \frac{1}{k^2 + m_{\widetilde{W}}^2}\, \delta^{(d)}(\boldsymbol{k}+\boldsymbol{q})\,, \\
\langle Z_0(\boldsymbol{k}) Z_0(\boldsymbol{q})\rangle &= \left(\frac{\cos^2(\theta-\widetilde{\theta})}{k^2 + m_{\widetilde{Z}}^2} + \frac{\sin^2(\theta-\widetilde{\theta})}{k^2 + m_{\widetilde{A}}^2} \right) \delta^{(d)}(\boldsymbol{k}+\boldsymbol{q})\,, \\
\langle Z_0'(\boldsymbol{k}) Z_0'(\boldsymbol{q})\rangle &= \left(\frac{\cos^2(\theta+\widetilde{\theta})}{k^2 + m_{\widetilde{Z}}^2} + \frac{\sin^2(\theta+\widetilde{\theta})}{k^2 + m_{\widetilde{A}}^2} \right) \delta^{(d)}(\boldsymbol{k}+\boldsymbol{q})\,.
\end{aligned} \tag{9.10}$$

In Fig. 16 (lower panel) we show how the gauge boson masses depend on temperature. Here we made a simple estimate using $g = \frac{2}{3}$ and $g' = \frac{1}{3}$. (That gives $\theta \approx 26.57°$.) We obtain $v(T)$ from (9.3) and use $v(0) = 246.22$ GeV, $\lambda = 0.13$ and $y_t = 1$. This 'back-of-the-envelope' calculation predicts that symmetry is restored for temperatures above $T \approx 140$ GeV, somewhat short of the known value [22]. The upper panel of Fig. 16 compares the new mixing angle $\widetilde{\theta}(T)$ with the constant Weinberg angle. It is self-evident that thermal effects are important, even for fairly low temperatures. Indeed, the applicability of the three-dimensional theory relies on the 'hard scale' πT exceeding $m_Z(v)$, i. e. $T \gtrsim 30$ GeV which is observed. Some refined discussion of the couplings and mass parameters comes next, but it does not change this conclusion.

	$U_{\rm Y}(1)$	$SU_{\rm L}(2)$	$SU_{\rm c}(3)$
β_0	$-41/(24\pi)$	$+19/(24\pi)$	$+21/(12\pi)$
Λ/GeV	1.1046×10^{43}	3.1459×10^{-24}	0.0694×10^{0}
$\alpha(m_Z)$	0.009737(8)	0.03383(1)	0.1181(11)

Table 1: Parameters for the 1-loop running couplings in the three-dimensional EFT (9.1).

Running (and crawling) couplings

The overall accuracy $\widetilde{g}^4$ requires that 1-loop renormalised couplings are used in order to make predictions for Γ, at a given temperature. That includes not only g and g', but also the strong ($g_{\rm s}$), scalar (λ) and Yukawa couplings which enter indirectly via the loop corrections that generate thermal masses. Only the top-quark's Yukawa coupling $y_{\rm t}$ is taken into account here. That leaves five coupling parameters, which can be fixed using the five well-measured quantities G_F, m_H, m_Z, $\alpha_{\rm s}(m_Z)$ and $m_{\rm t}$ [16]. The three gauge couplings have the form

$$\alpha(\mu^2) \;=\; \big[\beta_0 \log(\mu^2/\Lambda^2)\big]^{-1}\,,$$

where β_0 is predicted by the 1-loop structure of the theory and Λ is an energy scale that is conventionally obtained by fixing the coupling at $\mu = m_Z$. (In this discussion, we mean m_Z at zero temperature.) The evolution of the top Yukawa and the Higgs self-coupling for $\mu > m_Z$ can be obtained by numerically solving the coupled system [148]

$$\begin{aligned}
\frac{\partial\, y_{\rm t}^2}{\partial \log\mu} &= \frac{y_{\rm t}^2}{8\pi^2}\Big[\,\frac{9}{2}y_{\rm t}^2 - \frac{17}{12}g'^2 - \frac{9}{4}g^2 - 8g_{\rm s}^2\,\Big]\,, \\
\frac{\partial\lambda}{\partial \log\mu} &= \frac{1}{8\pi^2}\Big[\,12\lambda^2 + 6\lambda y_{\rm t}^2 - 3y_{\rm t}^4 + \frac{3}{16}\big(g'^4 + 2g'^2g^2 + 3g^4\big) - \frac{3}{2}\lambda\big(g'^2 + 3g^2\big)\,\Big]\,.
\end{aligned} \tag{9.11}$$

Like in any QFT, the parameters in the three-dimensional effective theory need to be related to physical quantities. The initial $\overline{\rm MS}$ values at $\mu = m_Z$ will be 'matched' before the 1-loop runnings can be used, as per Ref. [149]. For the gauge theory $SU(N)$ in contact with n_f fermions and n_s scalars transforming in the fundamental representation,

$$\beta_0 \;=\; \frac{11N - 2n_f - \frac{1}{2}n_s}{12\pi}\,, \tag{9.12}$$

For QCD we use $N = 3$, $n_f = 6$ (quarks) and $n_s = 0$. For the EW theory we use $N = 2$, $n_f = 6$ (all left handed doublets) and $n_s = 1$ (the Higgs doublet). The hypercharge part, being an Abelian theory, has $\beta_0 = -\big(\sum_i Y_i^2\big)/(6\pi)$. Colour and generation are to be included in the sum over squared-charges. The fields Φ, $q_{\rm L}$, $u_{\rm R}$, $d_{\rm R}$, $\ell_{\rm L}$, $\nu_{\rm R}$ and $e_{\rm R}$ have the assigned Y-eigenvalues of $-\frac{1}{2}$, $-\frac{1}{6}$, $-\frac{2}{3}$, $+\frac{1}{3}$, $+\frac{1}{2}$, 0 and $+1$. Table 1 shows the particulars for each gauge group of the SM. The uncertainties at the Z-mass value are small due to the high precision of measurements of G_F, m_Z and the strong coupling. The non-Abelian theories have $\beta_0 > 0$ as they are asymptotically free.

The Higgs-self coupling and the top Yukawa take on the values $\lambda = 0.145(5)$ and $y_{\rm t}^2 = 0.966(5)$ at the Z-mass, originating from the measured Higgs and top masses. The

uncertainties in these measurements are slightly higher than those that set the gauge couplings, but inconsequential next to the sensitivity in choice of μ. We show the dependence of the couplings on the renormalisation scale μ in Fig. 17. Notably, g and g' are basically flat and so their choice of scale will be rather robust. λ has very mild μ-dependence, but is small. The strong and top Yukawa couplings are both large and vary the most – but they only appear inside loops at NLO. (See footnote 34.)

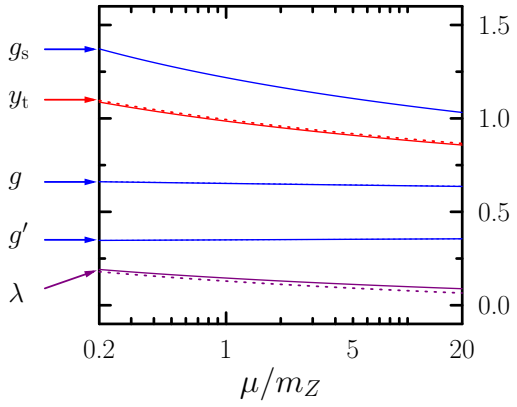

Figure 17: μ-dependence for 1-loop running; included are gauge couplings (blue), the scalar self-coupling (purple) and top Yukawa (red). Dashed lines (only visible for λ and y_t) indicate the SM runnings, differing by at most a few percent. The experimentally measured values are used to fixed the values of the couplings at $\mu = m_Z$, the uncertainty from them is insignificant.

Guided by the 'principle of minimal sensitivity', the optimal choice of scale with which to evaluate the couplings is $\mu \approx \pi T$ [108]. (See also Ref. [150] for recent developments at higher order.) To avoid an overcomplicated treatment when $\mu < m_Z$, in which one also leaves the scope of the EFT, we impose $\mu = \max[\pi T, m_Z]$. For temperatures below $m_Z/\pi \simeq 30$ GeV, the couplings are therefore frozen at their values, see Table 1.

10. Interaction rate to NLO accuracy

By virtue of loop diagrams being simpler in three-dimensions, the main work of calculating Γ is converted into careful bookkeeping. In Ref. [4] we applied the Feynman rules, given in Appendix B, and obtained the width from Eq. (8.11) for $k \sim T$. Recall that $S(\delta k) = b(k + \delta k, k)$, which is the Lorentz invariance breaking part of the self energy: $\Sigma(K) = -a\not{K} - b\gamma_0$. The LO contribution to S thus follows by adapting the graphs in Fig. 14 for the dimensionally reduced EFT. Since this theory incorporates thermal screening by using dressed propagators, taking the imaginary part already corresponds to $2 \to 2$ scattering processes [136]. The NLO contributions are those depicted in Fig. 18, each gauge boson line represents either a temporal or spatial propagation (as permitted by the interactions). As we shall see, $S'_{\text{LO}}(0)$ is a real quantity and therefore the LO and NLO contributions to the width are given by the first and second terms, respectively, in

$$\frac{\Gamma}{2} \;=\; \text{Im}\big[S_{\text{LO}}(0)\big] \;+\; \Big\{\text{Im}\big[S_{\text{NLO}}(0)\big] \;-\; S'_{\text{LO}}(0)\,\text{Im}\big[S_{\text{NLO}}(0)\big]\Big\} + \;\ldots\,, \tag{10.1}$$

where N^{2}LO and beyond are omitted.

We again specialise to a neutrino moving in the z-direction, so that the leptonic interactions occur through (8.12) and the free propagators for the negative helicity spinors, $\psi(k_0, \boldsymbol{k})$ and $\chi(k_0, \boldsymbol{k})$ (with $k_0 = k + \delta k$), are proportional to $(\delta k + i0^+)^{-1}$. The first perturbative order seems like (8.6), but performed in the effective three-dimensional theory.

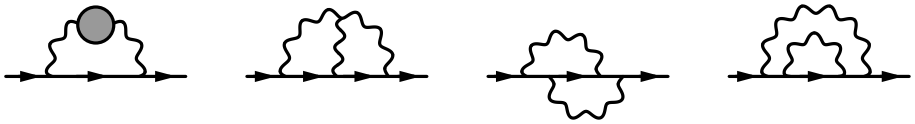

Figure 18: NLO contributions to the neutrino width. The wiggly lines are EW gauge bosons that couple with their temporal and z-components *à la* Eq. (8.12). These are treated in the dimensionally reduced EFT, meaning that each diagram above actually 'unpacks' into several graphs. The gray blob represents one-loop self-energies, which includes contributions from ghosts and the scalar field.

Rather than the function $\mathcal{B}$ encountered there, the exemplary integral here reads

$$\int_{\boldsymbol{p}} \frac{1}{\delta k - p_z + i0^+} \frac{1}{\boldsymbol{p}^2 + m_V^2} \;=\; \int_{\boldsymbol{p}_\perp} \left\{ \frac{i}{2}\Delta(m_V) + \delta k \; \mathcal{P}\!\int_{-\infty}^{+\infty} dp_z \, \frac{1}{p_z^2(\boldsymbol{p}^2 + m_V^2)} \right\} + \mathcal{O}(\delta k^2)\,, \tag{10.2}$$

where $\mathcal{P}$ indicates that the p_z-integration is meant in the Cauchy principal value sense, and $\Delta(m_V) = (p_\perp^2 + m_V^2)^{-1}$ arises from the propagator with $p_z \approx 0$. Here we have decomposed $\boldsymbol{p} = (\boldsymbol{p}_\perp, p_z)$ and used the shorthand notation

$$\int_{\boldsymbol{p}_\perp} \coloneqq \int \frac{d^{d-1}\boldsymbol{p}_\perp}{(2\pi)^{d-1}}$$

for integrals in the transverse plane. The first term in the curly braces of Eq. (10.2) is a prototype for each member of $\mathrm{Im}[S_{\text{LO}}(0)]$. Summing them all up gives

$$\Gamma_{\text{LO}} \;=\; \widetilde{g}^2 \frac{T}{4} \int_{\boldsymbol{p}_\perp} \Big\{ \Delta_Z - \cos^2(\theta - \widetilde{\theta})\Delta_{\widetilde{Z}} - \sin^2(\theta - \widetilde{\theta})\Delta_{\widetilde{A}} + 2\cos^2\theta\big(\Delta_W - \Delta_{\widetilde{W}}\big) \Big\}\,, \tag{10.3}$$

where $\Delta_i \coloneqq \Delta(m_i)$.

We do not discuss the individual contributions to NLO that arise from Fig. 18, here we simply state the result for completeness. Some basic functions A, $\dot{A}$, B, $\dot{B}$ and B_T, are enough to cover all types of loop integrals that arise. The simplest are

$$A(m) \;=\; \int_{\boldsymbol{q}} \frac{1}{q^2 + m^2}\,, \qquad B(m_1, m_2) \;=\; \int_{\boldsymbol{q}} \frac{1}{(q^2 + m_1^2)\big[(\boldsymbol{p} - \boldsymbol{q})^2 + m_2^2\big]}\,.$$

Evaluating their dimensionally regularised forms in $d = 3$ gives

$$A(m) \;=\; -\frac{m}{4\pi}\,, \qquad B(m_1, m_2) \;=\; \frac{1}{4\pi|\boldsymbol{p}|} \arctan\!\left(\frac{|\boldsymbol{p}|}{m_1 + m_2}\right). \tag{10.4}$$

In many cases, cutting the two-loop diagrams (with external momentum $\boldsymbol{k}$ in the z-direction) requires B at transverse external momentum: $\boldsymbol{p} = (\boldsymbol{p}_\perp, 0)$, as in (10.3). The shorthand for derivatives of these functions are defined by,

$$\dot{A} \;=\; \frac{\partial A}{\partial m^2}\,, \qquad \dot{B} \;=\; \frac{\partial B}{\partial m_1^2} + \frac{\partial B}{\partial m_2^2}\,. \tag{10.5}$$

Additionally, we require the transverse projection of a tensor integral,

$$\begin{aligned} B_T(m_1, m_2) \;&=\; \frac{1}{d-1}\Big(\delta_{ij} - \frac{p_i p_j}{p^2}\Big) \int_{\boldsymbol{q}} \frac{q_i q_j}{(q^2 + m_1^2)\big[(\boldsymbol{p} - \boldsymbol{q})^2 + m_2^2\big]} \\ &=\; \frac{1}{4(d-1)p^2}\Big\{ \big[p^2 - m_1^2 + m_2^2\big]A(m_1) + \big[p^2 - m_2^2 + m_1^2\big]A(m_2) \\ &\qquad - \big[p^4 + 2p^2(m_1^2 + m_2^2) + (m_1^2 - m_2^2)^2\big]B(m_1, m_2) \Big\}\,. \end{aligned}$$

Even though B_T is reducible into A and B, withholding that simplification keeps the end result shorter. Altogether, these 'masters' help to express the final NLO result, see Ref. [4] for more details.

Choosing to represent the two-loop contributions to the width as a linear combination of the functions introduced above, we find

$$\begin{aligned}\Gamma_{\rm NLO} \;=\; \widetilde{g}^4\frac{T^2}{8}\lim_{m_A\to 0}\int_{\boldsymbol{p}_\perp}\Big\{\sum_i\big(\,c_iA(m_i)+\dot{c}_i\dot{A}(m_i)\,\big) \\ +\sum_{i,j}\big(\,c_{ij}B(m_i,m_j)+c^T_{ij}B_T(m_i,m_j)+\dot{c}_{ij}\dot{B}(m_i,m_j)\,\big)\Big\}\,.\end{aligned} \tag{10.6}$$

We note that dependence on the gauge parameter falls away, i.e. no functions include the unphysical masses $\xi\, m_W^2$, etc. The 'photon mass' m_A was introduced as an intermediate regulator, appearing because charged particles crop up in loops at NLO. Explicit sums over masses, needed in (10.6), are as follows[34]:

$$\begin{aligned}\sum_i c_iA(m_i) \;=\; & \\ &\Big[\;A(m_H)+\frac{m_Z^2}{m_H^2}\Big\{\,(d-1)A(m_Z)+\cos^2(\theta-\widetilde{\theta})A(\widetilde{m}_Z)+\sin^2(\theta-\widetilde{\theta})A(\widetilde{m}_A)\,\Big\}\\ &+2\frac{m_W^2}{m_H^2}\Big\{\,(d-1)A(m_W)+A(\widetilde{m}_W)\,\Big\}\;\Big]\times\\ &\Big[\;\Delta_Z^2-\big(\cos^2(\theta-\widetilde{\theta})\Delta_{\widetilde{Z}}+\sin^2(\theta-\widetilde{\theta})\Delta_{\widetilde{A}}\big)^2+2\cos^4\theta\big(\Delta_W^2-\Delta_{\widetilde{W}}^2\big)\;\Big]\\ -4\cos^4\theta&\Big[\;(d-2)\cos^2\theta\,A(m_Z)+\cos^2\widetilde{\theta}\,A(\widetilde{m}_Z)+\sin^2\widetilde{\theta}\,A(\widetilde{m}_A)\\ &+(d-2)A(m_W)+A(\widetilde{m}_W)\;\Big]\big(\Delta_W^2-\Delta_{\widetilde{W}}^2\big)\\ +2\cos^2\theta&\Big[\;(d-2)A(m_W)+A(\widetilde{m}_W)\;\Big]\times\\ &\Big[\;\big(\cos\widetilde{\theta}\cos(\theta-\widetilde{\theta})\Delta_{\widetilde{Z}}-\sin\widetilde{\theta}\sin(\theta-\widetilde{\theta})\Delta_{\widetilde{A}}\big)^2-\cos^2\theta\,\Delta_Z^2\;\Big]\\ +A(m_W)&\sin(2\theta)\times\\ \Big[\;&\sin(2\theta)\Delta_Z^2+\sin(2\widetilde{\theta})\big(\sin^2(\theta-\widetilde{\theta})\Delta_{\widetilde{A}}^2-\cos^2(\theta-\widetilde{\theta})\Delta_{\widetilde{Z}}^2\big)-\cos(2\widetilde{\theta})\sin[2(\theta-\widetilde{\theta})]\Delta_{\widetilde{A}}\Delta_{\widetilde{Z}}\;\Big]\,,\end{aligned} \tag{10.7}$$

[34] The appearance of contributions from particles that do not couple directly to the negative helicity states in (8.12) arise due to the gauge boson self energy corrections,

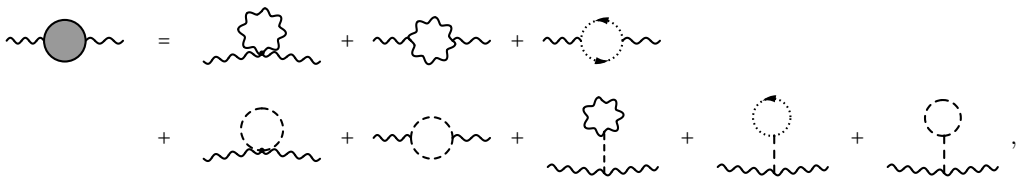

to 1-loop order. This explains why the NLO result depends on m_H etc. The diagrams are like in Fig. 18, with dashed lines being Higgs scalars and dotted lines being the ghosts. Each wiggly line stands for a gauge boson that could be a temporal or spatial field (as allowed by the Feynman rules, see Appendix B).

$$\sum_i \dot{c}_i \dot{A}(m_i) \;=\; \tag{10.8}$$
$$\begin{aligned}
&8\cos^4\theta\Big[\;\cos^2\theta\,\dot{A}(m_Z)-\cos^2\widetilde{\theta}\,\dot{A}(\widetilde{m}_Z)+\sin^2\theta\,\dot{A}(m_A)-\sin^2\widetilde{\theta}\,\dot{A}(\widetilde{m}_A)\\
&\qquad+\dot{A}(m_W)-\dot{A}(\widetilde{m}_W)\;\Big]\Big(\;\Delta_{\widetilde{W}}-\Delta_W\;\Big)\\
&+8\cos^3\theta\Big[\;\dot{A}(m_W)-\dot{A}(\widetilde{m}_W)\;\Big]\Big(\;\cos\widetilde{\theta}\cos(\theta-\widetilde{\theta})\,\Delta_{\widetilde{Z}}-\sin\widetilde{\theta}\sin(\theta-\widetilde{\theta})\,\Delta_{\widetilde{A}}-\cos\theta\,\Delta_Z\;\Big)\;,
\end{aligned}$$

$$\sum_{i,j} c_{ij} B(m_i,m_j) \;=\; \tag{10.9}$$
$$\begin{aligned}
&2m_Z^2 B(m_H,m_Z)\Delta_Z^2\\
&-2m_Z^2\Big[\cos^2(\theta-\widetilde{\theta})B(m_H,\widetilde{m}_Z)+\sin^2(\theta-\widetilde{\theta})B(m_H,\widetilde{m}_A)\Big]\times\\
&\qquad\Big(\cos^2(\theta-\widetilde{\theta})\Delta_{\widetilde{Z}}+\sin^2(\theta-\widetilde{\theta})\Delta_{\widetilde{A}}\Big)^2\\
&+4m_W^2\cos^4\theta\Big[\;\big(B(m_H,m_W)+B(m_Z,m_W)\big)\Delta_W^2-\big(B(m_H,\widetilde{m}_W)+B(m_Z,\widetilde{m}_W)\big)\Delta_{\widetilde{W}}^2\;\Big]\\
&-4m_W^2\cos^2\theta\Big(\cos^2(\theta+\widetilde{\theta})B(\widetilde{m}_Z,m_W)+\sin^2(\theta+\widetilde{\theta})B(\widetilde{m}_A,m_W)\Big)\Delta_W^2\\
&+16\cos^4\theta\Big[\;p_\perp^2\Big\{\;\cos^2\theta\,\big(B(m_Z,m_W)\Delta_W^2-B(m_Z,\widetilde{m}_W)\Delta_{\widetilde{W}}^2\big)\\
&\qquad\qquad+\;\sin^2\theta\,\big(B(m_A,m_W)\Delta_W^2-B(m_A,\widetilde{m}_W)\Delta_{\widetilde{W}}^2\big)\\
&\qquad\qquad-\;\big(\cos^2\widetilde{\theta}\,B(\widetilde{m}_Z,m_W)+\sin^2\widetilde{\theta}\,B(\widetilde{m}_A,m_W)\big)\Delta_{\widetilde{W}}^2\Big\}\\
&\qquad\qquad+\;\big(\cos^2\widetilde{\theta}\,B(\widetilde{m}_Z,\widetilde{m}_W)+\sin^2\widetilde{\theta}\,B(\widetilde{m}_A,\widetilde{m}_W)\big)\Delta_W\quad\Big]\\
&-4m_W^2(4\cos^2\theta-1)\big(B(m_W,m_W)\Delta_Z^2+\cos^2\theta B(m_Z,m_W)\Delta_W^2\big)\\
&+8\cos^4\theta\,\big(B(m_W,m_W)+B(\widetilde{m}_W,\widetilde{m}_W)\big)\Delta_Z+B(m_W,\widetilde{m}_W)\times\\
&\frac{4}{m_Z^2}\Big[\;\cos^2\theta-2m_W^2\Big(\cos^2(\theta-\widetilde{\theta})\,\Delta_{\widetilde{Z}}+\sin^2(\theta-\widetilde{\theta})\,\Delta_{\widetilde{A}}\Big)\\
&-\big((m_W^2-\widetilde{m}_W^2)^2+2p_\perp^2(m_W^2+\widetilde{m}_W^2)+p_\perp^4\big)\Big(\cos(\theta-\widetilde{\theta})\cos\widetilde{\theta}\,\Delta_{\widetilde{Z}}-\sin(\theta-\widetilde{\theta})\sin\widetilde{\theta}\,\Delta_{\widetilde{A}}\Big)^2\Big]\;,
\end{aligned}$$

$$\sum_{i,j} \dot{c}_{ij} \dot{B}(m_i,m_j) \;=\; \tag{10.10}$$
$$\begin{aligned}
&8\cos^4\theta\Big[\;\cos^2\theta\,\big(\dot{B}(m_Z,m_W)-\dot{B}(m_Z,\widetilde{m}_W)\big)+\cos^2\widetilde{\theta}\,\big(\dot{B}(\widetilde{m}_Z,\widetilde{m}_W)-\dot{B}(\widetilde{m}_Z,m_W)\big)\\
&\qquad+\;\sin^2\theta\,\big(\dot{B}(m_A,m_W)-\dot{B}(m_A,\widetilde{m}_W)\big)+\sin^2\widetilde{\theta}\,\big(\dot{B}(\widetilde{m}_A,\widetilde{m}_W)-\dot{B}(\widetilde{m}_A,m_W)\big)\\
&\qquad+\;\tfrac{1}{2}\big(\dot{B}(m_W,m_W)+\dot{B}(\widetilde{m}_W,\widetilde{m}_W)\big)-\dot{B}(\widetilde{m}_W,m_W)\;\Big]\;,
\end{aligned}$$

$$\sum_{i,j} c_{ij}^T B_T(m_i,m_j) \;=\; \tag{10.11}$$
$$\begin{aligned}
&2\Big[B_T(m_H,m_W)+\big(4(d-2)\cos^4\theta+1\big)B_T(m_W,m_W)+4\cos^4\theta\,B_T(\widetilde{m}_W,\widetilde{m}_W)\Big]\Delta_Z^2\\
&+4\cos^4\theta\Big[\;B_T(m_H,m_W)+\big(4(d-2)\cos^2\theta+1\big)B_T(m_Z,m_W)+4\cos^2\widetilde{\theta}\,B_T(\widetilde{m}_Z,\widetilde{m}_W)\\
&\qquad+4(d-2)\sin^2\theta\,B_T(m_A,m_W)+4\sin^2\widetilde{\theta}\,B_T(\widetilde{m}_A,\widetilde{m}_W)\;\Big]\Delta_W^2\;.
\end{aligned}$$

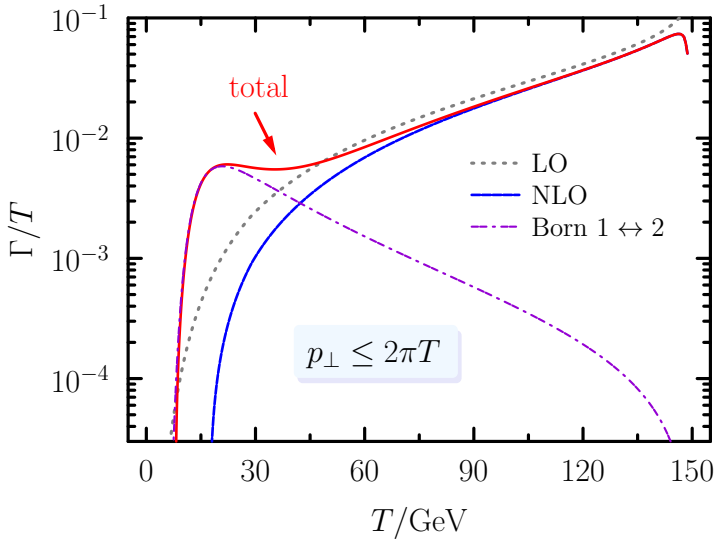

Figure 19: The active neutrino damping rate, to order $\widetilde{g}^4$, including both 'low' and 'high' temperature results. The former are Born $1 \leftrightarrow 2$ processes, and the latter originate from $2 \to 2$ scatterings involving soft gauge particles. The total is a sum of the Born rate and the NLO width.

The limit $m_A \to 0$ can be taken without issue in most cases, but a nuance crops up for terms in (10.8) and (10.10) where $\dot{A}$ or $\dot{B}$ contain the photon mass. Once these potentially divergent terms are combined, the limit is safe due to (here $d = 3$)

$$\lim_{m_A \to 0} \Big[\dot{B}(m_A, m_i) - \dot{A}(m_A) \Delta_i \Big] \;=\; \frac{m_i^2 - p^2}{8\pi\, m_i} \Delta_i^2 \,,$$

which is needed for $i = \{W, \widetilde{W}\}$. Besides this careful limit, there are no issues. The entire integrand matches up with the limit $|\boldsymbol{p}_\perp| \gg m_i$ (for all i) in Ref. [136]. For actually evaluating the integral over $\boldsymbol{p}_\perp$, we impose a cut-off of $2\,k$ with $k = \pi T$ (beyond which point, the integration has basically converged anyway [4]). We plot the result from (10.3) and (10.6), along with the Born result from (8.6) (with $\omega = \pi T$) in Fig. 19. The NLO correction is always negative, and $\sim 15\%$ for $80 < T/\mathrm{GeV} < 140$. It is worth noting that there is a significant cancellation between all the separate NLO pieces (10.7)-(10.11), which leads to the correction being small. At lower temperatures, the NLO correction can be as large as 40%, partly because the LO rate becomes unusually small there. This is not unexpected: When $m_i \gtrsim \pi T$ the EFT method is no longer applicable.

Returning to the discussion in Sec. 7, a hypothetical generation of sterile neutrinos in the early universe would have far-reaching consequences for matter-antimatter asymmetry [151, 152]. The feasibility of leptogenesis depends upon how 'efficient' the $\mathcal{CP}$-violating oscillations are at leading to lepton and baryon asymmetry [153]. Although our calculation is not expected to have much effect on the latter, lepton asymmetries in the benchmark point from Ref. [154] would be reduced by about one percent due to the NLO correction.

Part III

Gravitational waves and (shear) viscosity

11. Prospects for the weakest force

The first direct detection of gravitational waves (GWs) was announced by the LIGO and Virgo collaborations in 2016 [155]. This achievement has delivered scientists an entirely new way of observing the universe and, understandably, gained the topic a new vogue. A wealth of measurements have already been made of collapsing binary systems, consisting of co-orbiting black holes or neutron stars [156]. Cosmological sources of GWs are also a high priority target for future detectors, such as LISA [29].

Just as the CMB consists of *electromagnetic* radiation, the analogous background for GWs is expected to be produced by a large number of weak, stochastic sources. The spectral features of this radiation can be characterised by its distribution of energy density, as a function of frequency. This is conventionally done via the dimensionless ratio

$$\Omega_{\rm GW}(\omega) \;:=\; \frac{1}{\varepsilon_{\rm crit}}\frac{d\varepsilon_{\rm GW}}{d\log\omega}\,, \tag{11.1}$$

where $d\varepsilon_{\rm GW}$ is energy density of gravitational radiation in a frequency[35] range ω to $\omega + d\omega$. The critical energy density $\varepsilon_{\rm crit} = 3H_0^2/(8\pi G)$ is the minimum energy density required to 'close' the universe (today). Bayesian parameter estimates within the ΛCDM model give a present energy density nearly equal to $\varepsilon_{\rm crit}$. A conservative constraint on a GW background,

$$\Omega_{\rm GW} < 1.7\times10^{-7} \quad \text{for} \quad \frac{\omega}{2\pi} \in [20, 86]\ \text{Hz}\,, \tag{11.2}$$

has been obtained by LIGO [155]. We should note that there is still tension in the measured value of H_0 [125, 157] (which determines $\varepsilon_{\rm crit}$), but this will not concern us here.

There are many possible sources of a stochastic GW background, ranging from cosmological to astrophysical [158]. The relative importance among compact binaries, fluctuations during inflation, first order phase transitions and thermal noise is still being debated. We will focus on two possible mechanisms for GW radiation here. Those GWs generated through friction at the interface of expanding bubbles [30, 31], and the emission from a 'black body' in thermal equilibrium [33, 34].

Einstein's theory of gravity has so far resisted inclusion into the SM. Simply adding a 'graviton', as a massless gauge boson, cannot yet be done in a manner that *i*) the resulting quantum field theory is renormalisable and *ii*) is consistent with general relativity. This problem is one of the major contemporary issues in theoretical physics, and will hopefully be overcome in the future. A pragmatic (but well-founded) approach to incorporate gravitational effects into the SM is to view it as an effective theory [159]. Requirement *i*) is not an obstruction from this point of view, where we merely assume that the low energy limit of some yet-unknown theory is general relativity. EFTs benefit from a clear hierachy of scales, with corrections from the 'full theory' being suppressed by powers of $m_{\rm Pl} \simeq 1.22\times10^{19}$ GeV. Given the current mass spectrum and typical energies probed in SM physics, this programme should be quite robust. For instance, an extremely small coupling parameter,

$$\alpha_{\rm g} \;\equiv\; (m_t/m_{\rm Pl})^2 \;\sim\; 10^{-17}\,,$$

would result from the mediation of a graviton between two top quarks.

[35] We assume $\omega = k$ throughout this section, where $\boldsymbol{k}$ is the momentum of the wave.

In a 'weak' gravitational field, the curvature of spacetime is minimal. Hence we may suppose that the metric tensor has components almost equal to their Minkowskian values, which we now denote by $\eta_{\mu\nu} = \mathrm{diag}(+,-,-,-)$. The full metric can be written

$$g_{\mu\nu} \equiv \eta_{\mu\nu} + \kappa\, h_{\mu\nu}\ ; \quad \kappa^2 := 32\pi G\,. \tag{11.3}$$

The factor κ is not standard, but we include it so that $h_{\mu\nu}$ will correspond to a canonically normalised 'tensor boson' [160]. Since $G = 1/m_{\rm Pl}^2$ and $g_{\mu\nu}$ is scaleless, this field has a dimension of mass. If the perturbation from flat spacetime is small, we may assume that $h_{\mu\nu} \ll m_{\rm Pl}$. In this regime the inverse metric reads

$$g^{\mu\nu} \approx \eta^{\mu\nu} - \kappa\, h^{\mu\nu} + \ldots\ .$$

12. Effective theory of the gravitational field

Let us view general relativity as the low energy limit of some 'more general' theory, and accept it as provisional [159]. The Einstein-Hilbert action follows from the Lagrangian density,

$$\mathcal{L}_{\rm EH} = \frac{2}{\kappa^2}\sqrt{-\det g}\,\big(R + 2\Lambda\big)\,, \tag{12.1}$$

where the parameter Λ denotes the cosmological constant and $\det g$ is the determinant of the metric tensor[36]. We assume $\Lambda = 0$ and work in $D = d+1$ spacetime dimensions in what follows. Here $R = R^{\mu}{}_{\mu}$ and $R_{\mu\nu} = R^{\alpha}{}_{\mu\alpha\nu}$ in terms of the Riemann curvature tensor

$$R^{\alpha}{}_{\beta\mu\nu} = \big(\partial_\mu \Gamma^{\alpha}{}_{\beta\nu} + \Gamma^{\alpha}{}_{\mu\lambda}\Gamma^{\lambda}{}_{\nu\beta}\big) - \big(\mu \leftrightarrow \nu\big)\,.$$

The Christoffel symbols are given by derivatives of the metric $\Gamma^{\alpha}{}_{\mu\nu} = \frac{1}{2}\big(\partial_\mu g^{\alpha}{}_{\nu} + \partial_\nu g^{\alpha}{}_{\mu} - \partial^\alpha g_{\mu\nu}\big)$. The action derived from (12.1) is invariant under arbitrary coordinate transformations. Such a freedom in the metric $g_{\mu\nu}$ can be viewed as a generalised gauge transformation [161]. For instance, in the harmonic gauge[37] the metric satisfies

$$\Gamma^{\alpha}{}_{\mu\nu} g^{\mu\nu} = 0\ ; \quad \alpha = \{0, 1, \ldots, d\}\,,$$

which can be accommodated by augmenting (12.1) with a suitable gauge-fixing term [162].

Omitting self-interactions of the graviton field, we do not encounter any of the serious difficulties with renormalisation. We shall treat the GW as we treated the photon in Part I, focusing only on its coupling to the rest of the SM [163]. Now, without a cosmological constant, Einstein's field equations are

$$R_{\mu\nu} - \frac{1}{2} g_{\mu\nu}\, R = \frac{\kappa^2}{4}\, T_{\mu\nu}\,, \tag{12.2}$$

which constitutes a non-linear set of partial differential equations for $g_{\mu\nu}$. Eq. (12.2) follows from $\mathcal{L}_{\rm EH}$ by a variation with respect to the graviton field, which we conjecture to be close to flat. Upon substituting (11.3) into the field equations and ignoring terms of order κ^2 and higher, one obtains the classical wave equation

$$\ddot{h}_{\mu\nu} - \nabla^2 h_{\mu\nu} = \frac{\kappa}{2}\, T_{\mu\nu}\,. \tag{12.3}$$

Here a dot indicates differentiation with respect to time and ∇^2 is the Laplacian.

[36] In general, $\det g = \dfrac{1}{(d+1)!}\, \epsilon^{\mu_0\mu_1\cdots\mu_d} \epsilon^{\nu_0\nu_1\cdots\nu_d}\, g_{\mu_0\nu_0}\, g_{\mu_1\nu_1} \cdots g_{\mu_d\nu_d}$.

[37] Sometimes also referred to as the *de Donder* gauge.

Polarisation modes: h_+ and $h_\times$

The perturbed metric from Eq. (11.3) introduces a dynamical tensor gauge field, which is expected to have a redundancy in its components that represent the physical degrees of freedom.

Due to symmetry in the source in the Einstein equations (12.2), $h_{\mu\nu}$ has (at first glance) $\frac{1}{2}D(D+1)$ independent coefficients. Specialising to the harmonic gauge leads to $\partial^\mu h_{\mu\nu} = 0$ and thus imposes an additional D constraints. It can furthermore be shown, from the freedom to choose coordinates, that one can assume $h_\mu{}^\mu = 0$ and $u^\mu h_{\mu\nu} = 0$ where u^μ is a four-velocity of some distinguished frame [161]. The spin-2 GW is thus made traceless and transverse (TT).

We take $u^\mu = (1, \mathbf{0})$, i. e. the local rest frame, so that $g_{0\nu} = 0$ and $g_{00} = 1$. This implies that the metric does not distort measurements of time and such a frame[38] is sometimes called a *synchronous* reference system [164]. At each point in space, the time coordinate is the proper time. Since $h_{00} = 0$, the tensor h_{ij} is traceless and therefore represents the strain due to stretching and contracting of spatial measurements.

The TT requirements impose D new conditions overall, since one of the transverse conditions gives $\partial^\mu h_{\mu 0} = 0$ automatically. Altogether, the remaining degrees of freedom are

$$\underset{\text{(symmetry)}}{\frac{D(D+1)}{2}} \quad \underset{\text{(harmony)}}{-\,D} \quad \underset{\text{(traceless)}}{-\,1} \quad \underset{\text{(transverse)}}{-\,(D-1)} \quad = \quad \frac{D(D-3)}{2}\,,$$

which evaluates to two independent polarisations for $D = 4$. Compare that with a photon, which has $(D-2)$ polarisation states in general and thus also two in the physical case.

It is simple to transform any graviton into the TT-form by an appropriate projector,

$$h^{\mathrm{TT}}_{\mu\nu} \;=\; \mathbb{L}_{\mu\nu,\alpha\beta}\, h^{\alpha\beta}\,. \tag{12.4}$$

(Here the , separating $\mu\nu$ and $\alpha\beta$ does not represent a partial derivative.) To construct the explicit form for $\mathbb{L}$, let us consider the fields in momentum space. For a GW with frequency ω and momentum $\boldsymbol{k}$, the gauge condition yields $K^\mu h^{\mathrm{TT}}_{\mu\nu} = 0$ where $K = (\omega, \boldsymbol{k})$. Since $h^{\mathrm{TT}}_{0\nu} = 0$, we actually have $k^i h^{\mathrm{TT}}_{i\nu} = 0$. This latter equality can be acquired using an operator which projects onto the direction orthogonal with $\boldsymbol{k}$. Let us introduce the longitudinal (L) and transverse (T) projectors in the local rest frame,

$$\mathbb{P}^L_{\mu\nu} \;=\; \frac{1}{K^2}\begin{pmatrix} \boldsymbol{k}^2 & \omega\boldsymbol{k} \\ \omega\boldsymbol{k} & \omega^2 \hat{k}_i \hat{k}_j \end{pmatrix}, \qquad \mathbb{P}^T_{\mu\nu} \;=\; \begin{pmatrix} 0 & 0 \\ 0 & (\delta_{ij} - \hat{k}_i \hat{k}_j) \end{pmatrix}. \tag{12.5}$$

The latter allows us to construct

$$\mathbb{L}_{\mu\nu,\alpha\beta} \;\coloneqq\; \frac{1}{2}\big(\,\mathbb{P}^T_{\mu\alpha}\mathbb{P}^T_{\nu\beta} + \mathbb{P}^T_{\mu\beta}\mathbb{P}^T_{\nu\alpha}\big) \;-\; \frac{1}{D-2}\,\mathbb{P}^T_{\mu\nu}\mathbb{P}^T_{\alpha\beta}\,, \tag{12.6}$$

which achieves all the goals desired for (12.4) and is symmetric in $\mu\nu$ and $\alpha\beta$ separately, as well as pairwise. It is projector in the sense that $\mathbb{L}_{\mu\nu,\alpha\beta}\mathbb{L}_{\alpha\beta,\gamma\delta} = \mathbb{L}_{\mu\nu,\gamma\delta}$, namely idempotency in the first and second pairs of indices. Some properties are worth stating here:

$$\begin{aligned} g^{\mu\nu}\mathbb{L}_{\mu\nu,\alpha\beta} \;&=\; 0\,, \\ g^{\mu\alpha}\mathbb{L}_{\mu\nu,\alpha\beta} \;&=\; \frac{D(D-3)}{2(D-2)}\,\mathbb{P}^T_{\nu\beta}\,, \qquad g^{\mu\alpha}g^{\nu\beta}\mathbb{L}_{\mu\nu,\alpha\beta} = \frac{D(D-3)}{2}\,. \end{aligned} \tag{12.7}$$

[38] The choice is not unique because any transformation that only affects the spatial components will produce another frame with the same properties.

The last equality gives, of course, the number of polarisations in D spacetime dimensions.

Let us consider how gravitational waves are radiated by an arbitrary body of matter (for $D = 4$), whose components move with velocities small relative to the speed of light. The analogous problem in electrodynamics, concerning time-dependent fields, has a well known solution [165]. Here the same arguments are readily adapted for gravity [161].

We write the general solution to (12.3) in the form

$$h_{\mu\nu}(t,\boldsymbol{x}) \;=\; \frac{\kappa}{8\pi}\int_{\boldsymbol{x}'} \frac{T_{\mu\nu}\big(t-|\boldsymbol{x}-\boldsymbol{x}'|,\,\boldsymbol{x}'\big)}{|\boldsymbol{x}-\boldsymbol{x}'|}\,, \tag{12.8}$$

where the energy-momentum tensor is evaluated at a *retarded time*. Being non-relativistic, the constituents of the system cannot catch up with the propagating wave, i. e. to distances large compared with the wavelength of the radiated wave. Hence, if we choose the origin anywhere in the interior of the system,

$$h_{\mu\nu}(t,\boldsymbol{x}) \;=\; \frac{\kappa}{8\pi|\boldsymbol{x}|}\int_{\boldsymbol{x}'} T_{\mu\nu}\big(t-|\boldsymbol{x}|,\,\boldsymbol{x}'\big) \;+\; \ldots\,, \tag{12.9}$$

by approximating $|\boldsymbol{x}-\boldsymbol{x}'| \approx |\boldsymbol{x}|$ in (12.8). This is justified for coordinates $\boldsymbol{x}$ that are far away from the localised source and the solution represents an outgoing spherical wave that originated from the system, see Fig. 20.

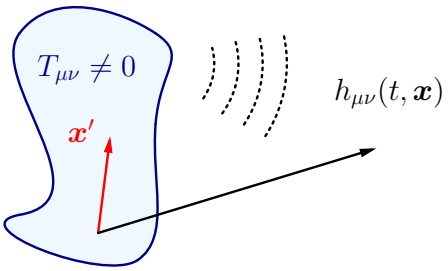

Figure 20: The GW far away from a localised distribution of mass and energy takes the form of a spherical wave. In Eq. (12.8), the integration extends over the volume where $T_{\mu\nu}$ is different from zero, so that $|\boldsymbol{x}| \gg |\boldsymbol{x}'|$. The source is evaluated at a retarded time, since the wave propagates at the speed of light.

In that case, $h_{0\nu} = h_{\nu 0}$ $(\nu = 0,1,2,3)$ is time independent thanks to Gauss' theorem: Integrating both sides of $\partial_t T_{0\nu} = \nabla_i T_{i\nu}$ over a volume enclosing the region where $T_{\mu\nu} \neq 0$ gives zero due to no flux on the volume's surface. As already discussed, we may take these time independent components of the field to vanish by a suitable change of reference frame that brings $h_{\mu\nu}$ into the TT gauge.

However, spatial components of the GW, h_{ij} $(i,j = 1,2,3)$, can vary with time. Equation (12.9) may be re-expressed through the virial theorem[39]:

$$h_{ij}(t,\boldsymbol{x}) \;\simeq\; \frac{\kappa}{48\pi\,|\boldsymbol{x}|}\,\ddot{\mathcal{Q}}_{ij}\big(t-|\boldsymbol{x}|\big)\,, \tag{12.10}$$

where the mass quadrupole moment is defined by [164]:

$$\mathcal{Q}_{ij}(t) \;:=\; \int_{\boldsymbol{x}} T_{00}(t,\boldsymbol{x})\,\big(3\,x_i\,x_j \;-\; x^2\,\delta_{ij}\big).$$

[39] Here we take the form

$$\int_{\boldsymbol{x}} T_{ij}(t,\boldsymbol{x}) \;=\; \frac{1}{2}\,\frac{\partial^2}{\partial t^2}\int_{\boldsymbol{x}} T_{00}(t,\boldsymbol{x})\,x_i\,x_j\;.$$

Although this does not directly give (12.10), the trace part of $h_{ii} = 0$ can be ensured by a coordinate transformation. That also brings the quadrupole moment as it is defined in textbooks like Ref. [164].

In other words, (12.10) gives the lowest-order contribution to radiation from slow-moving masses. Thus only quadrupole and higher moments of the energy density can radiate gravitationally, unlike in the electromagnetic case which can receive radiation from a charge dipole. A 'mass dipole' would correspond to the system's centre of mass, whose first time derivative yields a *conserved* quantity – the total momentum of the system.

Toy example

It is worth dwelling on a particularly simple case to illustrate the important features of GW production. We consider a point mass undergoing elliptical motion at a constant angular frequency in the xy-plane, and evaluate $h_{\mu\nu}$ far away (cf. Fig. 20).

Let the point mass' trajectory be described by

$$\boldsymbol{r}(t) \;=\; \big(\, a\cos(\omega t),\, b\sin(\omega t),\, 0\,\big)\,, \tag{12.11}$$

so that a and b are the semi-major and -minor axes of the ellipse (respectively, if $a \geq b$). If the mass of the object is denoted by m, the energy density reads $T_{00} = m\,\delta^{(3)}\big(\boldsymbol{x} - \boldsymbol{r}(t)\big)$ and the associated acceleration of the quadrupole moment can easily be calculated. Its only non-zero components are given by

$$\begin{aligned} \ddot{\mathcal{Q}}_{xx} \;&=\; -2m\,\omega^2\,a^2\,\cos(2\omega t)\,, \qquad \ddot{\mathcal{Q}}_{yy} \;=\; -2m\,\omega^2\,b^2\,\cos(2\omega t)\,, \\ \ddot{\mathcal{Q}}_{xy} \;&=\; \ddot{\mathcal{Q}}_{yx} \;=\; -m\,\omega^2\,ab\,\sin(2\omega t)\,. \end{aligned} \tag{12.12}$$

Since the motion is confined to the xy-plane, all other components of $\mathcal{Q}_{ij}$ are zero.

Using Eq. (12.10), the spherical wave at coordinate $\boldsymbol{x}$ (far away from the source) and time t may be calculated. Locally, it is a plane wave propagating along the direction of a unit vector perpendicular to the wave front, i. e. $\hat{n} = \boldsymbol{x}/|\boldsymbol{x}|$. To make the physical polarisations manifest, $h_{\mu\nu}$ needs to be projected onto the TT state using $\mathbb{L}$ as defined in Eq. (12.6). Table 2 summarises the propagating modes for a wave emerging in the x-, y- and z-directions.

Direction ($\hat{n}$)	Non-zero entries	Values	Mode
$(1,0,0)$	$h^{\mathrm{TT}}_{yy} = -h^{\mathrm{TT}}_{zz}$	$-B^2\cos[2\omega(t-x)]$	h_+
$(0,1,0)$	$h^{\mathrm{TT}}_{xx} = -h^{\mathrm{TT}}_{zz}$	$A^2\cos[2\omega(t-y)]$	h_+
$(0,0,1)$	$h^{\mathrm{TT}}_{xy} = h^{\mathrm{TT}}_{yx}$	$AB\,\sin[2\omega(t-z)]$	$h_\times$
	$h^{\mathrm{TT}}_{xx} = -h^{\mathrm{TT}}_{yy}$	$(A^2+B^2)\cos[2\omega(t-z)]$	h_+

Table 2: Explicit form of a GW generated by a mass undergoing elliptical motion in the xy-plane at a frequency ω. form of $h_{\mu\nu}$. A and B are trivial rescalings of a and b respectively so that $h_{\mu\nu}$ is still proportional to $m\kappa\omega^2/\big(16\pi|\boldsymbol{x}|\big)$.

Note that, as usual, acceleration parallel with the direction of the wave produces no radiation. By taking $b \to 0$ we reduce the problem to simple harmonic motion in one dimension, with no radiation being produced along its axis. In the general case, GWs emitted in the plane of the ellipse are 'linearly polarised'. However, observations in the z-direction

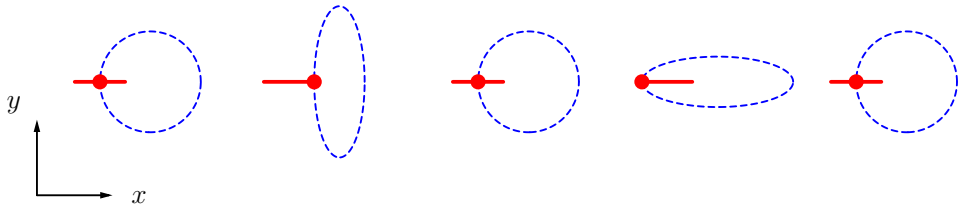

Figure 21: Here we track the geodesic deformation of a circle (blue) due to the metric perturbation $h_+ = h_{xx} = -h_{yy}$. A 'fixed' point on the circle (red) is shown to the negative x direction of the circle's centre. That point oscillates in the x-direction, and the entire circle undergoes sequential elongation and contraction in the x- and y-directions representing the '+' symbol. (The wave moves in the z-direction.)

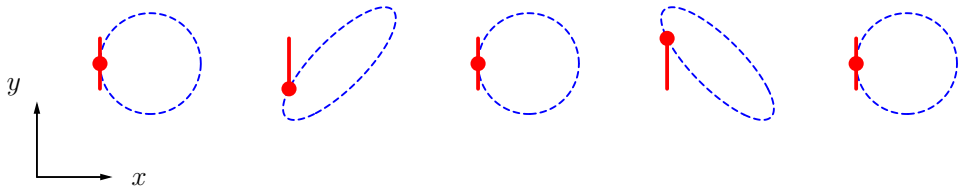

Figure 22: Same as Fig. 21, but for $h_\times$. Here the same point (red) on the circle oscillates only in the y-direction. The sequence of deformations for the circle (blue) resembles the '×' symbol.

will discern *two* independent polarisations, dubbed h_+ and $h_\times$.

In an arbitrary frame, a propagating GW may entail variations in dt, the infinitesimal element of time in that frame. A suitable boost puts the same wave into TT form, making a physical interpretation of $h_{\mu\nu}$ more transparent. In the case $\hat{n} = (0,0,1)$, both physical polarisations are present. The line element, using (11.3), takes the form

$$\begin{aligned} ds^2 &= g_{\mu\nu}\, dx^\mu\, dx^\nu \\ &= dt^2 - \big[\,(1+h_+)dx^2 + (1-h_+)dy^2 + 2h_\times dx\, dy + dz^2\,\big]\,. \end{aligned} \tag{12.13}$$

The influence of the h_+ polarisation on measurements in the x- and y-directions is shown in Fig. 21. The off-diagonal term, proportional $h_\times$, describes metric oscillations like those depicted in Fig. 22. One may construct a polarisation basis $\epsilon^{(\lambda)}_{\mu\nu}$, where $\lambda = \{+,\times\}$, which satisfies the completeness relation

$$\sum_\lambda \epsilon^{(\lambda)\,*}_{\mu\nu}\,\epsilon^{(\lambda)}_{\alpha\beta} = \mathbb{I}_{\mu\nu,\alpha\beta}\,, \tag{12.14}$$

according to Eq. (12.6).

Thanks to the choice of harmonic gauge, we have $\partial_\nu T^{\mu\nu} = 0$ from Eq. (12.3). If energy and momentum are locally conserved, how can gravitational waves carry away either? This paradox is due to the non-locality of defining gravitation energy in GR. Equation (12.3) is a truncated expansion of the Einstein equations in κ, higher-order terms should ensure $T^{\mu\nu}{}_{;\nu} = 0$ in general. By the equivalence principle, it is always possible to transform a

frame to be local Minkowskian. It follows that there is no covariant tensor representation for gravity satisfying a local conservation law. There is, however, a pseudotensor (frame dependent) $t^{\mu\nu}$ that can be uniquely constructed from the metric to satisfy

$$\partial_\mu\big[(\det g)\big(T^{\mu\nu} + t^{\mu\nu}\big)\big] \;=\; 0\,,$$

such that $t^{\mu\nu} = t^{\nu\mu}$ and it vanishes in an intertial reference frame. Explicitly,

$$t^{\mu\nu} \;:=\; -\frac{2}{\kappa^2}\Big\{2R^{\mu\nu} - g^{\mu\nu}R - \frac{1}{\det g}\,\partial_\alpha\partial_\beta\big[(\det g)\big(g^{\mu\nu}g^{\alpha\beta} - g^{\mu\alpha}g^{\nu\beta}\big)\big]\Big\}\,, \tag{12.15}$$

which is not a tensor because the partial derivatives are ordinary, and not covariant. Note that $t^{\mu\nu}$ is quadratic in the metric, making it zero to first order in $h_{\mu\nu}$ (the GW). The quadratic part is

$$t^{\mu\nu} \;=\; \big(\partial^\mu h^\alpha{}_\beta\big)\big(\partial^\nu h^\beta{}_\alpha\big) + O(\kappa^2)\,, \tag{12.16}$$

which follows from (12.15) upon substituting the perturbed metric, see Ref. [164]. By summing over α and β, both polarisations are taken into account and can be managed by specifying a gauge. For instance, consider a free GW moving in the z-direction which has the line element in (12.13), i. e. the axis along the direction of propagation is chosen to be Minkowskian. Since the two amplitudes h_+ and $h_\times$ depend on $(t-z)$, the momentum flux of the wave is

$$\begin{aligned} t^{0z} \;&=\; \tfrac{1}{2}(\dot h_+^2 + \dot h_\times^2) \\ &=\; \frac{\kappa^2}{(48\pi)^2|\boldsymbol{x}|^2}\,\ddot{\mathcal{Q}}_{ij}(t-|\boldsymbol{x}|)^2\,. \end{aligned} \tag{12.17}$$

This result, although derived in a special case, is actually a general one. Due to the completeness relation (12.14) for the polarisation tensors, the first line can be recast as $h_{ij}^2 = \frac{1}{2}(h_+^2 + h_\times^2)$ which gives the second line due to (12.10). Einstein first obtained this expression for the momentum flux [166]. In order to define the energy density carried by a GW, where the background metric is not the Minkowski one, one needs to average (12.17) over several wavelengths of oscillation. Adiabatic stellar systems, like inspiralling binaries, must account for the energy lost in GWs by a depletion in orbital energy, at a rate consistent with Eq. (12.17). The shrinking orbit of the neutron stars in PSR B1913+16 supplied the first *indirect* evidence for the existance of GWs [167].

The field generated by a source of energy and momentum can be expanded in 'monochromatic' waves, with different components taking the form $h_{ij}(\omega,\boldsymbol{x})\,e^{-i\omega t}$. The corresponding frequency mode of the source, T_{ij}, is responsible for that Fourier component in the field. To express this, we merely adapt Eq. (12.8) into the solution

$$h_{ij}(\omega,\boldsymbol{x}) \;=\; \frac{\kappa\,e^{i\,\omega\,|\boldsymbol{x}|}}{8\pi}\int_{\boldsymbol{x}'} T_{ij}\big(\,\omega,\,\boldsymbol{x}'\,\big)\,\frac{e^{-i\,\boldsymbol{k}\,\boldsymbol{x}'}}{|\boldsymbol{x}-\boldsymbol{x}'|}\,, \tag{12.18}$$

where $\boldsymbol{k} = \omega\,\hat{\boldsymbol{x}}$.

Let $dE_{\rm GW}$ be the energy radiated into the solid angle $d\Omega$ by GWs with frequencies in the interval $d\omega$. According to the spectral resolution of retarded potentials, the part of the total radiation in $d\omega/(2\pi)$ can be obtained from t^{0z} in (12.17) by replacing the square of the field by twice the squared modulus of its Fourier component. Thus,

$$dE_{\rm GW} \;=\; 2\omega^2\,|h_{ij}(\omega,\boldsymbol{x})|^2\,\frac{d\omega}{2\pi}\,|\boldsymbol{x}|^2 d\Omega\;.$$

Let us approximate $|\boldsymbol{x}-\boldsymbol{x}'| \approx |\boldsymbol{x}|$ in the denominator of (12.18), which amounts to the wavelength being small compared to the distance from the radiating system. In this limit, h_{ij} is a plane wave whose intensity is inversely proportional to $|\boldsymbol{x}|$ and hence $dE_{\rm GW}$ is the same for all distances. The differential energy can thus be expressed by

$$\begin{aligned}\frac{dE_{\rm GW}}{d\Omega\, d\log\omega} &= \frac{\omega^3\,\kappa^2}{32\pi^3}\int_{\boldsymbol{x}'}\int_{\boldsymbol{x}''} T_{ij}(\omega,\boldsymbol{x}')\,T_{ij}(\omega,\boldsymbol{x}'')\;e^{-i\boldsymbol{k}(\boldsymbol{x}'-\boldsymbol{x}'')}\\ &= \frac{\omega^3\,\kappa^2}{32\pi^3}\;T_{ij}(\omega,\boldsymbol{k})\,T_{ij}(\omega,-\boldsymbol{k})\,,\end{aligned}$$

where $\omega = |\boldsymbol{k}|$ and $\hat{\boldsymbol{k}}$ is oriented with the propagation of the GW.

We derive the formula for the rate of energy density emitted into GWs by a thermal plasma. For a homogeneous system, where the spatial $d^3\boldsymbol{x}'$- and $d^3\boldsymbol{x}''$-integration extends over a volume V, translational invariance implies

$$T_{ij}(\omega,\boldsymbol{k})\,T_{ij}(\omega,-\boldsymbol{k}) \;=\; V\int_{\boldsymbol{x}} T_{ij}(\omega,0)\,T_{ij}(\omega,\boldsymbol{x})\,. \tag{12.19}$$

It may also be shown that the rate at a specific time t is well defined as an average over one oscillation period [168]. Denoting $\varepsilon_{\rm GW} = E_{\rm GW}/V$ by the uniform energy density, its rate with respect to frequency and time is

$$\frac{d\varepsilon_{\rm GW}}{dt\,d\log\omega} \;=\; \kappa^2\frac{\omega^3}{16\pi^2}\int_X e^{iKX}\left\langle\, T_{ij}(0)T_{ij}(X)\,\right\rangle, \tag{12.20}$$

where the angular brackets represent the thermal average.

13. Hydrodynamic fluctuations

Smooth crossovers between phases in the early universe have beleaguered the proposal of baryogenesis in the SM. If the primordial plasma does not depart from thermal equilibrium, the third Sakharov condition is not met (see Sec. 1) [23]. This situation could be avoided for first order phase transitions, where both phases may be present in different parts of the system. That 'being out of equilibrium' is irreversible, i. e. breaks $\mathcal{T}$-symmetry, and entropy can be generated [113]. For this reason, it has become popular to consider extensions to the SM which would permit a first order transition (see, e. g. [169]). Here we will not consider a particular model, but rather investigate the general ramifications for long wavelength fluctuations and their GW spectrum.

For a wide variety of systems, there exists an *order parameter* that can be used to locally distinguish between two phases [170]. This might be a scalar function $\phi(t,\boldsymbol{x})$ that is non-zero below the phase transition temperature and becomes zero above it. A thermodynamic quantity that changes dramatically can serve this purpose. Alternatively, expectation values of the field configurations can be adopted for transitions induced by the breaking or restoring of a symmetry, e. g. the chiral condensate $\langle\bar{q}q\rangle$ in QCD. It is usual to take ϕ as the neutral component of the Higgs doublet in the EW theory. Dynamics of bubble nucleation, if a first order transition occurs, can then be studied via the spacetime dependence of ϕ. In hydrodynamics, the time and length scales characterising interactions within a plasma are considered infinitesimal. Fluctuations at the same time at different points are uncorrelated in this limit [171]. For the EW epoch, $T \sim 100$ GeV, the size of Higgs-phase bubbles was some few percent of the Hubble radius, $H^{-1} \sim 10^{15}\,T^{-1}$ (at that time). It follows that we

may regard their behaviour as hydrodynamic, insofar as the underlying plasma has a mean-free path $1/(g^4T) \ll H^{-1}$ where g is the weak isospin or hypercharge coupling. The universe expands so little during the weak transition that dilution of the plasma is negligible.

The main quantity characterising an equilibrium fluid is its energy momentum tensor $T^{\mu\nu} = (\varepsilon + p)u^\mu u^\nu - p g^{\mu\nu}$. Adding the scalar field as a dynamical quantity that may interact with the fluid, introduces an additional contribution to energy and momentum. The total energy and momentum is conserved, $T^{\mu\nu}{}_{;\nu} = 0$, but that of the two subsystems is not. The combined energy momentum tensor reads

$$T^{\mu\nu} \;=\; (\partial^\mu\phi)(\partial^\nu\phi) + (\varepsilon + p)u^\mu u^\nu - g^{\mu\nu}\Big(\frac{1}{2}(\partial_\alpha\phi)(\partial^\alpha\phi) + p\Big)\,. \tag{13.1}$$

The pressure p includes the scalar field's potential energy: $p = p_0(T) - \mathcal{V}(\phi, T)$. In the large-volume limit, and as a function of the temperature, $p(T)$ is a thermodynamic potential which allows all other thermodynamic properties of interest to be calculated. The entropy density, for example, is given by $s(T) = \partial p/\partial T$ and the energy density $\varepsilon(T) = sT - p$. Viscous corrections are not included in (13.1), but they are associated with fluctuations of variables that characterise the fluid[40] [172]. Here we shall focus on fluctuations in ϕ.

An effective potential can be introduced in a saddle-point approximation, in which ϕ is the 'condensate' mode [170]. To illustrate, taking inspiration from the Higgs sector from Sec. 9, we consider a potential

$$\mathcal{V}(\phi, T) \;=\; -\frac{1}{2}\mu^2\phi^2 \;+\; \frac{1}{4}\lambda\phi^4 \;+\; \Big[\, c_0\, T^2\phi^2 - c_1 T\phi^3 \,\Big] \;+\; \ldots\,, \tag{13.2}$$

where the terms in square brackets are the leading thermal corrections [35]. Coefficients c_0 and c_1 originate due to interactions, possibly including fields other than ϕ. [If just ϕ is included, $c_0 \simeq \lambda/8$ and $c_1 \simeq (3\lambda)^{3/2}/(12\pi)$ but the relative corrections are $\mathcal{O}(1)$.] The thermal 'Debye mass', equal to $2c_0T^2$, shifts a negative Higgs mass squared in the positive directions and thus counteracts the symmetry breaking. A cubic term, from $c_1 \neq 0$, could imply a first-order transition.

In order to couple the scalar field to the thermal plasma, we introduce a friction caused by the latter. The equation of motion for ϕ is modified:

$$\Box\,\phi + \gamma u_\mu(\partial^\mu\phi) - \frac{\partial\mathcal{V}}{\partial\phi} \;=\; 0\,, \tag{13.3}$$

by a term proportional to u_μ. ($\Box = g_{\mu\nu}\,\partial^\mu\partial^\nu$ is the d'Alembert operator.) We may interpret the coefficient γ by considering the role it plays in conserving energy and momentum: $T^{\mu\nu}{}_{;\nu} = 0$, using the explicit form in Eq. (13.1). Recall that for a scalar quantity, covariant differentiation is simply partial differentiation. Hence the divergence of the pressure component,

$$(p\,g^{\mu\nu})_{;\nu} \;=\; -\frac{\partial\mathcal{V}}{\partial\phi}\,\partial^\mu\phi \;+\; s\,\partial^\mu T\,,$$

where we used that $p(\phi, T) = p_0(T) - \mathcal{V}$ and the definition of the entropy. The entropy associated with the order parameter is $-\partial\mathcal{V}/\partial T$. Similarly, we find

$$\big[(\varepsilon + p)u^\mu u^\nu\big]_{;\nu} \;=\; Tu^\mu(su^\nu)_{;\nu} \;+\; su^\mu u^\nu\partial_\nu T \;+\; sTu^\nu u^\mu{}_{;\nu}\,.$$

[40] For a review of 'normal' hydrodynamic fluctuations, see Appendix A of Ref. [1].

For the energy momentum tensor of the scalar field, one obtains

$$\begin{aligned}\Big[(\partial^\mu\phi)(\partial^\nu\phi) - \frac{g^{\mu\nu}}{2}(\partial_\alpha\phi)(\partial^\alpha\phi)\Big]_{;\nu} &= (\partial^\mu\phi)(\Box\,\phi) \\ &= -(\partial^\mu\phi)\Big(\gamma u_\nu\partial^\nu\phi + \frac{\partial\mathcal{V}}{\partial\phi}\Big)\,,\end{aligned} \tag{13.4}$$

where we have substituted (13.3) in (13.4). These individual contributions to the flux of energy momentum yield, when projected onto the flow velocity,

$$0 = u_\mu T^{\mu\nu}{}_{;\nu} = T(su^\nu)_{;\nu} - \gamma(u_\mu\partial^\mu\phi)^2\,. \tag{13.5}$$

Thus γ parametrises local entropy production in regions where the scalar field varies, i. e. at the planar interface between the broken and unbroken phase, see Fig. (23). (We do not explicitly consider bubble collisions.) In kinetic theory, for relativistic particles, we may estimate $\gamma \sim n\,\sigma$ from the density n of particles that mutually scatter with a total cross section σ. Assuming $n \sim T^3$ and $\sigma \sim g^4/T^2$ reproduces the weak-coupling result $\gamma \sim g^4 T$.

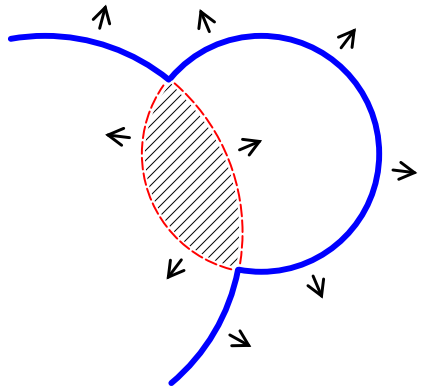

Figure 23: Low temperature bubbles expand to occupy the ambient environment (symmetric phase) in a first-order cosmological phase transition. The velocity of the interface is eventually constant due to friction, parametrised by γ. In the text, we focus on these boundary regions (blue), where entropy is produced. We do not concentrate on GWs generated by the hydrodynamical evolution, such as the wake of colliding bubbles, although thermal fluctuations would actually take place everywhere.

Detailed balance implies that equation (13.3) is incomplete: The *fluctuation-dissipation-relation* (FDR) is not respected unless a 'random' force is included [170]. This force adds to the drag and external forces acting on ϕ. The stochastic force ξ, has zero mean and is assumed to be Gaussian, i. e. the functional probability distribution takes the form

$$\int \mathcal{D}\xi\, \exp\Big[-\int_X \sqrt{-\det g}\;\frac{\xi(X)^2}{2\Omega}\Big]. \tag{13.6}$$

The coefficient Ω determines the relative strength of diffusion. Note that the noise is uncorrelated at different times and different points in space. Assuming d spatial dimensions and working in local Minkowskian coordinates, the covariance is

$$\langle\xi(X)\xi(Y)\rangle = \Omega\,\delta(x_0 - y_0)\delta^{(d)}(\boldsymbol{x}-\boldsymbol{y})\,.$$

Naturally, this has a consequence for the scalar field's motion. The value of ϕ can first be shifted in the broken symmetry phase, $\phi \to \phi_0(T) + \phi'$, where ϕ_0 minimises the effective potential, i. e.

$$\mathcal{V}(T,\phi) = \text{const.} + \frac{1}{2}m^2(T)\phi'^2 + \ldots\,, \tag{13.7}$$

where $m^2(T) = -\mu^2 + 2c_0\lambda T^2$ and the self interactions of ϕ' were omitted. From now on, we drop the $'$ to distinguish it from the original ϕ. Augmenting the equation of motion (13.3) with the noise term, and writing it for a flat metric in the fluid's frame, we get

$$\Box\,\phi + \gamma u_\mu(\partial^\mu\phi) - m^2\,\phi \;=\; \xi(X)\;; \quad \Box = \partial_t^2 - \nabla^2\,. \tag{13.8}$$

If we consider $\phi(t,\boldsymbol{x})$ for times $t \gg \gamma^{-1}$, all memory of initial conditions is lost and we focus on the steady-state solution sourced by the fluctuations. The solution is then $\phi(X) = \int_Y G(X-Y)\xi(Y)$ where G is the Green's function[41], which is given in Fourier space by

$$\widetilde{G}(P) \;=\; \frac{1}{P^2 - m^2 + i\gamma\,Pu}\,. \tag{13.9}$$

From that, the induced correlation function for scalar fields can be determined:

$$\langle\phi(P)\phi(Q)\rangle \;=\; \frac{\Omega\,\tilde{\delta}^{(d+1)}(P+Q)}{(P^2-m^2)^2 + \gamma^2(Pu)^2}\,. \tag{13.10}$$

The value of Ω can be fixed by calculating the same two-point function for the equilibrium ensemble [114]. Recalling the Saclay representation for the imaginary-time propagator, it may be approximated using (13.10) as

$$\Delta(\tau,\boldsymbol{p}) \;\simeq\; \Omega\int\frac{dp_0}{2\pi}\,\frac{e^{p_0\tau}}{(P^2-m^2)^2 + \gamma^2(Pu)^2}\,. \tag{13.11}$$

in the limit $|\boldsymbol{p}| \ll T$. We may readily perform the integration over p_0 using Cauchy's formula. To simplify, we may also set $u_\mu = (1,\boldsymbol{0})$ so that the poles in the upper half-plane are $\omega_\pm = \frac{1}{2}(i\gamma \pm \sqrt{4E_p^2 - \gamma^2}\,)$. From the sum of their residues[42], we are able to evaluate Eq. (13.11) for $\tau = 0$ by a semi-circular contour in the upper half-plane. This should be matched to the corresponding equilibrium result $\Delta(0,\boldsymbol{p}) = -\big[\,1 + 2n_{\rm B}(E_p)\,\big]/(2E_p)$ in the hydrodynamic limit, i.e. $E_p \ll T$. In so doing, we ensure that the long-time dynamics respects the correct equilibrium behaviour. Expanding $n_{\rm B}(x) \simeq T/x$ and identifying the equal-time correlators gives the FDR,

$$\Omega = 2\gamma T\,. \tag{13.12}$$

Response to metric perturbation

The production rate of gravitational waves can be calculated from the response of the combined system in (13.1) to a metric perturbation. For definiteness we study a GW propagating in the z-direction with a particular polarisation: $h_{xy} = h_{yx} = h_\times e^{-i\omega(t-z)}$ as the only non-zero deformations in Eq. (11.3). Then the scalar field satisfies, assuming small perturbations in ϕ and u^i,

$$(\partial_t^2 + \gamma\partial_t - \nabla^2 + m^2)\phi = \xi - 2\kappa\,h_\times\,\frac{\partial^2\phi}{\partial x\partial y} + \dots\,, \tag{13.13}$$

[41] The sign of γ indicates whether the poles of $\widetilde{G}$ lie in the upper or lower half-plane of complex frequencies and hence G is a retarded (advanced) propagator if γ is positive (negative). We assume $\gamma > 0$.

[42] In the overdamped case ($\gamma \gg m$), the two poles $\omega_\pm$ are purely imaginary for small $|\boldsymbol{p}|$. Supposing instead that $\gamma < 2m$, the poles in the upper half-plane differ only by the sign of their real parts for all $\boldsymbol{p}$. The sum of their residues is, in either case,

$$\sum_\pm \mathrm{Res}\Big[\,\frac{1}{(p_0^2 - E_p^2)^2 + \gamma^2 p_0^2}\,, p_0 \to \omega_\pm\,\Big] \;=\; \frac{i}{2\gamma\,E_p^2}\,.$$

up to quadratic terms in the field variables. The new solution $\phi \approx \phi^\star + \delta\phi$, departs from its original form $\phi^\star$, which satisfies Eq. (13.8). One iteration, with respect to an expansion in κ, gives [recalling the Green's function from (13.9)]

$$\delta\phi(X) \;=\; -2\kappa \int_{Y,Z} G(X-Y) h_\times(Y) G_{,x,y}(Y-Z)\xi(Z)\,, \tag{13.14}$$

where $G_{,x,y} = \partial_x\partial_y G$. The adjustment in the corresponding energy-momentum tensor is (only the xy-entry changes) $\delta T^\phi_{xy} = \phi^\star_{,x}\delta\phi_{,y} + \phi^\star_{,y}\delta\phi_{,x}$ and thus, energy may be transferred to the propagating gravitational wave. Indeed, there is a contribution to the emission rate (12.20) which can be obtained from the on-shell limit of

$$\int_X e^{i(\omega t - kz)} \left\langle \frac{1}{2}\big\{T_{xy}(0), T_{xy}(X)\big\} \right\rangle \;=\; \big[\,1 + 2n_{\rm B}(\omega)\,\big]\rho_\xi(\omega,k)\;;$$

where the particular spectral function reads

$$\rho_\xi \;\coloneqq\; \mathrm{Im}\Big[\,\frac{\delta\langle T^\phi_{xy}\rangle}{\delta g_{xy}}\,\Big], \tag{13.15}$$

in linear-response theory [173]. The functional derivative is to be understood in the $\kappa \to 0$ limit, where (11.3) is the deviation from the (flat) background metric. Damping of gravitational waves by matter is governed by the same response function, in a different context, see Ref. [174]. Averaging over the fluctuations, and denoting $K = (\omega, k\hat{z})$, we find

$$\frac{\delta\langle T^\phi_{xy}\rangle}{\delta g_{xy}} \;=\; 2\Omega \int_P p_x^2 p_y^2\, |\widetilde{G}(P)|^2\, |\widetilde{G}(L)|^2 \Big(\,2m^2 + P^2 + L^2 + i\gamma\, Ku\,\Big), \tag{13.16}$$

where $L = K - P$. The integration over p in (13.16) is power-divergent, an issue which arises because small gradients are assumed. And hence the integrand above is only meaningful for $|\boldsymbol{p}|, E_p \ll T$. Larger 'loop' momenta have small wavelengths that probe the microscopic medium, rather than its course-grained bulk properties.

Equation (13.16), being derived from the correlations between off-diagonal components of the energy momentum tensor, describes the system's ability to maintain shear stresses. A transport coefficient, the shear viscosity η, quantifies these forces in proportion to (small) velocity gradients. We may accordingly define, via a Kubo formula for the spectral function above

$$\eta_{\rm eff} \;\coloneqq\; \lim_{\omega\to 0} \frac{\rho_\xi(\omega,0)}{\omega}\;, \tag{13.17}$$

which sets the infrared contribution to the GW production rate.

In Appendix C we show how to complete the integration over p_0 in (13.16). The resulting expression, using the FDR (13.12) and for $\boldsymbol{k} \to 0$, is

$$\begin{aligned}\frac{\delta\langle T^\phi_{xy}\rangle}{\delta g_{xy}} \;&=\; 4T\left\{1 + \frac{i\gamma}{\omega + i\gamma}\right\} \int_{\boldsymbol{p}} \frac{p_x^2 p_y^2}{E_p^2\big[\,4E_p^2 - \omega^2 - 2i\gamma\omega\,\big]} \\ &=\; 2T \int_{\boldsymbol{p}} \frac{p_x^2 p_y^2}{E_p^4}\left[\,1 + \frac{i\omega}{2\gamma}\left(1 + \frac{\gamma^2}{E_p^2}\right) - \frac{\omega^2}{2\gamma^2}\left(1 + \frac{\gamma^4}{2E_p^4}\right) + \mathcal{O}\!\left(\frac{\omega^3}{\gamma^3}\right)\right],\end{aligned} \tag{13.18}$$

where $E_p = \sqrt{p^2 + m^2}$. The curly brackets of the unexpanded version above lead to a Lorentzian shape in the spectral peak in ρ_ξ (after taking the imaginary part) for fixed ω/γ

and $\gamma \ll E_p$. In the zero frequency limit, needed for (13.17), we obtain

$$\eta_{\text{eff}} \;=\; \frac{T}{d(d+2)\,\gamma} \int_{\boldsymbol{p}} \frac{p^4}{E_p^4} \left(1 + \frac{\gamma^2}{E_p^2} \right) , \tag{13.19}$$

making use of rotational symmetry in d spatial directions.

Equation (13.19) with $d = 3$ is formally divergent, due to the scope of working with a hydrodynamic approximation. The propagators (and the expression for ρ_ξ) are not applicable at large momenta [170]. Hence the calculation is only valid if restricted to momenta below a maximum wave number, e. g. $p_{\text{max}} < \pi/a$ where a is the lattice spacing. Imposing such a cut-off on the integration in (13.19), so that $|\boldsymbol{p}| \leq p_{\text{max}}$, and assuming that $m, \gamma \ll p_{\text{max}}$ we find

$$\eta_{\text{eff}} \;=\; \frac{T\,p_{\text{max}}}{90\pi^2\gamma} \big[\, p_{\text{max}}^2 + 3(\gamma^2 - 2m^2) \,\big] \,+\, \frac{T\,m}{96\pi\,\gamma} \big(4m^2 - 3\gamma^2 \big) . \tag{13.20}$$

after neglecting subleading terms. The power-like divergence is familiar from other settings (cf. Ref. [172]), but they are not detected unless d is fixed before doing the $d^3\boldsymbol{p}$-integral. The finite part of (13.20) can be found by carrying out the integration in general [1].

To elaborate how the leading divergence in (13.20) originates, let the spatial coordinates take values on a regular lattice with discrete separation of a in each direction. Rotational symmetry is thus broken to only the cubic isometries, meaning that we need to return to Eq. (13.18). Appropriately coarse graining the autocorrelator for ξ and restricting the momenta to the first Brillouin zone, $p_i \leq \pi/a$ where $i = \{x, y, z\}$, gives (for $m, \gamma \to 0$)

$$\eta_{\text{latt}} \;=\; \frac{T}{\gamma} \int_{\boldsymbol{p}} \frac{\widetilde{p}_x^2 \widetilde{p}_y^2}{\widetilde{\boldsymbol{p}}^4} \;; \quad \widetilde{p}_i \,\coloneqq\, \frac{2}{a} \sin\Big(\frac{a p_i}{2} \Big) . \tag{13.21}$$

This expression can be simplified starting with the trivial identity:

$$\int_{-\pi/2}^{\pi/2} dx \; \frac{\partial}{\partial x} \left(\frac{\sin x \, \cos x}{\sum \sin^2 x} \right) \;=\; 0 ,$$

and expanding the partial derivative on the left hand side. When applied in a suitable way for (13.21), cyclic invariance of the pair $\widetilde{p}_x \widetilde{p}_y$ with respect to the denominator allows one to replace the numerator

$$\widetilde{p}_x^4 \quad \to \quad \frac{1}{3} \big(\widetilde{p}_x^2 + \widetilde{p}_y^2 + \widetilde{p}_z^2 \big)^2 - 2\,\widetilde{p}_x^2 \widetilde{p}_y^2 \;.$$

Following these steps, the lattice viscosity can be re-expressed as

$$\eta_{\text{latt}} \;=\; \frac{T\iota}{3\,\gamma\,a^3} \;; \tag{13.22}$$

$$\iota \;\coloneqq\; \frac{1}{(2\pi)^3} \int_{-\pi/2}^{\pi/2} \int_{-\pi/2}^{\pi/2} \int_{-\pi/2}^{\pi/2} \frac{2\,dx\,dy\,dz}{\sin^2 x + \sin^2 y + \sin^2 z} \;.$$

Integrals of this type were studied by Watson [175]. ι can be represented in terms of special values the Γ-function, its value is [176]

$$\iota \;=\; \Gamma\Big(\frac{1}{24} \Big)^2 \Gamma\Big(\frac{11}{24} \Big)^2 \frac{\sqrt{3} - 1}{192\pi^3} \;\approx\; 0.252731 ,$$

yielding a cut-off of $p_{\text{max}} \approx 4.213987\,/a$ in (13.20). Although actual simulations would include this tunable contribution to viscosity, the continuum limit $a \to 0$ is spoiled by a

formal divergence. Perhaps a different framework can be used to remove cut-off dependence in fluctuation-induced viscosities by 'renormalising' thermodynamic functions [177].

In any case, Eq. (12.20) would predict a late time GW rate,

$$\lim_{\omega\to 0}\frac{d\varepsilon_{\rm GW}}{dt\,d^3\boldsymbol{k}} \;=\; \frac{\kappa^2 T}{(2\pi)^3}\,\eta\,, \tag{13.23}$$

where η can be replaced by one of the appropriate regularisations above. Turning to the finite part of (13.20), we recall that $\gamma\sim g^4T$ in kinetic theory, whereas the weak coupling expansion gives $\eta_{\rm LL}\sim T^3/(g^4\log g^{-1})$ [178]. Supposing $m\sim g^l T^2$, the contribution from $\eta_{\rm eff}$ is of order $\max[3l-4,l+4]$ in the coupling, making it highly suppressed with respect to the leading-log result, even with the conservative assumption $l\le 2$.

Although difficult to include in practice (due to large statistical samplings required), fluctuations would enrich the scope of hydrodynamic simulations of cosmological phase transitions. Not only would they shed light on the stability of growing bubbles [179], fluctuations also automatically seed the initial nucleations [180]. We have demonstrated a self-consistency check, for when ϕ approaches equilibrium and the FDR needs to be respected. Changing the noise-correlation amplitude Ω with the lattice spacing a, would test the predicted scaling behaviour in (13.12) and the regulated viscosities.

14. Coupling to matter and thermal production

Just as a (neutral) plasma of charged elements can emit photons due to changing electromagnetic currents caused by scatterings, so an equilibrium plasma can radiate gravitational waves owing to the microscopic transport of energy and momentum. The GW-emission rate is proportional to $G=1/m_{\rm Pl}^2$, making it tiny for temperatures far below the Planck scale. Nevertheless, the total energy it has withdrawn[43] over the course of the universe's lifetime may be appreciable. Indeed, as far as the radiation epoch's budget is concerned,

$$\Omega_{\rm rad} \;=\; \Omega_\gamma+\Omega_\nu+\Omega_{\rm GW}\,. \tag{14.1}$$

If one assumes that only photons and light neutrinos contribute, $\Omega_{\rm rad}$ is determined by ε_γ and the effective number of neutrino species present. From the earlier discussion [below (7.2)], it may be shown that

$$\frac{\Omega_\nu}{\Omega_\gamma} \;=\; \frac{7}{8}\Big(\frac{4}{11}\Big)^{4/3}N_{\rm eff}\;;\quad \text{with}\quad N_{\rm eff}\simeq 3.045(1)\,.$$

Corrections to the naive $N_{\rm eff}\to 3$ are a prediction of the SM and come about after e^+e^- annihilation effects, etc. are taken into account with the thermal history [181]. Any additional radiation in Eq. (14.1) may be interpreted as a deviation from this value. Attributing what is allowed by the theoretical uncertainty $\Delta N_{\rm eff}\simeq 10^{-3}$ to GWs was considered in Refs. [5,182], and constrains the maximal temperature of the radiation epoch.

The leading-log (LL) rate for graviton production from the SM in the symmetric phase was calculated in Ref. [168]. Soft scatterings due to gauge bosons are responsible for the

[43] Since the coupling of the plasma to the gravitational field is weak, re-absorption is negligible for LO considerations. In the early universe, GWs have a mean scattering time of $2/(\kappa^2\eta)$ which is larger than the Hubble time.

logarithmic enhancement, giving

$$\frac{d\varepsilon_{\rm GW}}{dt\,d\log\omega} \;=\; \frac{\kappa^2\,\omega^4\,n_{\rm B}(\omega)}{16\pi^3}\Big[\,\sum_i d_i m_i^2 \log\frac{T^2}{m_i^2} \,+\, \mathcal{O}(g_i^2 T^2)\,\Big], \tag{14.2}$$

where the sum runs over all massless gauge fields in the SM. The degeneracies are $d_{\rm Y} = 1$, $d_{\rm W} = 3$ and $d_{\rm s} = 8$. The Debye masses are $m_{\rm Y} = \sqrt{11/6}\,g'T$, $m_{\rm W} = \sqrt{11/6}\,gT$ and $m_{\rm s} = \sqrt{2}\,g_{\rm s}T$. To calculate $\Omega_{\rm GW}$ in (11.1), the rate needs to be integrated over time in an expanding cosmological background. The result is plotted in Fig. 24, showing the LL expression (14.2) for $k > T/200$ with an 'error band' from varying $\bar{c} \in [3, 30]$ in the parametric form $m_i^2[\log(T^2/m_i^2) + \bar{c}]$. The hydrodynamic estimate uses $\eta = [1, 4] \times 100\,T^3$, where the rate is from Eq. (13.23). Like the CMB, the GW energy spectrum peaks in the microwave range at around 100 GHz. A full LO calculation can better resolve the shape of the peak, marking frequencies at the typical thermal scale $\omega \sim T$ (after redshift).

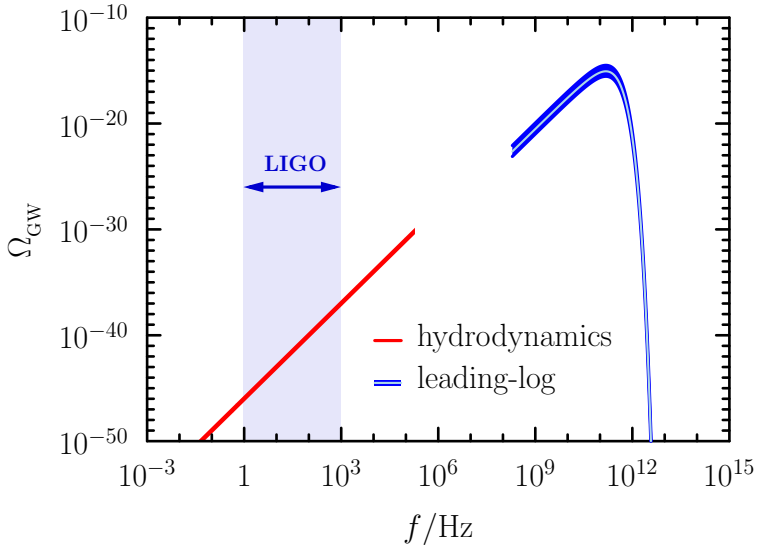

Figure 24: The ratio of the GW energy density to the closure density of the universe, see Eq. (11.1). These estimates are based on Ref. [168], where the differential rate was integrated from $T_{\rm max} = 10^6$ GeV to around the end of the EW epoch $T_0 = 160$ GeV. The frequency is redshifted: $f = \omega_0 a(t_0)/(2\pi a(t_{\rm now}))$. See main text for details.

The LO production rate, as discussed in Part I for photoemission in QCD, has very recently been determined for GWs in Ref. [5]. We will discuss a few important ingredients of that calculation, without going into the details. At LO it is sufficient to neglect the self-interaction of the 'graviton' field $h_{\mu\nu}$. Just as $\alpha_{\rm em} \ll \alpha_{\rm s}$ in the QCD plasma, this is justified for a SM plasma at temperatures well below the Planck scale. In this sense, we may consider incorporating a 'graviton' field into the SM by a minimal coupling [183]. Although the first observation of GWs is no evidence for a hypothetical quantum attributed to the gravitational force, it should be a massless spin-2 boson if it exists. The masslessness is expected from the long-range nature of GR, and the tensor structure just follows from the source $T_{\mu\nu}$ in the Einstein equations (12.2). Severe problems of renormalisation do not occur in Feynman diagrams without graviton loops, granting the EFT some predictive power.

Let us examine the general action, for a Lagrangian $\mathcal{L}$ which is a functional of one or

more fields,

$$\mathcal{S} \;=\; \int_X \sqrt{-\det g}\;\mathcal{L}\big[\,g_{\mu\nu}\,,\;\cdots\big]\,, \tag{14.3}$$

for the induced metric (11.3). $\mathcal{L}$ itself depends on $g_{\mu\nu}$ through the explicit terms that are polynomials of Lorentz invariant combinations of field operators. Since the perturbation with respect to the flat metric $\eta_{\mu\nu}$ is combined with factors of κ, the graviton is canonically quantised and κ plays the role of a coupling constant. The leading effect of interactions with the ordinary fields in (14.3) is via the interaction term

$$\mathcal{L}_{\rm int} \;=\; -\frac{\kappa}{2}\,h^{\mu\nu}\,T_{\mu\nu}\,, \tag{14.4}$$

where $T_{\mu\nu}$ is the aggregate energy-momentum tensor for all fields included in $\mathcal{L}$ (except the graviton) and indices can be raised and/or lowered with the flat metric. Equation (14.4) may be derived by formally expanding the integrand of (14.3) for $\kappa\,h_{\mu\nu} \ll 1$. The energy-momentum tensor for the field content is derivable from variations with respect to the metric,

$$T_{\mu\nu} \;=\; \Big(-g_{\mu\nu}\,\mathcal{L} + 2\frac{\partial\mathcal{L}}{\partial g^{\mu\nu}}\Big)\Big|_{\kappa=0}\,.$$

We may use the flat metric above since (14.4) already includes the leading part, which comes from the second term in

$$\sqrt{-\det g} \;\approx\; 1 + \frac{\kappa}{2}\,h_\mu{}^\mu + \mathcal{O}(\kappa^2)\,.$$

From this perspective, Eq. (12.20) is familiar: The production rate is given by the imaginary part of the graviton self-energy.

Scalar theory

Let us examine the simple case of the interacting scalar ϕ^4-theory,

$$\mathcal{L} \;=\; \frac{1}{2}\,(\partial_\mu\phi)^2 + \frac{m^2}{2}\phi^2 + \frac{\lambda}{4}\,\phi^4\,. \tag{14.5}$$

The energy-momentum tensor for ϕ is included in Eq. (13.1), although here we disregard the fluid component. Hence the interaction described by (14.4) couples a single graviton-field with two ϕ-fields. The terms in $T_{\mu\nu}$ that are proportional to $g_{\mu\nu}$ do not contribute in the TT gauge. Directing the flow of momentum into the vertex, and associating P and Q with the two scalar fields, the fundamental interaction reads

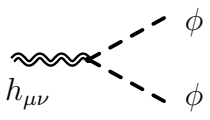

$$\;=\; \frac{\kappa}{2}\big(\,P_\mu Q_\nu + P_\nu Q_\mu\,\big)\,. \tag{14.6}$$

This, in addition to the usual self-interaction proportional to λ, allows Eq. (12.20) to be taken up for evaluating the GW production rate. The leading perturbative corrections to the appropriate correlation of energy and momentum are shown in Fig. 25. For convenience, we define the retarded correlator

$$\mathcal{G}(K) \;=\; \mathbb{L}^{\mu\nu,\alpha\beta}\int_X e^{iKX}\,\big\langle\,T_{\mu\nu}(X)T_{\alpha\beta}(0)\,\big\rangle\,, \tag{14.7}$$

which needs to be evaluated on the light cone. A spectral function associated with the same correlator has been studied for quenched QCD in Refs. [184–186]. Following that work (here in the far easier case) we make use of a decomposition to master integrals $\mathcal{J}$ and $\mathcal{I}$. Our goal here is to provide the simplest example that demonstrates a few of the more general techniques used in Ref. [5] to calculate GW production in the SM.

(a) (b) (c)

Figure 25: Graphs contributing to LO, (a), and NLO, (b) and (c). The scalar field propagator is represented by a single line, and the (external) GW is represented by a double wavy line.

To define the master integrals, we abbreviate the projections

$$\mathbb{P}_T(X) \;:=\; X^\mu X^\nu \mathbb{P}^T_{\mu\nu} \;=\; x^2 - \frac{(\boldsymbol{x}\boldsymbol{k})^2}{\boldsymbol{k}^2}\,,$$

which gives the magnitude of $\boldsymbol{x}$ in the plane transverse to the GW momentum. The one- and two-loop master integrals needed to express $\mathcal{G}$ are

$$\begin{aligned}
\mathcal{J}^{[c]}_{ab}(K) &\equiv \int\!\!\!\!\!\!\diagup_P \Delta_P^a \Delta_L^b \left[\mathbb{P}_T(P)\right]^c\,, \\
\mathcal{I}^{[fgh]}_{abcde}(K) &\equiv \int\!\!\!\!\!\!\diagup_{P,Q} \Delta_P^a \Delta_Q^b \Delta_R^c \Delta_L^d \Delta_V^e \left[\mathbb{P}_T(P)\right]^f \left[\mathbb{P}_T(Q)\right]^g \left[\mathbb{P}_T(R)\right]^h\,.
\end{aligned} \tag{14.8}$$

For the latter, we partially recycle the notation from (4.16) albeit with all bosonic propagators where the transverse projector was defined in (12.5). The overall dimension of $\mathcal{J}$ and $\mathcal{I}$ is given by $[\mathrm{GeV}]^{2\vartheta}$ where $\vartheta = 2-(a+b)+c$ and $\vartheta = 4-(a+b+c+d+e)+(f+g+h)$ respectively. The master functions that were used in Ref. [184] can be obtained with the change of variables $P \to L = K - P$.

Direct evaluation of the LO and NLO diagrams in Fig. 25, with the same principles as illustrated in Appendix A, produces a linear combination of (14.8). The result reads

$$\begin{aligned}
\mathcal{G}(K) &= 4(D-3)\,\mathcal{J}^{[2]}_{11} \\
&+ 12\lambda\Big\{(D-3)\,\mathcal{I}^{[200]}_{11020} + \frac{1}{4}(D-4)\,\mathcal{I}^{[110]}_{11011} + \frac{1}{4}(D-2)\big(\mathcal{I}^{[200]}_{11011} - 2\mathcal{I}^{[101]}_{11011} + 2\mathcal{I}^{[002]}_{11011}\big)\Big\} \\
&+ \mathcal{O}(\lambda^2)\,,
\end{aligned}$$

which has dimensions of $[\mathrm{GeV}]^4$. Two reduction formulae help to simplify the expression considerably. The first follows by noting that

$$\mathbb{P}_T(R) \;=\; \mathbb{P}_T(P) + \mathbb{P}_T(Q) + 2P^\mu Q^\nu\,\mathbb{P}^T_{\mu\nu}\,,$$

where the last term drops out in a rotationally symmetric integration over $\boldsymbol{p}$ or $\boldsymbol{q}$, combined with the projection operator. That leads to

$$\mathcal{I}^{[101]}_{11011} \;=\; \mathcal{I}^{[200]}_{11011} + \mathcal{I}^{[110]}_{11011}\,. \tag{14.9}$$

The second relation is slightly less obvious. To derive it, we note that

$$\mathbb{P}_T(R)^2 \;=\; \mathbb{P}_T(P)^2 \;+\; \mathbb{P}_T(Q)^2 \;+\; 2\mathbb{P}_T(P)\,\mathbb{P}_T(Q) \;+\; P^\alpha Q^\beta P^\mu Q^\nu\,\mathbb{P}^T_{\alpha\beta}\mathbb{P}^T_{\mu\nu} + \ldots\,,$$

where the missing terms will vanish after carrying out the integrals in (14.8). For the last term, rotational symmetry justifies replacing

$$P^\alpha Q^\beta P^\mu Q^\nu \, \mathbb{P}^T_{\alpha\beta} \mathbb{P}^T_{\mu\nu} \;\to\; \frac{4}{D-2} \, \mathbb{P}_T(P) \mathbb{P}_T(Q)$$

within the integrand. Hence we obtain

$$\mathcal{I}^{[110]}_{11011} \;=\; \frac{D-2}{2D} \Big(\mathcal{I}^{[002]}_{11011} - 2\mathcal{I}^{[200]}_{11011} \Big) . \tag{14.10}$$

Together Eqs. (14.9) and (14.10) give

$$\mathcal{G}(K) \;=\; 4(D-3) \Big\{ \mathcal{J}^{[2]}_{11} \,-\, 3\lambda \mathcal{I}^{[200]}_{11020} \Big\} \,+\, \mathcal{O}(\lambda^2) \, . \tag{14.11}$$

The Wightman correlator in Eq. (12.20) implies that the GW rate is obtained from the imaginary part of $\mathcal{G}$, namely (after setting $D = 4$)

$$\frac{d\varepsilon_{\rm GW}}{dt \, d\log\omega} \;=\; \frac{\kappa^2 \, \omega^3}{16\pi^2} \, n_{\rm B}(\omega) \, \mathrm{Im}\big[\mathcal{G}(K)\big]_{k_0 \to (\omega + i0^+)} \, , \tag{14.12}$$

in direct analogy with the photon rate, see (3.2). It turns out the the two master functions in Eq. (14.11) vanish on the light cone for massless scalars. This is perhaps not surprising, as each cut diagram includes an amplitude for $\phi + \phi \to \mathrm{GW}$. Once the whole SM is considered, $2 \leftrightarrow 2$ processes get generated by the cutting rules and HTL resummation is needed to cure the same kind of logarithmic divergence as in the photon case [5]. That LO computation is quite technical (and was undertaken as this thesis was being completed), so we do not discuss it further here.

15. Conclusion

Our understanding of physical theories is bolstered by considering them at an extreme point along some parameter axis. At high temperatures T, for instance, the 'strong' interaction $\alpha_{\rm s}$ diminishes until quarks and gluons are no longer confined. At still higher T, the Higgs mechanism is undone to render all the gauge bosons massless $m_W, m_Z \to 0$. How far the solutions in these 'known limits' can be extrapolated to physically realistic scenarios is an important issue. It calls on us to test the underlying assumptions and establish where (and why) they break down. That can be managed by comparing with non-perturbative data, e.g. from lattice QCD, and/or carefully considering NLO corrections together with the effect of running couplings.

This thesis has examined rate observables that are relevant for heavy ion experiments and the early universe – two settings, seemingly unrelated, that actually have much in common on the methodological side. The tool of choice, perturbation theory, is useful for solving problems that cannot be solved exactly. While (by its very nature) *approximate*, it is capable of making predictions from 'first principles'. Although QCD has a small cosmological footprint and, conversely, EW interactions are too slow to matter for nucleus-nucleus collisions, we have profited by the exchange of ideas.

Taking stock of the techniques used, several are worth re-iterating. Firstly, the symbolic reduction that produced the strict NLO spectral functions in Eqs. (4.4) and (4.5) is a widely adopted strategy in higher-order computations. The same ideas have also been tailored to Part III and for obtaining the LO gravitational rate in Ref. [5]. A second concept that helps to describe global features of transport quantities, is the hydrodynamic regime and its predictions for various spectral functions. The connection between η (shear viscosity) and GW production is based on this, as is the last remark of Part I. Finally, the unifying approach of EFTs has been indispensable throughout. It enabled us to use Ref. [92]'s argument and dramatically simplify the calculation in Part II for the neutrino width.

Summary & outlook

The central findings of this thesis and Refs. [1–5] are as follows.

Photons (and dileptons) offer themselves as clean probes of the QGP because they are unlikely to reinteract with the medium once produced. Their emission rates are given via the vector channel spectral function $\rho_{\mu\nu}$, an object that can be strongly constrained by lattice data [136]. We have scrutinised the associated imaginary-time correlator $G_{\mu\nu}(\tau)$ ($\tau = it$, where t is the real time) [3], building on earlier determinations of $\rho_{\mu\nu}$ [101]. As the NLO corrections to $\rho_{\mu\nu}$ were not known for spacelike virtualities, we calculated them there, thus establishing the QCD spectral function for energies above, below and in the vicinity of the light cone for a photon of momentum k [2]. Our results for $G_{\rm V}$ and G_{Δ}, in Figs. 12 and 13, lie somewhat above the lattice data, possibly indicating a non-perturbative suppression of the QCD spectral function. The outlook for more stringent tests is promising, especially as new lattice data become available.

Neutrinos, prior to their decoupling at $T_{\rm dec} \simeq 2$ MeV, are interesting 'test particles' to consider because of their connection with physics beyond the SM. We considered the next-to-leading order (NLO) thermal interaction rate of an active neutrino (mass $<$ eV), as it passes through a SM plasma in the range 90 GeV $< T <$ 160 GeV [4]. To do so, we

made use of the breakthrough in Ref. [92] that enables light-like correlators to be calculated in a much simpler, dimensionally reduced, EFT. The result is displayed in Fig. 19. Our calculation clarifies the accuracy of computations like those in Ref. [136], which concern the role sterile neutrinos (mass ~ GeV) might play in the generation of lepton asymmetry through active-sterile oscillations.

Gravitational waves (GWs) of primordial origin might be detectable by the proposed LISA interferometer [29]. Cosmological phase transitions that disturb the system from equilibrium would provide sufficiently violent sources (e.g. sound waves), whereas thermal 'radiation' of GWs is way below the anticipated detector sensitivity. Nevertheless, the connection between damping and thermal noise, provided by the fluctuation-dissipation theorem, is necessary for self-consistency. We explored a setting wherein the scalar field ϕ (representing an order parameter) interacts with the energy-momentum tensor of a thermal plasma, and suggested that including its thermal fluctuations would enlarge the scope of numerical simulations [1]. The thermal GW production rate from the SM is the subject of ongoing work [5], that has helped to refine the peak-region in Fig. 24 and constrain the maximal temperature in the radiation epoch.

Appendices

A. FORM code and reduction

In this appendix, we supply the FORM procedures that can be used to refine the output of Listing 1 (in Sec. 4) of the main text. The following will put the strict NLO photon self-energy into a conventional basis, i. e. the one defined by (4.16), and make use of symmetries and relationships between the integrals to put the final expression into a 'minimal' form. The steps lead to Eqs. (4.17) ad (4.18); see also Refs. [2,3,54].

Listing 2 (below) is the procedure that favours inverse propagators over products between four momenta, like in Eq. (4.13). The vectors `k`, `p`, `q`, `r`, `l` and `v` are declare in List. 1. Lines 3-6 of List. 2 simply express the definition of R in (4.3). The remaining identities follow by 'completing the square', like $P_\mu L^\mu = \frac{1}{2}(K^2 + P^2 - L^2)$ where $L = K - P$. This is the reason we only need to consider powers of energies, $p_0^m q_0^n$ in the numerator of (4.16) to describe also $\mathrm{Im}[\Pi^{00}_{(1)}]$. We note that this step can yield inverse propagators in the numerator, as encountered with $\rho^{(0,0)}_{1111(-1)}$ in (4.17).

```
1  #procedure Squares()
2
3    id p.r = k.p - p.p - p.q;
4    id q.r = k.q - q.p - q.q;
5    id l.r = k.l - l.p - l.q;
6    id v.r = k.v - v.p - v.q;
7
8    id p.q = ( r.r + k.k - l.l - v.v )/2;
9    id l.v = ( r.r + k.k - q.q - p.p )/2;
10   id p.l = ( k.k - p.p - l.l )/2;
11   id q.v = ( k.k - q.q - v.v )/2;
12   id q.l = ( l.l + q.q - r.r )/2;
13   id p.v = ( v.v + p.p - r.r )/2;
14
15   id k.p = ( p.p + k.k - l.l )/2;
16   id k.l = ( l.l + k.k - p.p )/2;
17   id k.q = ( q.q + k.k - v.v )/2;
18   id k.v = ( v.v + k.k - q.q )/2;
19
20 #endprocedure
```

Listing 2: Procedure to apply the definitions in (4.3) and re-express all products by squares of the loop and external momenta, *à la* Eqs. (4.13).

The master integral (4.16) is represented by the function `I(...)`, defined in line 1 of List. 3. Calling the procedure `Masters()` will then match the suitable pattern of squared loop momenta onto a particular 'vector' of indices a, b, d, c, e (lines 8-17) and m, n (lines 25-26).

```
1  cfunction I;
2  symbols a,b,c,d,e,m,n,;
3
4  #procedure Masters()
5
6    multiply I(0,0,0,0,0);
7    repeat;
8      id I(a?,b?,c?,d?,e?)/p.p = I(a+1,b,c,d,e);
9      id I(a?,b?,c?,d?,e?)/q.q = I(a,b+1,c,d,e);
10     id I(a?,b?,c?,d?,e?)/r.r = I(a,b,c+1,d,e);
11     id I(a?,b?,c?,d?,e?)/l.l = I(a,b,c,d+1,e);
12     id I(a?,b?,c?,d?,e?)/v.v = I(a,b,c,d,e+1);
13     id I(a?,b?,c?,d?,e?)*p.p = I(a-1,b,c,d,e);
14     id I(a?,b?,c?,d?,e?)*q.q = I(a,b-1,c,d,e);
15     id I(a?,b?,c?,d?,e?)*r.r = I(a,b,c-1,d,e);
16     id I(a?,b?,c?,d?,e?)*l.l = I(a,b,c,d-1,e);
17     id I(a?,b?,c?,d?,e?)*v.v = I(a,b,c,d,e-1);
18   endrepeat;
19
20   id I(a?,b?,c?,d?,e?) = I(a,b,c,d,e,0,0);
21   id l = k-p;
22   id v = k-q;
23   id r = k-p-q;
24   repeat;
25     id I(a?,b?,c?,d?,e?,m?,n?)*p(0) =
       I(a,b,c,d,e,m+1,n);
26     id I(a?,b?,c?,d?,e?,m?,n?)*q(0) =
       I(a,b,c,d,e,m,n+1);
27   endrepeat;
28   .sort
29
30 #endprocedure
```

Listing 3: Identification of the master integrals by 'raising' and 'lowering' indices.

Once the self-energy is expressed as a (potentially very long) linear combination of master integrals, the next task is to eliminate those that are not independent from the rest. This requires a 'priority' order to the integrals, a natural choice being to accept those with as few propagators and the lowest powers. Relations between the integrals are applied in List. 4. We shall not prove them all here but, for example, line 8 replaces

$$\not\int_{P,Q} \frac{(K-P-Q)^2}{P^2\,Q^2\,(K-P)^2\,(K-Q)^2} = \not\int_{P,Q} \frac{2}{P^2\,Q^2\,(K-P)^2} - \not\int_{P,Q} \frac{\frac{1}{2}K^2}{P^2\,Q^2\,(K-P)^2\,(K-Q)^2}\,, \tag{A.1}$$

where the dependence on loop momenta are made obvious. The equality above follows from expanding the numerator and using 1-loop identities like

$$\not\int_P \frac{P_\mu}{P^2(K-P)^2} = \frac{1}{2}K_\mu \not\int_P \frac{1}{P^2(K-P)^2}\,.$$

Another important symmetry in the master integrals, due to the fermionic nature of momenta P and Q, is the component-wise swap of (a, d, m) with (b, e, n) as expressed by line 10 which symmetrises the corresponding arguments of `I`.

```
1  #procedure Reduce()
2
3    id I(0,0,1,1,1,0,0)   = I(1,1,1,0,0,0,0);
4    id I(1,1,1,1,1,1,0)   = I(1,1,1,1,1,0,0)*k(0)/2;
5    id I(1,1,1,1,1,0,1)   = I(1,1,1,1,1,0,0)*k(0)/2;
6    id I(1,1,0,1,1,1,n?)  = I(1,1,0,1,1,0,n)*k(0)/2;
7    id I(1,1,0,1,1,m?,1)  = I(1,1,0,1,1,m,0)*k(0)/2;
8    id I(1,1,-1,1,1,0,0)  = 2*I(1,1,0,1,0,0,0)
                           - k.k*I(1,1,0,1,1,0,0)/2;
9
10   symmetrize I (1,4,6) (2,5,7);
11   .sort
12
13   id I(a?,b?,c?,0,e?,m?,n?) = I(b,a,c,e,0,n,m);
14   id I(0,b?,c?,d?,e?,m?,n?) = I(b,0,c,e,d,n,m);
15   .sort
16
17   id I(a?,0,c?,d?,e?,0,0) = I(d,e,c,a,0,0,0);
18   id I(a?,0,c?,d?,e?,1,0) = I(d,e,c,a,0,0,0)*k(0)
                             - I(d,e,c,a,0,1,0);
19   id I(a?,0,c?,d?,e?,0,1) = I(d,e,c,a,0,0,0)*k(0)
                             - I(d,e,c,a,0,0,1);
20   id I(a?,0,c?,d?,e?,1,1) = I(d,e,c,a,0,0,0)*k(0)^2
                             - I(d,e,c,a,0,1,0)*k(0)
                             - I(d,e,c,a,0,0,1)*k(0)
                             + I(d,e,c,a,0,1,1);
21   id I(a?,0,c?,d?,e?,2,0) = I(d,e,c,a,0,0,0)*k(0)^2
                             - I(d,e,c,a,0,1,0)*2*k(0)
                             + I(d,e,c,a,0,2,0);
22   id I(a?,0,c?,d?,e?,0,2) = I(d,e,c,a,0,0,0)*k(0)^2
                             - I(d,e,c,a,0,0,1)*2*k(0)
                             + I(d,e,c,a,0,0,2);
23   .sort
24
25 #endprocedure
```

Listing 4: This procedure implements the reduction steps by explicitly identifying relations between master integrals. These relations are derived by hand, like (A.1) for line 8. Lines 4 and 5 follow from exchanging $(P, Q) \leftrightarrow (L, V)$ and lines 6 and 7 follow because $c = 0$ means that the integrals over P and Q decouple. Most of the other identities are simple shifts in the integration variables to obtain a 'canonical' ordering on a, b, c, d, e.

To recap, the symbolic output of List. 1 can be processed by the FORM procedures `Squares()`, `Masters()` and `Reduce()` in that order. One arrives at Eqs. (4.17) and (4.18) after taking the imaginary part, which removes a few terms. This also allows one, if `xi` is kept non-zero, to check gauge independence. A few further reduction steps beyond those in List. 4 are required to verify this.

B. Feynman rules for a reduced weak sector

The interaction of the temporal gauge fields with the scalar Higgs sector can be attributed to the last line of (9.1). Expressed in terms of the relevant fields, this reveals their mutual interactions in the broken phase

$$\begin{aligned}\frac{g^2}{4}\vec{W}_0^{\,2}\Phi^\dagger\Phi+\frac{g'^2}{4}B_0^2\Phi^\dagger\Phi-\frac{gg'}{2}B_0\Phi^\dagger\big(\vec{W}_0\cdot\vec{\sigma}\big)\Phi \;&=\; \frac{g^2}{2}W_0^+W_0^-\big(\Phi^\dagger\Phi\big) \\ &-\; \frac{g\widetilde{g}}{4}\big(Z_0+Z_0'\big)\Big[\,W_0^+\phi^-(v+\phi_0+i\phi_3)+\text{c.c.}\,\Big] \\ &+\; \frac{\widetilde{g}^2}{8}\Big[\,Z_0^2\big((v+\phi_0)^2+\phi_3^2\big)+2Z_0'^2\phi^+\phi^-\,\Big]\,.\end{aligned} \tag{B.1}$$

This expression includes the W- and Z-boson masses (at zero temperature), which get combined with their effective thermal masses. That is why we substitute

$$Z_0 \;=\; +\cos(\theta-\widetilde{\theta})\widetilde{Z}_0+\sin(\theta-\widetilde{\theta})\widetilde{A}_0\,, \tag{B.2}$$

$$Z_0' \;=\; -\cos(\theta+\widetilde{\theta})\widetilde{Z}_0+\sin(\theta+\widetilde{\theta})\widetilde{A}_0\,, \tag{B.3}$$

in (B.1) to derive the following Feynman rules.

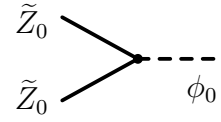

$$=\; -\widetilde{g}\cos^2(\theta-\widetilde{\theta})\;m_Z \tag{B.4}$$

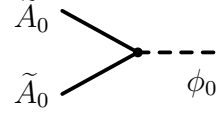

$$=\; -\widetilde{g}\sin^2(\theta-\widetilde{\theta})\;m_Z \tag{B.5}$$

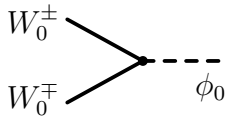

$$=\; -\widetilde{g}\cos^2\theta\;m_W \tag{B.6}$$

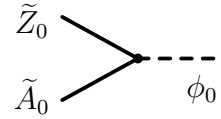

$$=\; -\frac{\widetilde{g}}{2}\sin\big[2(\theta-\widetilde{\theta})\big]\;m_Z \tag{B.7}$$

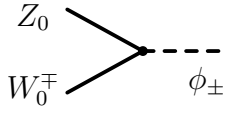

$$=\; +\widetilde{g}\sin\theta\sin\widetilde{\theta}\;m_W \tag{B.8}$$

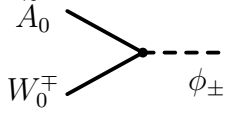

$$=\; +\widetilde{g}\sin\theta\cos\widetilde{\theta}\;m_W \tag{B.9}$$

Temporal and scalar fields were denoted using solid and dashed lines respectively. Here (and throughout this appendix) the coupling $\widetilde{g}$ is preferred over $g=\widetilde{g}\cos\theta$. Note that we

include a symmetry factor wherever identical fields emanate from a vertex. The masses are related by $\widetilde{g}/g = m_Z/m_W$ in the broken phase.

The neutral $\widetilde{Z}_0$ and $\widetilde{A}_0$ fields have quartic interactions with all the scalars.

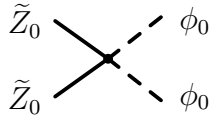

$$= \quad -\frac{\widetilde{g}^2}{2}\cos^2(\theta-\widetilde{\theta}) \tag{B.10}$$

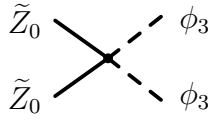

$$= \quad -\frac{\widetilde{g}^2}{2}\cos^2(\theta-\widetilde{\theta}) \tag{B.11}$$

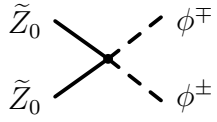

$$= \quad -\frac{\widetilde{g}^2}{2}\cos^2(\theta+\widetilde{\theta}) \tag{B.12}$$

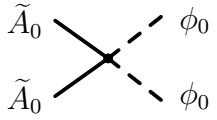

$$= \quad -\frac{\widetilde{g}^2}{2}\sin^2(\theta-\widetilde{\theta}) \tag{B.13}$$

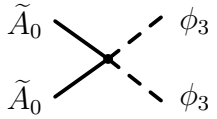

$$= \quad -\frac{\widetilde{g}^2}{2}\sin^2(\theta-\widetilde{\theta}) \tag{B.14}$$

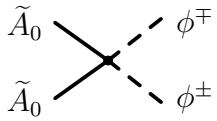

$$= \quad -\frac{\widetilde{g}^2}{2}\sin^2(\theta+\widetilde{\theta}) \tag{B.15}$$

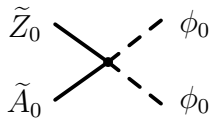

$$= \quad -\frac{\widetilde{g}^2}{4}\sin\left[2(\theta-\widetilde{\theta})\right] \tag{B.16}$$

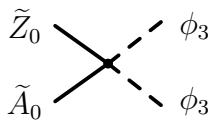

$$= \quad -\frac{\widetilde{g}^2}{4}\sin\left[2(\theta-\widetilde{\theta})\right] \tag{B.17}$$

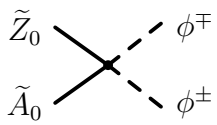

$$= \quad +\frac{\widetilde{g}^2}{4}\sin\left[2(\theta+\widetilde{\theta})\right] \tag{B.18}$$

Similarly, the charged $W_0^\pm$ fields have vertices from the first line in (B.1), describing its

mutual interactions with the Higgs. They are just (B.10), (B.11) and (B.12) with $\widetilde{\theta} \to 0$.

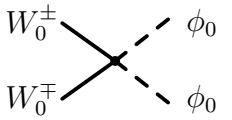

$$= \quad -\frac{\widetilde{g}^2}{2}\cos^2\theta \tag{B.19}$$

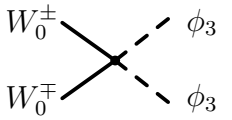

$$= \quad -\frac{\widetilde{g}^2}{2}\cos^2\theta \tag{B.20}$$

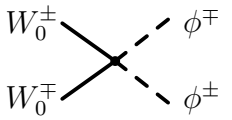

$$= \quad -\frac{\widetilde{g}^2}{2}\cos^2\theta \tag{B.21}$$

The second line in (B.1) involves four-point interactions which mix neutral and charged scalars and temporal fields. There are several terms, leading to these vertices:

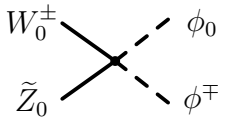

$$= \quad -\frac{\widetilde{g}^2}{4}\sin(2\theta)\sin\widetilde{\theta} \tag{B.22}$$

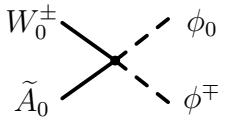

$$= \quad -\frac{\widetilde{g}^2}{4}\sin(2\theta)\cos\widetilde{\theta} \tag{B.23}$$

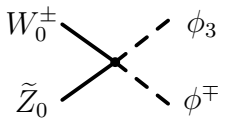

$$= \quad \mp i\frac{\widetilde{g}^2}{4}\sin(2\theta)\sin\widetilde{\theta} \tag{B.24}$$

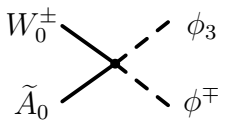

$$= \quad \mp i\frac{\widetilde{g}^2}{4}\sin(2\theta)\cos\widetilde{\theta} \tag{B.25}$$

The mutual interactions between the temporal and spatial gauge fields follows from the kinetic term for $\vec{W}_0$, which may be expanded

$$\begin{aligned}\frac{1}{2}(D_i\vec{W}_0)(D_i\vec{W}_0) \;&=\; \frac{1}{2}(\partial_i\vec{W}_0)(\partial_i\vec{W}_0) \\ &+\; g(\partial_i\vec{W}_0)\cdot(\vec{W}_i\times\vec{W}_0) \;+\; \frac{g^2}{2}(\vec{W}_i\times\vec{W}_0)^2\,.\end{aligned} \tag{B.26}$$

We substitute $gW_0^3 = \widetilde{g}\cos\theta\,\big(\,\cos\widetilde{\theta}\,\widetilde{Z}_0 - \sin\widetilde{\theta}\,\widetilde{A}_0\,\big)$ to involve the correct temporal mass eigenstates and similarly for W_i^3 (with $\widetilde{\theta}\to\theta$) to bring in Z_i and A_i. These spatial gauge fields will be denoted by a wiggly line in Feynman diagrams. Then the $O(g)$ terms in (B.26) provide the following cubic vertices, which is momentum dependent due to the derivative interaction (e. g. $\nabla \to i\,\boldsymbol{p}$).

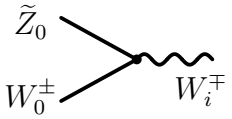

$$= \pm\,\widetilde{g}\cos\theta\,\cos\widetilde{\theta}\;(p-q)_i \tag{B.27}$$

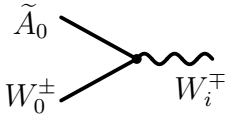

$$= \mp\,\widetilde{g}\cos\theta\,\sin\widetilde{\theta}\;(p-q)_i \tag{B.28}$$

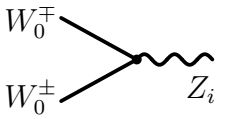

$$= \mp\,\widetilde{g}\cos^2\theta\;(p-q)_i \tag{B.29}$$

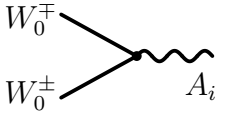

$$= \pm\,\frac{\widetilde{g}}{2}\sin(2\theta)\;(p-q)_i \tag{B.30}$$

Here $\boldsymbol{p}$ and $\boldsymbol{q}$ denote the momenta for the upper and lower scalar lines respectively, so that the vertices are antisymmetric under interchange of the temporal fields. We direct the momentum flow (not explicitly shown) *into* the vertex.

The quartic terms in (B.26) each contain two vector and two scalar fields. Those with all charged external legs can take the following forms, being consistent with charge conservation. We prefer to substitute $g = \widetilde{g}\cos\theta$ for the coupling.

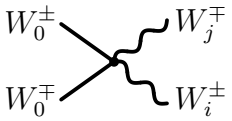

$$= -\,\widetilde{g}^2\cos^2\theta\,\delta_{ij} \tag{B.31}$$

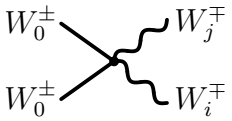

$$= +\,2\widetilde{g}^2\cos^2\theta\,\delta_{ij} \tag{B.32}$$

Neutral fields can couple in many different ways to the charged ones. The quartic vertices for them are as follows.

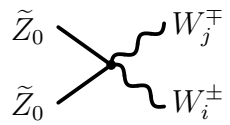

$$= \quad -2\widetilde{g}^2 \cos^2\theta \cos^2\widetilde{\theta}\,\delta_{ij} \tag{B.33}$$

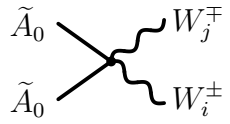

$$= \quad -2\widetilde{g}^2 \cos^2\theta \sin^2\widetilde{\theta}\,\delta_{ij} \tag{B.34}$$

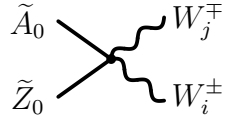

$$= \quad +\frac{\widetilde{g}^2}{2} \cos^2\theta \sin(2\widetilde{\theta})\,\delta_{ij} \tag{B.35}$$

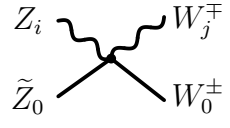

$$= \quad -\widetilde{g}^2 \cos^3\theta \cos\widetilde{\theta}\,\delta_{ij} \tag{B.36}$$

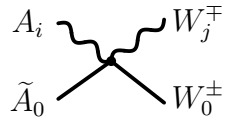

$$= \quad -\widetilde{g}^2 \cos^2\theta \sin\theta \sin\widetilde{\theta}\,\delta_{ij} \tag{B.37}$$

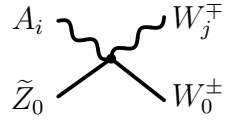

$$= \quad +\widetilde{g}^2 \cos^2\theta \sin\theta \cos\widetilde{\theta}\,\delta_{ij} \tag{B.38}$$

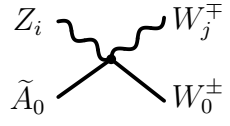

$$= \quad +\widetilde{g}^2 \cos^3 \sin\widetilde{\theta}\,\delta_{ij} \tag{B.39}$$

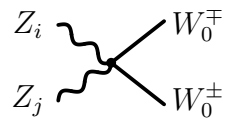

$$= \quad -2\widetilde{g}^2 \cos^4\theta\,\delta_{ij} \tag{B.40}$$

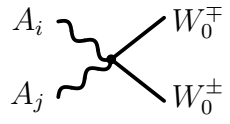

$$= \quad -2\widetilde{g}^2 \cos^2\theta \sin^2\theta\,\delta_{ij} \tag{B.41}$$

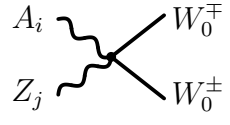

$$= \quad +\frac{\widetilde{g}^2}{2} \cos^2\theta \sin(2\theta)\,\delta_{ij} \tag{B.42}$$

(We will now discuss the rules that carry over from ordinary electroweak perturbation theory at finite temperature. They are, point of fact, recoverable by keeping only the non-zero spacetime indices μ, ν, etc. Furthermore, many can be found from those above by setting $\widetilde{\theta} \to \theta$ due to no additional mass mixing.)

Moving on to the Higgs sector, we recal that $m_H = \sqrt{2\lambda v^2}$ to rewrite the vertices in terms of the masses. (Remember that symmetry factors for identical lines are included.)

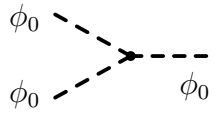

$$= \quad -\widetilde{g}\,\frac{3\,m_H^2}{2\,m_Z} \tag{B.43}$$

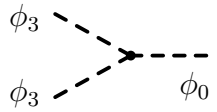

$$= \quad -\widetilde{g}\,\frac{m_H^2}{2\,m_Z} \tag{B.44}$$

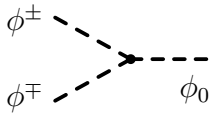

$$= \quad -\widetilde{g}\,\frac{m_H^2}{2\,m_Z} \tag{B.45}$$

$$= \quad -\widetilde{g}^2\,\frac{3\,m_H^2}{4\,m_Z^2} \tag{B.46}$$

$$= \quad -\widetilde{g}^2\,\frac{3\,m_H^2}{4\,m_Z^2} \tag{B.47}$$

$$= \quad -\widetilde{g}^2\,\frac{m_H^2}{4\,m_Z^2} \tag{B.48}$$

$$= \quad -\widetilde{g}^2\,\frac{m_H^2}{4\,m_Z^2} \tag{B.49}$$

$$= \quad -\widetilde{g}^2\,\frac{m_H^2}{4\,m_Z^2} \tag{B.50}$$

$$= \quad -\widetilde{g}^2\,\frac{m_H^2}{2\,m_Z^2} \tag{B.51}$$

Spatial gauge fields also interact with the (Higgs) scalar sector. This happens in the usual way, due to the kinetic term $(D_i\Phi)^\dagger(D_i\Phi)$ in (9.1). In the broken-symmetric phase, Φ is rewritten according to (9.2) and Z_i, A_i and $W_i^\pm$. Momenta $\boldsymbol{p}$ and $\boldsymbol{q}$ flow into the vertex and correspond to the upper and lower left legs respectively.

$$= \quad -\frac{\widetilde{g}}{2}\cos(2\theta)\ (p-q)_i \tag{B.52}$$

$$= \quad -i\frac{\widetilde{g}}{2}\ (p-q)_i \tag{B.53}$$

$$= \quad -\frac{\widetilde{g}}{2}\sin(2\theta)\ (p-q)_i \tag{B.54}$$

$$= \quad \mp\frac{\widetilde{g}}{2}\cos\theta\ (p-q)_i \tag{B.55}$$

$$= \quad -i\frac{\widetilde{g}}{2}\cos\theta\ (p-q)_i \tag{B.56}$$

The cubic vertices with two spatial fields and one scalar do not depend on momentum. But the two indices (i and j) must be equal, as δ_{ij} ensures.

$$= \quad +\widetilde{g}\sin^2\theta\, m_W\ \delta_{ij} \tag{B.57}$$

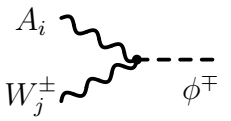

$$= \quad -\frac{\widetilde{g}}{2}\sin(2\theta)\, m_W\ \delta_{ij} \tag{B.58}$$

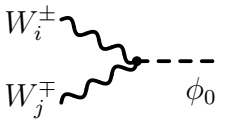

$$= \quad -\widetilde{g}\cos^2\theta\, m_Z\ \delta_{ij} \tag{B.59}$$

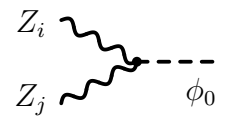

$$= \quad -\widetilde{g}\, m_Z\ \delta_{ij} \tag{B.60}$$

As far as the quartic interactions go, each contains two gauge fields and two scalar fields.

The charged boson interacts with all Goldstone modes equally:

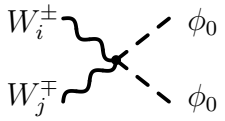

$$= \quad -\frac{\widetilde{g}^2}{2}\cos^2\theta\ \delta_{ij} \tag{B.61}$$

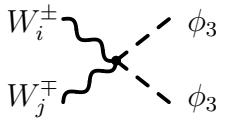

$$= \quad -\frac{\widetilde{g}^2}{2}\cos^2\theta\ \delta_{ij} \tag{B.62}$$

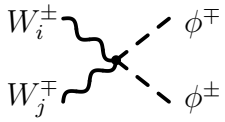

$$= \quad -\frac{\widetilde{g}^2}{2}\cos^2\theta\ \delta_{ij} \tag{B.63}$$

The Z-boson interacts with both neutral scalar fields in the same manner, while the charged scalars mix differently with the two neutral bosons. Spatial photons, A_i, interact only with the charged scalar bosons (unlike $\widetilde{A}_0$). Compare this to Eqs. (B.10)-(B.18), with $\widetilde{\theta} \to \theta$ to replace temporal fields with spatial ones.

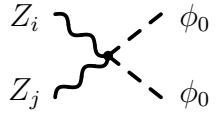

$$= \quad -\frac{\widetilde{g}^2}{2}\ \delta_{ij} \tag{B.64}$$

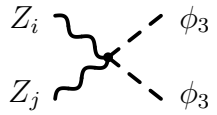

$$= \quad -\frac{\widetilde{g}^2}{2}\ \delta_{ij} \tag{B.65}$$

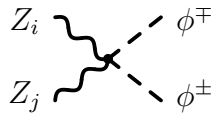

$$= \quad -\frac{\widetilde{g}^2}{2}\cos^2(2\theta)\ \delta_{ij} \tag{B.66}$$

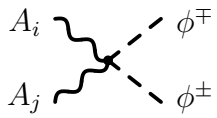

$$= \quad -\frac{\widetilde{g}^2}{2}\sin^2(2\theta)\ \delta_{ij} \tag{B.67}$$

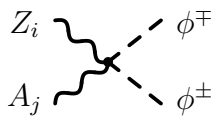

$$= \quad -\frac{\widetilde{g}^2}{2}\sin(2\theta)\cos(2\theta)\ \delta_{ij} \tag{B.68}$$

Then there are also the interactions between charged scalars, neutral scalars, charged bosons and neutral bosons.

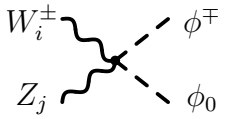

$$= \quad + \frac{\widetilde{g}^2}{2} \cos\theta \sin^2\theta \ \delta_{ij} \tag{B.69}$$

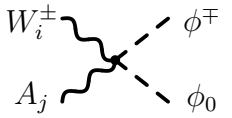

$$= \quad + \frac{\widetilde{g}^2}{2} \cos^2\theta \sin\theta \ \delta_{ij} \tag{B.70}$$

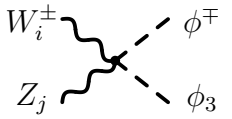

$$= \quad \pm i \frac{\widetilde{g}^2}{2} \cos\theta \sin^2\theta \ \delta_{ij} \tag{B.71}$$

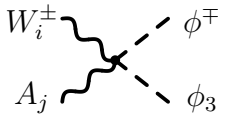

$$= \quad \pm i \frac{\widetilde{g}^2}{2} \cos^2\theta \sin\theta \ \delta_{ij} \tag{B.72}$$

As usual, the non-abelian self interactions get inherited by the spatial vector fields. It is useful to define (for external vectors $\boldsymbol{p}$ and $\boldsymbol{q}$)

$$Y_{ijk} = \delta_{ij}(p-q)_k + \delta_{ki}(p+2q)_j - \delta_{jk}(2p+q)_i \ ,$$

a general three point function, already accounting for momentum conservation. In what follows, we associate the momenta $\boldsymbol{p}$ and $\boldsymbol{q}$ with the external fields $W_i^\pm$ and $W_j^\mp$ respectively. Momentum flows *into* the vertex.

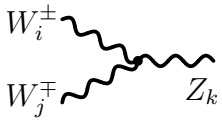

$$= \quad -\widetilde{g} \cos^2\theta \ Y_{ijk}(\boldsymbol{p}, \boldsymbol{q}) \tag{B.73}$$

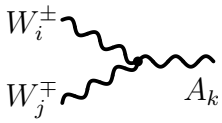

$$= \quad -\frac{\widetilde{g}}{2} \sin(2\theta) \ Y_{ijk}(\boldsymbol{p}, \boldsymbol{q}) \tag{B.74}$$

The quartic couplings are momentum independent, but proportional to the rank four tensor

$$X_{ijkl} = 2\delta_{ij}\delta_{kl} - \delta_{ik}\delta_{jl} - \delta_{il}\delta_{jk}\,.$$

Allowable configurations and their relative interaction strengths are as follows. Consistency with Eqs. (B.33)-(B.42) can be checked by setting $\widetilde{\theta} \to \theta$.

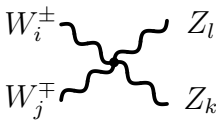

$$= \quad -\widetilde{g}^2 \cos^4\theta \; X_{ijkl} \tag{B.75}$$

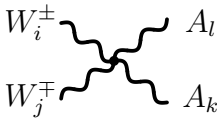

$$= \quad -\widetilde{g}^2 \cos^2\theta \sin^2\theta \; X_{ijkl} \tag{B.76}$$

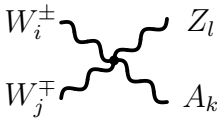

$$= \quad -\widetilde{g}^2 \cos^3\theta \sin\theta \; X_{ijkl} \tag{B.77}$$

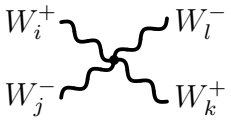

$$= \quad -\widetilde{g}^2 \cos^2\theta \; X_{ijkl} \tag{B.78}$$

The vector fields, in a general (linear) gauge, require ghost fields to be included. Their interactions are the same as at $T = 0$ and follow by incorporating Fadeev-Popov terms in the Lagrangian for the spatial components. Thus, denoting by $\boldsymbol{p}$ the momentum of the

outgoing fermion, the vertices are

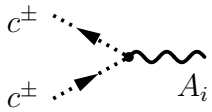

$$= \mp\, \widetilde{g} \sin\theta \cos\theta \; p_i \tag{B.79}$$

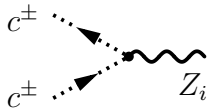

$$= \mp\, \widetilde{g} \cos^2\theta \; p_i \tag{B.80}$$

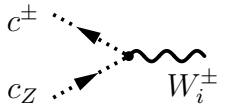

$$= \pm\, \widetilde{g} \cos^2\theta \; p_i \tag{B.81}$$

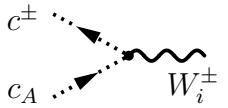

$$= \pm\, \widetilde{g} \sin\theta \cos\theta \; p_i \tag{B.82}$$

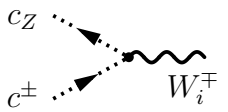

$$= \pm\, \widetilde{g} \cos^2\theta \; p_i \tag{B.83}$$

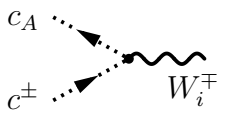

$$= \pm\, \widetilde{g} \sin\theta \cos\theta \; p_i \tag{B.84}$$

The ghosts do not interact with $\widetilde{A}_0$, $\widetilde{Z}_0$ or $W_0^\pm$ because no gauge fixing is needed for the temporal scalars. We apply gauge fixing uniformly to the $\vec{W}_i$ and B_i fields, in a covariant manner parametrised by ξ:

$$\begin{aligned} \mathcal{L}_{\text{g.f.}} &= -\frac{1}{2\xi}\Big(\partial_i \vec{W}_i + \xi \frac{gv}{2}\vec{\phi}\Big)^2 - \frac{1}{2\xi}\Big(\partial_i B_i + \xi \frac{g'v}{2}\phi_3\Big)^2 \qquad \text{(B.85)} \\ &= -\frac{1}{2\xi}(\partial_i \vec{W}_i)^2 - \frac{1}{2\xi}(\partial_i B_i)^2 - \frac{gv}{2}(\partial_i \vec{W}_i)\cdot\vec{\phi} - \frac{g'v}{2}(\partial_i B_i)\phi_3 - \xi m_W^2\, \phi^+\phi^- - \frac{1}{2}\xi m_Z^2 \phi_3^2 \,. \end{aligned}$$

This leads to $\phi^\pm$ and ϕ_3 acquiring masses ξm_W^2 and ξm_Z^2 respectively. The two mixing terms that fell out of (B.85) combine with similar terms in the kinetic energy for the Higgs field, to give a total derivative. (So that they can be ignored.)

Therefore the Goldstone bosons also interact with the ghosts, except if $\xi \to 0$ (Landau

gauge).

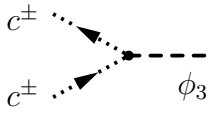

$$= \mp i\,\frac{\widetilde{g}}{2}\cos^2\theta\;\xi\,m_Z \tag{B.86}$$

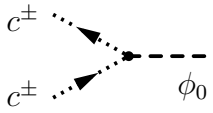

$$= -\frac{\widetilde{g}}{2}\cos^2\theta\;\xi\,m_Z \tag{B.87}$$

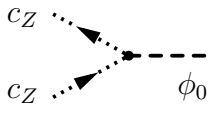

$$= -\frac{\widetilde{g}}{2}\;\xi\,m_Z \tag{B.88}$$

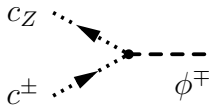

$$= +\frac{\widetilde{g}}{2}\cos\theta\;\xi\,m_Z \tag{B.89}$$

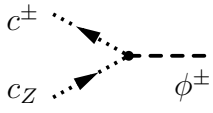

$$= -\frac{\widetilde{g}}{2}\cos(2\theta)\;\xi\,m_W \tag{B.90}$$

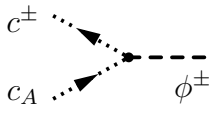

$$= -\widetilde{g}\sin\theta\cos\theta\;\xi\,m_W \tag{B.91}$$

C. Energy integral within $\delta\langle T^\phi_{xy}\rangle/\delta g_{xy}$

In Sec. 13 we encountered a linear response function of the energy-momentum tensor with respect to a perturbed metric. The 1-loop effect of fluctuations involved an integration over the intermediate energy, see Eq. (13.16), which we discuss further in this appendix. After recognising that the numerator of that expression is a quadratic polynomial in the energy variable, we study

$$I_\alpha \;:=\; \int_{-\infty}^{+\infty}\frac{dp_0}{2\pi}\,\frac{p_0^\alpha}{\big[\,(\epsilon_{\boldsymbol{p}}^2-p_0^2)^2+\gamma^2p_0^2\,\big]\Big[\,\big(\epsilon_{\boldsymbol{\ell}}^2-(\omega-p_0)^2\big)^2+\gamma^2p_0^2\,\Big]}\;, \tag{C.1}$$

for $\alpha=\{0,1,2\}$. The on-shell energies that appear in the denominators are

$$\epsilon_{\boldsymbol{p}} \;=\; \sqrt{\boldsymbol{p}^2+m^2}\quad\text{and}\quad \epsilon_{\boldsymbol{\ell}} \;=\; \sqrt{(\boldsymbol{k}-\boldsymbol{p})^2+m^2}\,.$$

For non-zero γ, there are eight distinct poles from the integrand of I_α. Each pole is simple, and altogether they are summarised by the set

$$\left\{\;\pm i\frac{\gamma}{2}\pm\frac{d_p}{2}\,,\;\omega\pm i\frac{\gamma}{2}\pm\frac{d_\ell}{2}\;\right\};\qquad d_p\;=\;\sqrt{4\epsilon_{\boldsymbol{p}}^2-\gamma^2}\quad\text{and}\quad d_\ell\;=\;\sqrt{4\epsilon_{\boldsymbol{\ell}}^2-\gamma^2}\,. \tag{C.2}$$

The momentum $\boldsymbol{p}$ is 'fixed', but unrestricted with respect to the outer integration. Hence we should be careful in considering the positions of the poles. In particular, the discriminants d_p and d_ℓ may either be real or purely imaginary. This depends upon whether $|\boldsymbol{p}| < \frac{1}{4}\gamma^2 - m^2$ or in the alternative case $|\boldsymbol{k}-\boldsymbol{p}| < \frac{1}{4}\gamma^2 - m^2$. In Fig. 26 we depict a configuration where d_p is real and d_ℓ is imaginary. We note that, taking the principal branch of the square root, $\mathrm{Im}\,[d_{p,\ell}] > \gamma$, and hence the same four poles always remain in the upper or lower half-plane. Since γ is assumed to be positive, the poles in the former have a plus sign for $i\gamma$ in (C.2).

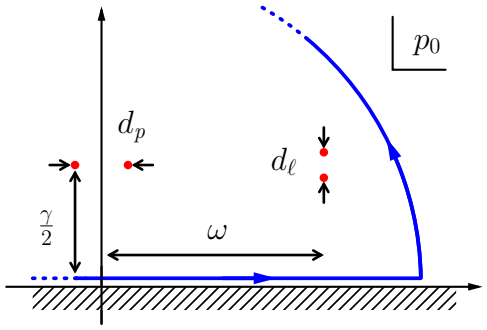

Figure 26: Upper half of the complex p_0-plane, where a semicircular contour (blue) is used to evaluate I_α. The poles from (C.2) are indicated by red points and their conjugates are reflected in the lower half-plane. Here the external vector $\boldsymbol{k}$ is such that d_p is real but d_ℓ is imaginary.

We can then proceed to evaluate (C.1) by standard methods, using a semicircular contour closed in the upper half-plane, see Fig. 26. As the radius of this contour becomes arbitrarily large, the contribution from the semi-circle vanishes. Cauchy's theorem then implies that I_α may be obtained from the sum of enclosed residues.

In the $\boldsymbol{k} \to 0$ limit we have $d_p = d_\ell$. Since this is the case of interest for the hydrodynamic calculation (before considering small ω), the structures needed are

$$I_0 = \frac{2}{\Xi}\big(4(\epsilon_{\boldsymbol{p}}^2+\gamma^2)+\omega^2\big), \qquad I_1 = \frac{\omega}{\Xi}\big(4(\epsilon_{\boldsymbol{p}}^2+\gamma^2)+\omega^2\big),$$
$$I_2 = \frac{1}{\Xi}\big(8\epsilon_{\boldsymbol{p}}^4 - 2(\epsilon_{\boldsymbol{p}}^2-2\gamma^2)+\omega^4\big), \tag{C.3}$$

where we introduced

$$\Xi = 2\gamma\epsilon_{\boldsymbol{p}}^2(\gamma^2+\omega^2)\big((4\epsilon_{\boldsymbol{p}}^2-\omega^2)^2+4\gamma^2\omega^2\big).$$

Returning now to the expression in Eq. (13.16), we recognise that it may be written as a linear combination of I_α. The response to the metric perturbation is thus

$$\frac{\delta\langle T^\phi_{xy}\rangle}{\delta g_{xy}} = 2\Omega\int_{\boldsymbol{p}} p_x^2 p_y^2\,\big[\,(2\epsilon_{\boldsymbol{p}}^2-\omega^2+i\gamma\omega)I_0 + 2\omega I_1 - 2I_2\,\big], \tag{C.4}$$

which gives (13.18) after using Eqs. (C.3).

Bibliography

[1] G. Jackson and M. Laine *Eur. Phys. J.* **C78** (Apr, 2018) 304, arXiv:1803.01871 [hep-ph].

[2] G. Jackson *Phys. Rev.* **D100** no. 11, (2019) 116019, arXiv:1910.07552 [hep-ph].

[3] G. Jackson and M. Laine *JHEP* **11** (2019) 144, arXiv:1910.09567 [hep-ph].

[4] G. Jackson and M. Laine *Nucl. Phys.* **B950** (2020) 114870, arXiv:1910.12880 [hep-ph].

[5] J. Ghiglieri, G. Jackson, M. Laine, and Y. Zhu *JHEP* **07** (2020) 092, arXiv:2004.11392 [hep-ph].

[6] A. A. Penzias and R. W. Wilson *Astrophys. J.* **142** (1965) 419–421.

[7] S. Weinberg, *The First Three Minutes*. Basic Books, 1977.

[8] F. Halzen and A. Martin, *Quarks and Leptons*. Wiley, 1984.

[9] G. 't Hooft and M. J. G. Veltman *Nucl. Phys.* **B44** (1972) 189–213.

[10] P. W. Anderson *Science* **177** (1972) 393–396.

[11] D. Maoz, *Astrophysics in a Nutshell*. Princeton University Press, 2016.

[12] D. Clowe, M. Bradac, A. H. Gonzalez, M. Markevitch, S. W. Randall, C. Jones, and D. Zaritsky *Astrophys. J.* **648** (2006) L109–L113, arXiv:astro-ph/0608407 [astro-ph].

[13] S. Gasiorowicz and J. L. Rosner *Am. J. Phys.* **49** (1981) 954.

[14] S. Weinberg *Phys. Rev. Lett.* **19** (1967) 1264–1266.

[15] R. Hagedorn *Nuovo Cim. Suppl.* **3** (1965) 147–186.

[16] **Particle Data Group** Collaboration, M. Tanabashi *et al. Phys. Rev.* **D98** no. 3, (2018) 030001.

[17] J. Cleymans and D. Worku *Mod. Phys. Lett.* **A26** (2011) 1197–1209, arXiv:1103.1463 [hep-ph].

[18] D. J. Gross and F. Wilczek *Phys. Rev. Lett.* **30** (1973) 1343–1346.

[19] A. Bazavov *et al. Phys. Rev.* **D85** (2012) 054503, arXiv:1111.1710 [hep-lat].

[20] P. Braun-Munzinger and J. Stachel *Nature* **448** (2007) 302–309.

[21] R. D. Pisarski *Phys. Lett. B* **110** (1982) 155–158.

[22] M. D'Onofrio and K. Rummukainen *Phys. Rev.* **D93** no. 2, (2016) 025003, arXiv:1508.07161 [hep-ph].

[23] A. D. Sakharov *Pisma Zh. Eksp. Teor. Fiz.* **5** (1967) 32–35.

[24] D. E. Morrissey and M. J. Ramsey-Musolf *New J. Phys.* **14** (2012) 125003, arXiv:1206.2942 [hep-ph].

[25] B. W. Lee and S. Weinberg *Phys. Rev. Lett.* **39** (1977) 165–168.

[26] M. Drewes *et al.* *JCAP* **1701** (2017) 025, arXiv:1602.04816 [hep-ph].

[27] N. Turok *Phys. Rev. Lett.* **68** (1992) 1803–1806.

[28] A. Klein *et al.* *Phys. Rev. D* **93** no. 2, (2016) 024003, arXiv:1511.05581 [gr-qc].

[29] C. Caprini *et al.* *JCAP* **1604** no. 04, (2016) 001, arXiv:1512.06239 [astro-ph.CO].

[30] D. Bödeker and G. D. Moore *JCAP* **0905** (2009) 009, arXiv:0903.4099 [hep-ph].

[31] D. Bödeker and G. D. Moore *JCAP* **1705** no. 05, (2017) 025, arXiv:1703.08215 [hep-ph].

[32] M. Hindmarsh, S. J. Huber, K. Rummukainen, and D. J. Weir *Phys. Rev.* **D96** no. 10, (2017) 103520, arXiv:1704.05871 [astro-ph.CO].

[33] T. L. Smith, E. Pierpaoli, and M. Kamionkowski *Phys. Rev. Lett.* **97** (2006) 021301, arXiv:astro-ph/0603144.

[34] S. Henrot-Versille *et al.* *Class. Quant. Grav.* **32** no. 4, (2015) 045003, arXiv:1408.5299 [astro-ph.CO].

[35] M. Laine and A. Vuorinen, *Basics of Thermal Field Theory*, vol. 925. Springer, 2016. arXiv:1701.01554 [hep-ph].

[36] S. Davidson, P. Gambino, M. Laine, M. Neubert, and C. Salomon, *Effective Field Theories in Particle Physics and Cosmology*. Oxford University Press, 2020.

[37] **STAR** Collaboration, L. Adamczyk *et al.* *Phys. Rev. C* **92** no. 2, (2015) 024912, arXiv:1504.01317 [hep-ex].

[38] **STAR** Collaboration, J. Adam *et al.* arXiv:1810.10159 [nucl-ex].

[39] E. M. Lifshitz and L. P. Pitaevskii, *Physical Kinetics*. Pergamon Press, 1981.

[40] G. Vujanovic, J.-F. Paquet, C. Shen, G. S. Denicol, S. Jeon, C. Gale, and U. Heinz *Phys. Rev. C* **101** (2020) 044904, arXiv:1903.05078 [nucl-th].

[41] T. Song, W. Cassing, P. Moreau, and E. Bratkovskaya *Phys. Rev. C* **98** no. 4, (2018) 041901, arXiv:1806.09377 [nucl-th].

[42] J. I. Kapusta, P. Lichard, and D. Seibert *Phys. Rev.* **D44** (1991) 2774–2788. [Erratum: Phys. Rev.D47,4171(1993)].

[43] R. Baier, H. Nakkagawa, A. Niégawa, and K. Redlich *Z. Phys.* **C53** (1992) 433–438.

[44] R. Baier, B. Pire, and D. Schiff *Phys. Rev.* **D38** (1988) 2814.

[45] Y. Gabellini, T. Grandou, and D. Poizat *Annals Phys.* **202** (1990) 436–466.

[46] T. Altherr and P. Aurenche *Z. Phys.* **C45** (1989) 99.

[47] E. Braaten, R. D. Pisarski, and T.-C. Yuan *Phys. Rev. Lett.* **64** (1990) 2242.

[48] T. Altherr and P. V. Ruuskanen *Nucl. Phys.* **B380** (1992) 377–390.

[49] M. H. Thoma and C. T. Traxler *Phys. Rev. D* **56** (1997) 198–202, arXiv:hep-ph/9701354.

[50] P. B. Arnold, G. D. Moore, and L. G. Yaffe *JHEP* **11** (2001) 057, arXiv:hep-ph/0109064 [hep-ph].

[51] P. B. Arnold, G. D. Moore, and L. G. Yaffe *JHEP* **12** (2001) 009, arXiv:hep-ph/0111107 [hep-ph].

[52] P. Aurenche, F. Gelis, G. D. Moore, and H. Zaraket *JHEP* **12** (2002) 006, arXiv:hep-ph/0211036 [hep-ph].

[53] M. Laine *JHEP* **05** (2013) 083, arXiv:1304.0202 [hep-ph].

[54] M. Laine *JHEP* **11** (2013) 120, arXiv:1310.0164 [hep-ph].

[55] J. Ghiglieri, J. Hong, A. Kurkela, E. Lu, G. D. Moore, and D. Teaney *JHEP* **05** (2013) 010, arXiv:1302.5970 [hep-ph].

[56] J. Ghiglieri and G. D. Moore *JHEP* **12** (2014) 029, arXiv:1410.4203 [hep-ph].

[57] K. Dusling and I. Zahed *Phys. Rev.* **C82** (2010) 054909, arXiv:0911.2426 [nucl-th].

[58] C.-H. Lee and I. Zahed *Phys. Rev.* **C90** no. 2, (2014) 025204, arXiv:1403.1632 [hep-ph].

[59] Y.-M. Kim, C.-H. Lee, D. Teaney, and I. Zahed *Phys. Rev.* **C96** no. 1, (2017) 015201, arXiv:1610.06213 [nucl-th].

[60] C. Shen, U. W. Heinz, J.-F. Paquet, and C. Gale *Phys. Rev.* **C89** no. 4, (2014) 044910, arXiv:1308.2440 [nucl-th].

[61] G. Aarts, C. Allton, J. Foley, S. Hands, and S. Kim *Phys. Rev. Lett.* **99** (2007) 022002, arXiv:hep-lat/0703008 [hep-lat].

[62] Y. Burnier and M. Laine *Eur. Phys. J. C* **72** (2012) 1902, arXiv:1201.1994 [hep-lat].

[63] H.-T. Ding, A. Francis, O. Kaczmarek, F. Karsch, E. Laermann, and W. Soeldner *Phys. Rev. D* **83** (2011) 034504, arXiv:1012.4963 [hep-lat].

[64] B. B. Brandt, A. Francis, H. B. Meyer, and H. Wittig *JHEP* **03** (2013) 100, arXiv:1212.4200 [hep-lat].

[65] A. Amato, G. Aarts, C. Allton, P. Giudice, S. Hands, and J.-I. Skullerud *Phys. Rev. Lett.* **111** no. 17, (2013) 172001, arXiv:1307.6763 [hep-lat].

[66] J. Ghiglieri, O. Kaczmarek, M. Laine, and F. Meyer *Phys. Rev. D* **94** no. 1, (2016) 016005, arXiv:1604.07544 [hep-lat].

[67] B. B. Brandt, A. Francis, T. Harris, H. B. Meyer, and A. Steinberg *EPJ Web Conf.* **175** (2018) 07044, arXiv:1710.07050 [hep-lat].

[68] M. Cè, T. Harris, H. B. Meyer, A. Steinberg, and A. Toniato arXiv:2001.03368 [hep-lat].

[69] L. D. McLerran and T. Toimela *Phys. Rev.* **D31** (1985) 545.

[70] H. A. Weldon *Phys. Rev.* **D42** (1990) 2384–2387.

[71] C. Gale and J. I. Kapusta *Nucl. Phys.* **B357** (1991) 65–89.

[72] D. Bödeker, M. Sangel, and M. Wörmann *Phys. Rev. D* **93** no. 4, (2016) 045028, arXiv:1510.06742 [hep-ph].

[73] E. Braaten and R. D. Pisarski *Nucl. Phys. B* **337** (1990) 569–634.

[74] H. B. Meyer *Eur. Phys. J.* **A47** (2011) 86, arXiv:1104.3708 [hep-lat].

[75] G. Cuniberti, E. De Micheli, and G. A. Viano *Commun. Math. Phys.* **216** (2001) 59–83, arXiv:cond-mat/0109175 [cond-mat.str-el].

[76] F. Ferrari *Nucl. Phys.* **B909** (2016) 880–920, arXiv:1602.07355 [hep-lat].

[77] S. Caron-Huot *Phys. Rev.* **D79** (2009) 125009, arXiv:0903.3958 [hep-ph].

[78] J. I. Kapusta and S. M. H. Wong *Phys. Rev.* **D62** (2000) 037301, arXiv:hep-ph/0002192 [hep-ph].

[79] J. I. Kapusta and S. M. H. Wong *Phys. Rev.* **C62** (2000) 027901, arXiv:hep-ph/0003196 [hep-ph].

[80] T. Kinoshita *J. Math. Phys.* **3** (1962) 650–677.

[81] T. D. Lee and M. Nauenberg *Phys. Rev.* **133** (1964) 1549–1562.

[82] P. Aurenche, R. Baier, T. Becherrawy, Y. Gabellini, F. Gelis, T. Grandou, M. Le Bellac, B. Pire, D. Schiff, and H. Zaraket *Phys. Rev.* **D65** (2002) 038501, arXiv:hep-ph/0009074 [hep-ph].

[83] A. Majumder and C. Gale *Phys. Rev. C* **65** (2002) 055203, arXiv:hep-ph/0111181.

[84] J. I. Kapusta and S. M. H. Wong *Phys. Rev.* **D65** (2002) 038502.

[85] G. D. Moore and J.-M. Robert arXiv:hep-ph/0607172.

[86] P. Gubler and D. Satow *Phys. Rev. D* **96** no. 11, (2017) 114028, arXiv:1710.02256 [hep-ph].

[87] M. Carrington, A. Gynther, and P. Aurenche *Phys. Rev. D* **77** (2008) 045035, arXiv:0711.3943 [hep-ph].

[88] A. Peshier, K. Schertler, and M. H. Thoma *Annals Phys.* **266** (1998) 162–177, arXiv:hep-ph/9708434 [hep-ph].

[89] S. Jeon *Phys. Rev. D* **47** (1993) 4586–4607, arXiv:hep-ph/9210227.

[90] J. Kuipers, T. Ueda, J. A. M. Vermaseren, and J. Vollinga *Comput. Phys. Commun.* **184** (2013) 1453–1467, arXiv:1203.6543 [cs.SC].

[91] H. A. Weldon *Phys. Rev. D* **65** (2002) 076010, arXiv:hep-ph/0203057.

[92] S. Caron-Huot *Phys. Rev.* **D79** (2009) 065039, arXiv:0811.1603 [hep-ph].

[93] O. Bär and U. Wiese *Nucl. Phys. B* **609** (2001) 225–246, arXiv:hep-ph/0105258.

[94] P. Aurenche, F. Gelis, R. Kobes, and H. Zaraket *Phys. Rev.* **D58** (1998) 085003, arXiv:hep-ph/9804224 [hep-ph].

[95] L. Landau and I. Pomeranchuk *Dokl. Akad. Nauk Ser. Fiz.* **92** (1953) 535–536.

[96] A. Migdal *Phys. Rev.* **103** (1956) 1811–1820.

[97] P. Aurenche, F. Gelis, and H. Zaraket *Phys. Rev. D* **62** (2000) 096012, arXiv:hep-ph/0003326.

[98] P. Aurenche, F. Gelis, and H. Zaraket *JHEP* **05** (2002) 043, arXiv:hep-ph/0204146 [hep-ph].

[99] G. Baym, J.-P. Blaizot, F. Gelis, and T. Matsui *Phys. Lett. B* **644** (2007) 48–53, arXiv:hep-ph/0604209.

[100] D. Besak and D. Bödeker *JHEP* **05** (2010) 007, arXiv:1002.0022 [hep-ph].

[101] I. Ghisoiu and M. Laine *JHEP* **10** (2014) 083, arXiv:1407.7955 [hep-ph].

[102] M. J. Strassler and M. E. Peskin *Phys. Rev. D* **43** (1991) 1500–1514.

[103] I. Gradshteyn and I. Ryzhik, *Table of Integrals, Series, and Products*. Academic Press, 1994.

[104] G. Jackson, Oct., 2019. https://doi.org/10.5281/zenodo.3478144.

[105] P. Baikov, K. Chetyrkin, and J. Kühn *Phys. Rev. Lett.* **118** no. 8, (2017) 082002, arXiv:1606.08659 [hep-ph].

[106] P. Baikov, K. Chetyrkin, J. Kühn, and J. Rittinger *Phys. Lett. B* **714** (2012) 62–65, arXiv:1206.1288 [hep-ph].

[107] S.-z. Huang and M. Lissia *Nucl. Phys. B* **438** (1995) 54–66, arXiv:hep-ph/9411293.

[108] M. Laine and Y. Schröder *JHEP* **03** (2005) 067, arXiv:hep-ph/0503061.

[109] A. Francis, O. Kaczmarek, M. Laine, T. Neuhaus, and H. Ohno *Phys. Rev. D* **91** no. 9, (2015) 096002, arXiv:1503.05652 [hep-lat].

[110] B. B. Brandt, A. Francis, H. B. Meyer, O. Philipsen, D. Robaina, and H. Wittig *JHEP* **12** (2016) 158, arXiv:1608.06882 [hep-lat].

[111] **Flavour Lattice Averaging Group** Collaboration, S. Aoki *et al. Eur. Phys. J. C* **80** no. 2, (2020) 113, arXiv:1902.08191 [hep-lat].

[112] A. Vuorinen *Phys. Rev. D* **67** (2003) 074032, arXiv:hep-ph/0212283.

[113] M. Kardar, *Statistical Physics of Particles*. Cambridge University Press, 2007.

[114] E. Lifshitz and L. Pitaevskii, *Statistical Physics, Part 2*. Butterworth-Heinemann, 1980.

[115] H.-T. Ding, O. Kaczmarek, and F. Meyer *Phys. Rev. D* **94** no. 3, (2016) 034504, arXiv:1604.06712 [hep-lat].

[116] J.-P. Blaizot and F. Gelis *Eur. Phys. J. C* **43** (2005) 375–380, arXiv:hep-ph/0504144.

[117] **Super-Kamiokande** Collaboration, Y. Fukuda *et al. Phys. Rev. Lett.* **81** (1998) 1562–1567, arXiv:hep-ex/9807003 [hep-ex].

[118] **SNO** Collaboration, Q. R. Ahmad *et al. Phys. Rev. Lett.* **89** (2002) 011301, arXiv:nucl-ex/0204008 [nucl-ex].

[119] I. Avignone, Frank T., S. R. Elliott, and J. Engel *Rev. Mod. Phys.* **80** (2008) 481–516, arXiv:0708.1033 [nucl-ex].

[120] I. Esteban, M. C. Gonzalez-Garcia, A. Hernandez-Cabezudo, M. Maltoni, and T. Schwetz *JHEP* **01** (2019) 106, arXiv:1811.05487 [hep-ph].

[121] **T2K** Collaboration, K. Abe *et al. Nature* **580** no. 7803, (2020) 339–344, arXiv:1910.03887 [hep-ex].

[122] **KamLAND** Collaboration, K. Eguchi *et al. Phys. Rev. Lett.* **90** (2003) 021802, arXiv:hep-ex/0212021 [hep-ex].

[123] **T2K** Collaboration, K. Abe *et al. Phys. Rev. D* **91** no. 7, (2015) 072010, arXiv:1502.01550 [hep-ex].

[124] **KATRIN** Collaboration, M. Aker *et al. Phys. Rev. Lett.* **123** no. 22, (2019) 221802, arXiv:1909.06048 [hep-ex].

[125] **Planck** Collaboration, N. Aghanim *et al.* arXiv:1807.06209 [astro-ph.CO].

[126] P. Minkowski *Phys. Lett. B* **67** (1977) 421–428.

[127] M. Gell-Mann, P. Ramond, and R. Slansky *Conf. Proc. C* **790927** (1979) 315–321, arXiv:1306.4669 [hep-th].

[128] T. Yanagida *Prog. Theor. Phys.* **64** (1980) 1103.

[129] S. Tremaine and J. E. Gunn *Phys. Rev. Lett.* **42** (1979) 407–410.

[130] M. Fukugita and T. Yanagida *Phys. Lett.* **B174** (1986) 45–47.

[131] E. Hand *Nature* **464** (2010) 334–335.

[132] S. Alekhin *et al. Rept. Prog. Phys.* **79** no. 12, (2016) 124201, arXiv:1504.04855 [hep-ph].

[133] T. Asaka and M. Shaposhnikov *Phys. Lett. B* **620** (2005) 17–26, arXiv:hep-ph/0505013.

[134] S. Dodelson and L. M. Widrow *Phys. Rev. Lett.* **72** (1994) 17–20, arXiv:hep-ph/9303287 [hep-ph].

[135] B. Follin, L. Knox, M. Millea, and Z. Pan *Phys. Rev. Lett.* **115** no. 9, (2015) 091301, arXiv:1503.07863 [astro-ph.CO].

[136] J. Ghiglieri and M. Laine *JCAP* **07** (2016) 015, arXiv:1605.07720 [hep-ph].

[137] H. Weldon *Phys. Rev. D* **28** (1983) 2007.

[138] H. A. Weldon *Phys. Rev.* **D26** (1982) 2789.

[139] D. Nötzold and G. Raffelt *Nucl. Phys.* **B307** (1988) 924–936.

[140] H. Weldon *Phys. Rev. D* **40** (1989) 2410.

[141] K. Farakos, K. Kajantie, K. Rummukainen, and M. E. Shaposhnikov *Nucl. Phys.* **B425** (1994) 67–109, arXiv:hep-ph/9404201 [hep-ph].

[142] T. Appelquist and R. D. Pisarski *Phys. Rev. D* **23** (1981) 2305.

[143] E. Braaten and A. Nieto *Phys. Rev. D* **51** (1995) 6990–7006, arXiv:hep-ph/9501375.

[144] K. Kajantie, M. Laine, K. Rummukainen, and M. E. Shaposhnikov *Phys. Rev. Lett.* **77** (1996) 2887–2890, arXiv:hep-ph/9605288.

[145] K. Kajantie, M. Laine, K. Rummukainen, and Y. Schröder *Phys. Rev. D* **67** (2003) 105008, arXiv:hep-ph/0211321.

[146] D. Bödeker and M. Sangel *JCAP* **04** (2015) 040, arXiv:1501.03151 [hep-ph].

[147] M. Carrington *Phys. Rev. D* **45** (1992) 2933–2944.

[148] B. Pendleton and G. G. Ross *Phys. Lett. B* **98** (1981) 291–294.

[149] K. Kajantie, M. Laine, K. Rummukainen, and M. E. Shaposhnikov *Nucl. Phys.* **B458** (1996) 90–136, arXiv:hep-ph/9508379 [hep-ph].

[150] M. Laine, P. Schicho, and Y. Schröder *JHEP* **05** (2018) 037, arXiv:1803.08689 [hep-ph].

[151] J. Ghiglieri and M. Laine *JHEP* **05** (2017) 132, arXiv:1703.06087 [hep-ph].

[152] D. Bödeker and D. Schröder *JCAP* **02** (2020) 033, arXiv:1911.05092 [hep-ph].

[153] J. Ghiglieri and M. Laine *JHEP* **07** (2019) 078, arXiv:1905.08814 [hep-ph].

[154] J. Ghiglieri and M. Laine *JHEP* **02** (2019) 014, arXiv:1811.01971 [hep-ph].

[155] **LIGO Scientific, Virgo** Collaboration, B. P. Abbott *et al. Phys. Rev. Lett.* **118** no. 12, (2017) 121101, arXiv:1612.02029 [gr-qc]. [Erratum: Phys. Rev. Lett.119,no.2,029901(2017)].

[156] **LIGO Scientific, Virgo** Collaboration, B. P. Abbott *et al. Phys. Rev.* **X9** no. 3, (2019) 031040, arXiv:1811.12907 [astro-ph.HE].

[157] A. G. Riess *et al. Astrophys. J.* **855** no. 2, (2018) 136, arXiv:1801.01120 [astro-ph.SR].

[158] N. Christensen *Rept. Prog. Phys.* **82** no. 1, (2019) 016903, arXiv:1811.08797 [gr-qc].

[159] J. F. Donoghue *Phys. Rev.* **D50** (1994) 3874–3888, arXiv:gr-qc/9405057 [gr-qc].

[160] B. S. DeWitt *Phys. Rev.* **160** (1967) 1113–1148.

[161] S. Carroll, *Spacetime and Geometry: An Introduction to General Relativity*. Pearson, 2014.

[162] S. Weinzierl *Phys. Rept.* **676** (2017) 1–101, arXiv:1610.05318 [hep-th].

[163] S. Weinberg, *Gravitation and Cosmology*. John Wiley & Sons, 1972.

[164] L. D. Landau and E. M. Lifshitz, *The Classical Theory of Fields*. Butterworth-Heinemann, 1980.

[165] J. D. Jackson, *Classical Electrodynamics*. Wiley, 1975.

[166] A. Einstein *Sitzungsber. Preuss. Akad. Wiss. Berlin (Math. Phys.)* (1916) 688–696.

[167] J. Weisberg, J. Taylor, and L. Fowler *Sci. Am.* **245** (1981) 66–74.

[168] J. Ghiglieri and M. Laine *JCAP* **1507** (2015) 022, arXiv:1504.02569 [hep-ph].

[169] L. Niemi, H. H. Patel, M. J. Ramsey-Musolf, T. V. Tenkanen, and D. J. Weir *Phys. Rev. D* **100** no. 3, (2019) 035002, arXiv:1802.10500 [hep-ph].

[170] M. Kardar, *Statistical Physics of Fields*. Cambridge University Press, 2007.

[171] L. D. Landau and E. Lifshitz, *Fluid Mechanics*. Butterworth-Heinemann, 1987.

[172] P. Kovtun, G. D. Moore, and P. Romatschke *Phys. Rev. D* **84** (2011) 025006, arXiv:1104.1586 [hep-ph].

[173] G. D. Moore and K. A. Sohrabi *Phys. Rev. Lett.* **106** (2011) 122302, arXiv:1007.5333 [hep-ph].

[174] G. Baym, S. P. Patil, and C. J. Pethick *Phys. Rev.* **D96** no. 8, (2017) 084033, arXiv:1707.05192 [gr-qc].

[175] G. N. Watson *Q. J. Math.* **10** (1939) 266–276.

[176] M. L. Glasser and J. Boersma *J. Phys. A: Math. Gen.* **33** (2000) 5017–5023.

[177] Y. Akamatsu, A. Mazeliauskas, and D. Teaney *Phys. Rev. C* **97** no. 2, (2018) 024902, arXiv:1708.05657 [nucl-th].

[178] G. Baym, H. Monien, C. Pethick, and D. Ravenhall *Phys. Rev. Lett.* **64** (1990) 1867–1870.

[179] P. Y. Huet, K. Kajantie, R. G. Leigh, B.-H. Liu, and L. D. McLerran *Phys. Rev. D* **48** (1993) 2477–2492, arXiv:hep-ph/9212224.

[180] G. D. Moore and K. Rummukainen *Phys. Rev. D* **63** (2001) 045002, arXiv:hep-ph/0009132.

[181] P. F. de Salas and S. Pastor *JCAP* **07** (2016) 051, arXiv:1606.06986 [hep-ph].

[182] B. X. Hu and A. Loeb arXiv:2004.02895 [astro-ph.CO].

[183] M. J. G. Veltman *Conf. Proc.* **C7507281** (1975) 265–327.

[184] Y. Schröder, M. Vepsäläinen, A. Vuorinen, and Y. Zhu *JHEP* **12** (2011) 035, arXiv:1109.6548 [hep-ph].

[185] Y. Zhu and A. Vuorinen *JHEP* **03** (2013) 002, arXiv:1212.3818 [hep-ph].

[186] A. Vuorinen and Y. Zhu *JHEP* **03** (2015) 138, arXiv:1502.02556 [hep-ph].

Declaration of consent

on the basis of Art. 18 of the PromR Phil.-nat. 19

Surname, first name:	Jackson, Greg
Registration number:	16-109-373
Study programme:	Physics
	Bachelor ☐ Master ☐ Dissertation ☒
Thesis title:	Rate observables for cosmology and heavy ion collision experiments
Supervisor:	Prof. Dr. Mikko Laine

I declare herewith that this thesis is my own work and that I have not used any sources other than those stated. I have indicated the adoption of quotations as well as thoughts taken from other authors as such in the thesis. I am aware that the Senate pursuant to Article 36 paragraph 1 litera r of the University Act of September 5th, 1996 and Article 69 of the University Statute of June 7th, 2011 is authorized to revoke the doctoral degree awarded on the basis of this thesis.

For the purposes of evaluation and verification of compliance with the declaration of originality and the regulations governing plagiarism, I hereby grant the University of Bern the right to process my personal data and to perform the acts of use this requires, in particular, to reproduce the written thesis and to store it permanently in a database, and to use said database, or to make said database available, to enable comparison with theses submitted by others.

Bern, 18 June 2020

Greg Jackson